DYNAMIC CHARACTERIZATION AND SEISMIC ASSESSMENT OF HISTORIC MASONRY STRUCTURE OF RUMI DARWAZA

A Thesis Submitted
in Partial Fulfillment of the Requirements
for the Degree of

MASTER OF TECHNOLOGY

by

Amanpreet Singh

DEPARTMENT OF CIVIL ENGINEERING
INDIAN INSTITUTE OF TECHNOLOGY KANPUR
KANPUR 208016

August 2016

CERTIFICATE

It is certified that the work contained in this thesis entitled "*Dynamic characterization and seismic assessment of historic masonry structure of Rumi Darwaza*" by *Mr. Amanpreet Singh* (Y11907075), has been carried out under my supervision and this work has not been submitted elsewhere for a degree.

August 2016

Dr. Durgesh C Rai
Professor
Department of Civil Engineering
Indian Institute of Technology Kanpur
Kanpur - 208016

ABSTRACT

Historical monuments portray the architectural heritage and cultural wealth of a civilization. They are symbols of pride and a gateway to our past. Therefore it is of paramount importance that these monuments be preserved for future generations. Foremost symbol of Lucknow Awadhi architecture, Rumi Darwaza is an 18th century gateway structure characterized by a half spherical dome resting on half octagonal plan and further supported by an arch. The masonry structure, built using thin burnt clay bricks (Lakhauri) and lime-crushed brick aggregate (surkhi) mortar, has developed major cracks in the arch due to natural aging and other environmental factors. Past earthquakes in India have highlighted the poor seismic performance of our monuments. Seismic assessment of historic monuments needs to be carried out to evaluate their structural response and draw out retrofitting plans to ensure their longevity.

To assess the seismic performance of Rumi Darwaza, dynamic characteristics, such as natural frequencies, mode shapes and damping ratios, are required for realistic numerical simulation which have been obtained from field vibration tests. Laboratory experiments were conducted to characterize the mechanical properties of Lakhauri bricks and lime surkhi mortar, as well as masonry prisms. A detailed Finite Element (FE) model was developed to understand the structural behaviour under gravity and seismic loads. Dynamic characterization results are seen to match closely with analytical predictions validating the FE model. Response spectrum analysis showed the stiffening arch at the open face of half dome to be the critical structural element with high tensile stresses at the same locations where damages have been observed in the structure. Two strengthening techniques using latticed structure of concrete filled hollow steel tubes to support the dome arch from the inside have been proposed to reduce its vulnerability for seismic forces.

ACKNOWLEDGMENT

I would like to express my deepest and sincerest gratitude to my thesis supervisor, Prof. Durgesh C Rai for his valuable guidance and encouragement. He has been a constant source of inspiration for me and I feel privileged to have gotten the opportunity to do research with him as my guide. The opportunities provided by him to work on interesting projects have helped me broaden my knowledge and develop my overall personality. I would also like to thank my professors at IIT Kanpur who taught me and helped to build my technical knowledge.

I would like to express my sincere thanks to Dr. K. K. Bajpai, Senior Scientific Officer, Structural Engineering Laboratory for his support and assistance in the experimental study. I am thankful to Pankaj Sir, Mohit Sir, Dhruv Bhaiya & Abrar ji for helping me at different stages of my work. Appreciations are extended to all the staff, especially Lal ji, Raj Kishor ji, Jitender & Mohit for their help in conducting the experiments.

I am grateful to my friends, Nitin and Alok, for providing a healthy learning environment in the lab. The fun we had during the course of our theses will be deeply missed. I would also like thank Anurag, Pragya, Piyush and Faizan for sparing their valuable time to help me with my experiments and proofreading my thesis. I would like to appreciate my seniors Abhijit and Bhushan for their guidance at the beginning of my thesis. I must also thank Vaibhav Bhaiya, Puneet, Supratik and Rajarshi for their help and support. I am grateful to all my wingmates who made my stay in the campus wonderful and fun filled. No account of my story at IIT Kanpur will be complete without the mention of Shrey, Aditya and Amit who have stood by me through thick and thin. I will always cherish the memorable moments I have shared with them.

Last but not the least, I express my gratitude to my parents for their love, affection and support throughout my life. I would not have reached where I am today if it had not been for their confidence in me. To them, I owe everything in my life.

Amanpreet Singh

TABLE OF CONTENTS

LIST OF TABLES

LIST OF FIGURES

CHAPTER 1

INTRODUCTION

1.1 OVERVIEW

Historic preservation is a worldwide endeavor that aims to protect and conserve buildings of historical significance. Monuments remind the society about its cultural heritage. They are symbols of pride of our civilization helping us to appreciate our past. Therefore it is the society's duty to preserve and protect these monuments inherited from past generations and bestow for the benefit of future generations. Every nation has at least a few, if not many, old buildings like temples, towers, churches, memorials, palaces etc. which have historical and cultural significance as they are a repository of archaeological treasures and a gateway to our past.

These monuments, some of them several centuries old, have withstood the ravages of time and nature. Many structures have survived through the ages experiencing several earthquakes and other natural calamities. However, their survival was not without undergoing damages and cracking due to natural aging and intermittent severe events. Therefore, the responsibility of protecting the monuments from deteriorating agents and restoring their former glory should be borne by the society. Assessment of historic monuments needs to be done so that remedial measures to ensure their longevity can be determined and implemented. Every historical monument is unique and presents new difficulties in seismic assessment, making it a very challenging problem. Only recently our society has started to realize that protecting architectural heritage is important. A worldwide effort has led to increased interest in developing tools and methods for assessment of monuments and their protection and conservation.

India too has a very rich cultural heritage with a huge and diverse pool of ancient monuments and archaeological sites. Particularly, one of the best traditions of Indian art is architecture of Awadh which excels in variety and numerousness of its buildings.

1.2 STRUCTURAL SYSTEM AND MATERIALS USED IN AWADH ARCHITECTURE

The city of Lucknow, situated on the banks of river Gomti and famously called the 'Constantinople of India' derives its charm from the glorious Awadhi architecture and monumental heritage. Art and culture flourished in Lucknow during the Nawabi period (1770*s* – 1850*s*). During that period, Lucknow saw scores of monuments, palaces, mosques, Imambaras, tombs etc. come up. These buildings employed traditional elements of Mughal architecture such as a sanctuary covered by dome, tall minarets with cupolas, arches and kiosks, combined with local elements and European features. Thick walls, large sized columns, arches, vaults and domes were the general structural components of most of the monuments. Walls were the main gravity load resisting members. Arches were used to transfer load from domes above to the walls underneath. Masonry arches are particularly strong under compressive stress, and have been used for large span constructions. Monuments built during the Nawabi era were considerably more massive compared to structures of the same period elsewhere. The main feature of the Imambaras constructed by the Nawabs are their spaciousness and provision for a central hall. The Bada Imambara is the world's largest vault structure having a dimension of 50 m × 16 m and a height of 15 m without any supporting pillars in between. This huge vault, which has been used to enclose the space, was successfully built by the architect to counter the thrust from vault by providing thick walls. Domes, also commonly seen in these monuments, rested on top of walls or a drum below it, or supported by arches (Güngör 1988).

Rumi Darwaza, the main gateway of the Bara Imambara Complex, is a magnificent and unparalleled creation of Hindu-Muslim architecture constructed during the period of Nawab Asaf-ud-daula by the architect Kaifayatullah. It is an ASI (Archaeological Survey of India) protected monument which was completed in 1784. A half spherical dome rests on a half octagonal plan and the half dome is further supported by an arch. Viewed from the west, the structure looks like a large *mehrab*, formed by two extra areas, which intersect at a point on the apex. All along, cursive engravings of lotus petals and other intricate patterns with a series of *Guldastas* were provided to adorn the lofty gateway and within this, three medium sized arched gateways appear in a semi-circular fashion. From the eastern side, it appears like a half crescent shaped building, influenced

by the Rajput style, having three medium sized gateways adorned with multi foiled arches and floral designs, flanked by two minarets on both the sides. On the roof of the gateway, there is another pentagonal structure with five doorways on each wall. The roof of this geometric structure culminates in a small platform, resembling the top of Mexican hat. Above this, a red sand stone octagonal *chhatri* (cupola) visible from all the sides, serves as the *mukuta* (crown) of the structure as shown in Figure 1.1. The *Rumi Darwaza* is flanked by two three-storey structures on either sides, along with two four-storey octagonal bastions on their extreme ends (Chandra 2003).

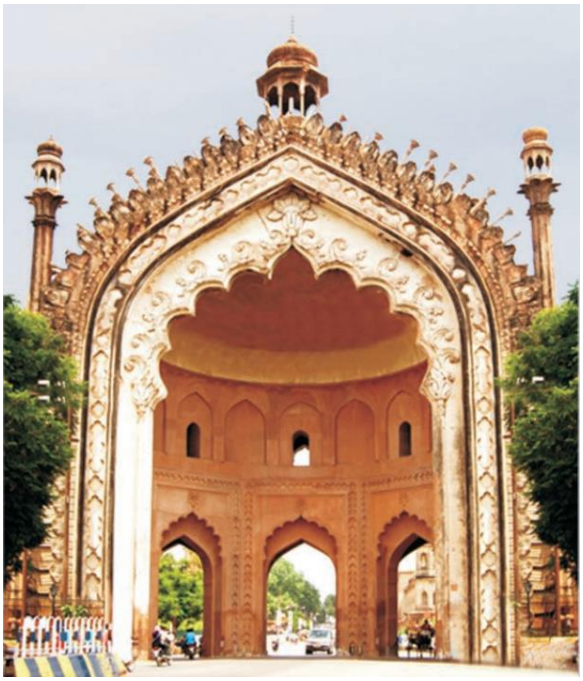

Figure 1.1. Rumi Darwaza, Lucknow (asilucknowcircle.nic.in)

Nawabi era saw the use of brick, mortar and stucco instead of stone and marble which was commonly used during the Mughal period. *Rumi Darwaza* was built using Lakhauri bricks with lime-surkhi mortar as binding material. Lakhauri bricks were rectangular, burnt bricks with typical size of 120 mm × 80 mm × 20 mm. These bricks were not of standard size as they were hand molded, and so their surfaces were not levelled and the thickness was not uniform. Because of this reason, thick mortar was used to level the surface of masonry at each course. Lucknow monuments are characterized by mortar joints of 10-25 mm thickness. Lime, sand and surkhi (crushed brick) were used as

constituents of mortar. Through research and experiments, it is now known that addition of surkhi to mortar imparts hydraulic properties to the otherwise non-hydraulic lime putty (Teutonico et al. 1993). Even though discarded brick fragments were easily available, their use in construction in those times shows that the architects were very knowledgeable and vastly experienced about how the material would behave and hugely confident in their design of massive structures for gravity load. This lime surkhi mortar imparted ductility to the structure, even though it took a longer time to reach its full strength. Lime surkhi mortar used in Lucknow monuments, has also been used in other parts of the world and is known by different names. Ancient Romans referred to it as *Opus Signinum*, and was later called as *Cocciopesto* in Italy and *Argamasa* in Spain (Verhosek 2006).

1.3 SEISMIC PERFORMANCE AND NEED FOR SEISMIC ASSESSMENT

Majority of historical monuments had been built using brick masonry and mortar which is characterized by low tensile and shear strength. Even though the monuments had been constructed to perform satisfactorily under service loads, they were not built to resist seismic events. Past earthquakes have highlighted the deficient seismic performance of monuments. Several earthquake reconnaissance reports mention about the poor seismic performance of historical monuments (Rai et al. 2012, Rai et al. 2015b) as shown in Figures 1.2 and 1.3.

Figure 1.2. Collapse of historical monuments in Kathmandu, Nepal due to M7.8 Gorkha (Nepal) earthquake of 25th April, 2015 (Rai et al. 2015b)

Figure 1.3. Damaged Buddhist monastic temples in Sikkim after M6.9 Sikkim (India–Nepal Border) earthquake of 18th September, 2011 (Rai et al. 2012)

In 2001 Bhuj earthquake, a large number of heritage structures suffered extensive damage. In Kutch and Rajkot regions of Gujrat alone, 250 monuments were inspected by a team from Indian National Trust for Art and Cultural Heritage (INTACH) and it was reported that more than 40% structures suffered extensive damage, while only 10% escaped undamaged (INTACH Field Report 2001). Figure 1.4 shows damages incurred by heritage structures in 2001 Bhuj earthquake.

Figure 1.4. Damage to heritage structures in Kutch region of Gujrat due to M7.7 Bhuj earthquake of 26th January, 2001 (UNESCO Report 2001)

Observed damages to the monuments indicate that they are seismically deficient and point towards the need for urgent retrofitting to safeguard the monuments against future earthquakes and mitigate the associated risk. In order to determine the extent of retrofitting required, seismic evaluation of the as-built structure is necessary. As every monument is unique in terms of its material, construction practice, geometry and layout, seismic evaluation does not have straightforward procedures and requires considerable expertise. Outcomes of seismic evaluation can give a better idea about the structural response, which can serve as a guide for the measures to be adopted for retrofitting.

1.4 MOTIVATION AND OBJECTIVES

Historical monuments are cultural assets worth preserving. Therefore, governmental agencies, academia and the whole society in general should pay attention to the maintenance and preservation of historic monuments. The repair work carried out by ASI at Lucknow monuments has worn-out within a very short span of time because the intervention material being used has not been checked through prior analysis to be compatible with the original material. Due to the incompatibility between the two materials, the intervention material is not able to establish a bond with the older material. This is mainly because the binder-aggregate ration in renovation mortar is lower than existing mortar, so there is lesser lime content in renovation mortar (Rai et al. 2015a). Such incompatibility between the two materials can in fact lead to accelerated deterioration of original material due to unexpected chemical interactions. Furthermore, the major cracks that have been observed in the arch are due to structural problems, due to natural aging, vehicular movement through the gate and other deteriorating natural influences, but still no remedial measures have been undertaken. Figure 1.5 shows the cracks in the monument and the poor quality of renovation work carried out by ASI, Lucknow Circle.

General public, activists and media have, over the years, voiced their concerns about the deteriorating state of *Rumi Darwaza* and other monuments (Ahmed 1998, Bose 2011, Sharda 2012, Malhotra 2013).

(a) (b)

Figure 1.5. Rumi Darwaza: (a) Major cracks in arch and (b) Poor quality of renovation work carried out by ASI on Lucknow monuments (Rai and Dhanapal 2013)

Historic monuments were not built according to seismic provisions, since they did not exist at the time of their construction. Therefore, they need to be assessed as per current seismic code requirements, and retrofitted to upgrade their seismic capacity. Considering their heritage value, it is important that the proposed retrofitting techniques should preserve the original characteristics as far as possible while at the same time adequately improving its seismic capacity. Addition of new elements should preferably not interfere with the original appearance of the structure. Further, any proposed intervention material should be based on analysis to ensure their compatibility with the original material.

In the current study, seismic assessment of historic masonry structure of *Rumi Darwaza* has been carried out. The objectives of the study can be summarized as:

i. Dynamic characterization of structure of *Rumi Darwaza* for its natural frequencies, mode shapes and damping ratios through field vibration testing.

ii. Characterization of materials used, Lakhauri bricks and lime surkhi mortar, as well as masonry assemblages for their mechanical properties.

iii. Develop a Finite Element (FE) model, of the structure and calibrate it using experimental results, to understand the structural behaviour under dead load and seismic loads.

iv. Propose strengthening techniques to mitigate the vulnerability of structure to seismic forces based on the developed understanding of structural behaviour and observed damages in the structure.

1.5 ORGANIZATION OF DISSERTATION

The dissertation has been organized in six chapters. Chapter 1 introduces the importance of preserving historical monuments and the need for seismic assessment. A brief introduction about the structural system and materials used in *Rumi Darwaza*, and other monuments of that period, is also provided. Chapter 2 presents some studies by past researchers for seismic assessment of monuments by performing material characterization, dynamic characterization and finite element modelling of monuments for numerical analyses. Chapter 3 presents the procedure of experimental testing done at *Rumi Darwaza* for its dynamic characterization. The procedure for processing the structural response measurement data has been explained and extracted modal parameters have been presented. Chapter 4 presents the results of tests conducted for the mechanical characterization of the materials used in 18th century Lucknow monuments – bricks, mortar and masonry assemblages. Formulation of lime-surkhi mortar for preparation of masonry specimens has also been explained. Chapter 5 describes the steps involved in FE modelling of the monument and presents the results of different analyses done in Abaqus software to predict the structural response. A comparison between the experimental and analytical results is also presented. Based on the evaluated structural behaviour, strengthening techniques have been proposed and their effect on improving the structural response has been demonstrated. Chapter 6 gives an overall summary of the seismic assessment procedure adopted and presents the conclusions of the study. Some recommendations for future work have also been listed.

CHAPTER 2

LITERATURE REVIEW

2.1 OVERVIEW

Seismic assessment and retrofitting of historical monuments and heritage structures is an issue of paramount importance for countries, such as India, which have a great built cultural heritage and also suffer from high seismicity. Even though considerable research advances have been made in methods for non-destructive evaluation, techniques for material characterization and tools for advanced computational analyses, conservation of historical structures is still a challenging problem. This chapter presents the various studies carried out by different researchers for material properties, dynamic characterization, and finite element modelling of monuments which constitute the different steps involved in the seismic assessment of monuments.

2.2 ASPECTS OF SEISMIC ASSESSMENT

Seismic assessment of a monument is based on the following three main steps (Lagomarsino and Cattari 2015):

- Survey of monument site for gaining knowledge about the structure and damages incurred due to previous earthquakes, augmented by non-destructive testing, structural identification, laboratory tests on material specimens etc.,
- Computer/numerical modelling of structure or structural elements accompanied by verification of model for seismic analysis of monument, and
- Rehabilitation/retrofitting decisions with design of strengthening interventions.

Various researchers have carried out studies to tackle this problem from one or more aspects in order to assess seismic vulnerability of monuments and tried to provide retrofitting solutions to enhance their structural integrity and prolong their life.

2.3 MATERIAL CHARACTERIZATION

Maravelaki-Kalaitzaki (2007) performed physio-chemical analyses of original mortar materials used in castle of Firkas, one of the bastions of the Venetian fortifications of the city of Chania (Canea), on the north-western side of Crete, Greece. The objective of the restoration project was conservation and rehabilitation of the central building of the castle. The Venetian fortifications had been declared a historical, artistic and monumental patrimony of the Greek State in 1965. Although no structural problems were observed in the structure, it was deemed important to protect the structure against natural deteriorating agents of moisture, salts and rain which had led the mortar into an advanced state of decay by waterproofing the roof. Principles of compatibility with original mortar material dictated the design of repair mortars so that they had similar properties and composition. Natural hydraulic lime was used as a binding material in the design of repair mortar simulating the grain size distribution of the analysed original mortars. Figure 2.1 compares the grain size distribution of aggregates in original mortar samples and repair mortar samples. Mechanical characteristics of repair mortars were also evaluated keeping in mind that compatibility with old masonry would require that repair mortars have lower strength than original stone. Stone and mortars of old masonry are characterized by low mechanical resistance and modulus of elasticity. However, the repair materials showed lower strength than the original stone, which demonstrated that they can be used for repointing purposes. Visual inspection of designed mortar used for waterproofing of the roof showed no microcracks or efflorescence formation after 14 months suggesting that a compatible system had been achieved.

Baronio et al. (1997) studied the characteristics of mortar based on lime and crushed brick. This type of mortar had been used extensively in monuments. Mortar samples were collected from churches San Vitale and San Michele in Ravenna, Italy. Binder-aggregate ratio and grain size distribution were evaluated from chemical analyses and a similar material was reproduced in lab based on the results. Figure 2.2 shows the grain size distibution of samples collected from church sites. Binder-aggregate ratio of 1:3 was used in the formulated mortar.

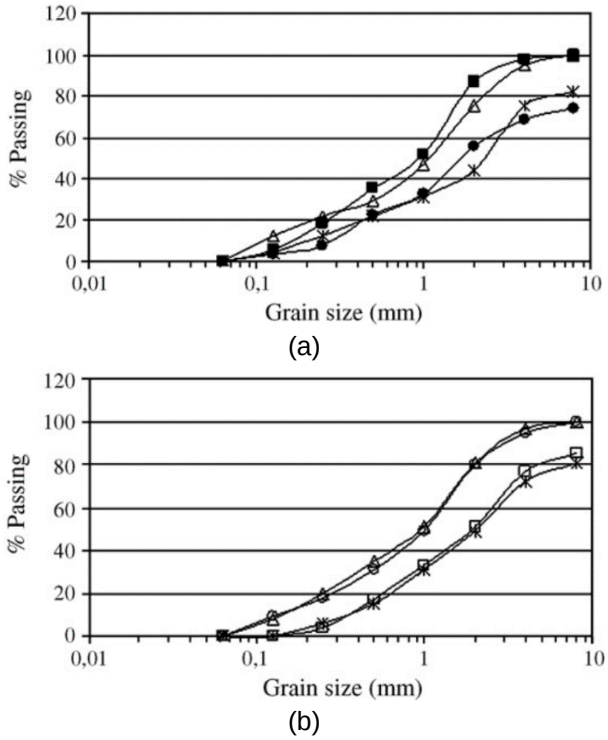

Figure 2.1. Comparison of grain size distribution of aggregates in (a) original mortar used in Firkas castle and (b) repair mortar (Maravelaki-Kalaitzaki 2007)

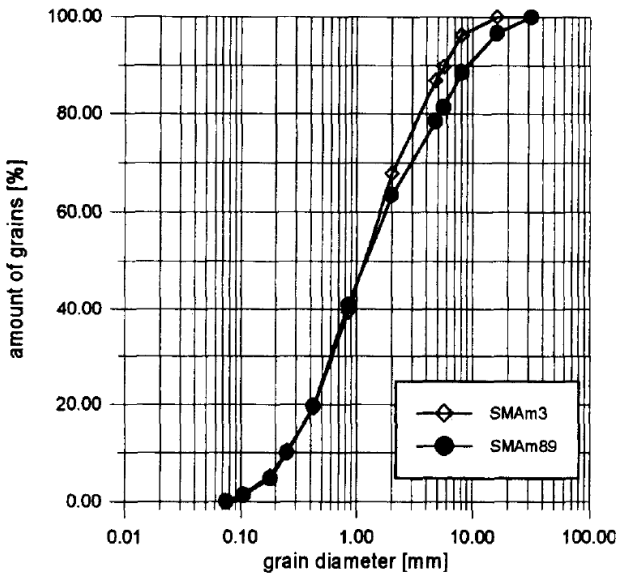

Figure 2.2. Grain size distribution of aggregates in mortar samples from San Michele in Italy (Binda et al. 2000)

Mortar specimens of dimensions $40\,\text{mm} \times 40\,\text{mm} \times 160\,\text{mm}$ were tested under compression and flexure at different ages of curing. It was seen that the mortars

exhibited very low compressive strength which continued to increase even till a period of 240 days with only a slight increase in 365 days strength, as shown in Figure 2.3a. The low growth of strength is attributed to the slow rate of carbonation, which is shown in Figure 2.3b. This shows that the reaction continues to happen, even though it may take a long time.

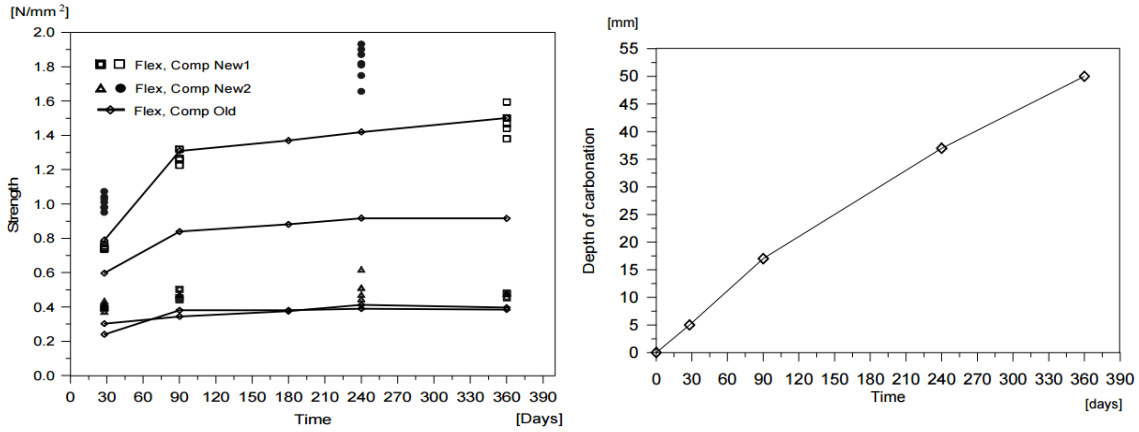

(a) (b)

Figure 2.3. Effect of addition of crushed brick on characteristics of lime based mortar: (a) Compressive and flexural strength and (b) Carbonation for different curing age (Binda et al. 1999)

Binda et al. (1999) also prepared masonry specimens using the same type of mortar and bricks as used in Basilica of San Vitale to understand the behaviour of masonry with very thick mortar joints, as shown in Figure 2.4a. Stack bond prisms made of mortar joints thickness 45 mm were prepared and tested under compression at different curing age. The test setup has been shown in Figure 2.4b.

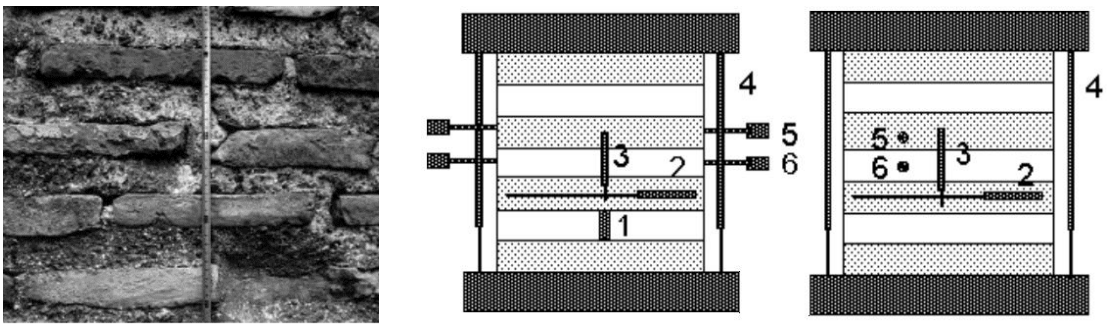

(a) (b)

Figure 2.4. (a) Thick mortar joints in San Vitale masonry and (b) Experimental setup for stack bond compression test (Binda et al. 1999)

From the experimental results, it was observed that although the mortar strength continued to grow over the period of one year, the increase in mortar strength is not that significant. At shorter ages of curing, the specimen showed greater ability to undergo deformation with lower elastic modulus. Specimens at longer curing age showed lower deformation capacity with approximately 2-3 times higher elastic modulus for 365 days cured specimen as compared to 28 days cured specimen. These observations can also be made from the stress-strain curves shown in Figure 2.5.

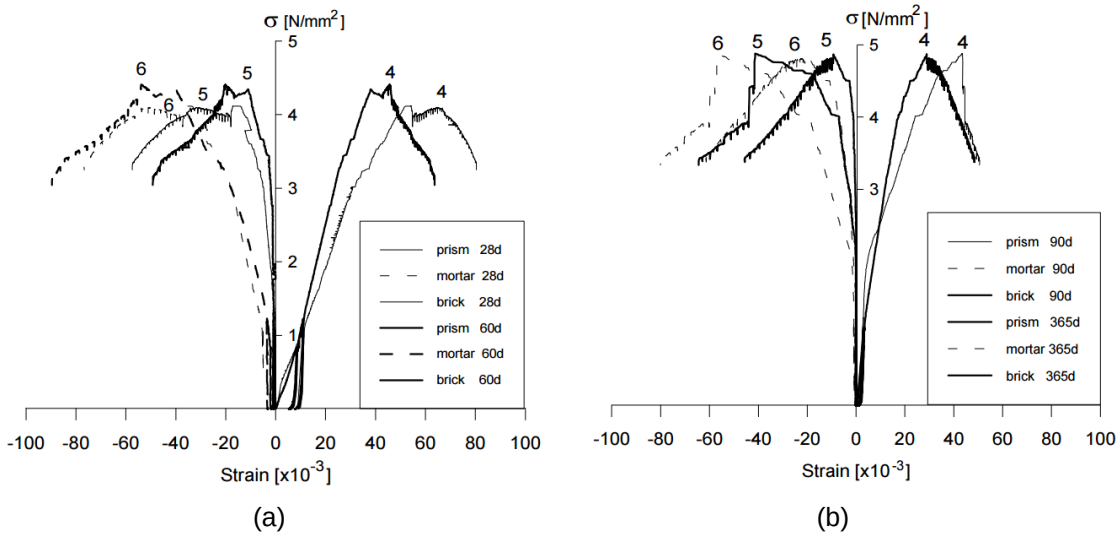

Figure 2.5. Stress-strain curves of prisms tested at (a) 28 and 60 days and (b) 90 and 365 days (Binda et al. 1999)

Vintzileou et al. (2008) conducted experiments on three-leaf masonry specimens grouted with ternary or hydraulic lime based grouts to evaluate their mechanical properties. The aim of the study was to select an appropriate grout mix for restoration of Katholikon church of Dafni Monastery, Greece. Masonry specimens were prepared to simulate the in situ masonry conditions by using radar and boroscopy to get in-depth geometry of the perimeter stone. Geometry of specimens was chosen to simulate the more vulnerable part of masonry. Six specimens were constructed, three each for testing in compression and diagonal tension. On the basis of observed enhancement of compressive strength of masonry, achieved homogenization of masonry, delayed separation between the three leaves and physical–chemical compatibility with the in-situ materials, hydraulic lime-based grouts were selected for use in monastery.

2.4 DYNAMIC CHARACTERIZATION AND FINITE ELEMENT MODELLING

Due to uncertainties in modeling masonry structures, it is required that the analytical models be validated by structural characteristics obtained from field tests. Jaishi et al. (2003) tested traditional multi-tiered temples in Nepal by ambient vibration testing under wind-induced excitation to obtain their dynamic properties. These old temples are monuments having historic and archaeological importance and have drawn much national and international concern. The temples have experienced damages due to previous earthquakes. Historical records also show that some of these temples have been destroyed completely and no trace can be seen anymore. Figure 2.6a shows one of the temples which were tested. Two identification methods, Peak Picking and Stochastic Subspace Identification, were used for modal parameter extraction. Idealized finite element (FE) models of the temples were prepared and the analytical models were verified using experimental results. Structural and non-structural elements contributing to mass and stiffness of structure were modelled in the structural idealization. The different materials used in structural components were assumed as homogeneous, isotropic and linearly elastic. It was seen that natural frequency predicted by analytical models were significantly different than the experimentally obtained values. The modulus of elasticity for masonry used in FE model was updated to 800 MPa to obtain good correlation between experimental and analytical results, as shown in Figure 2.6b.

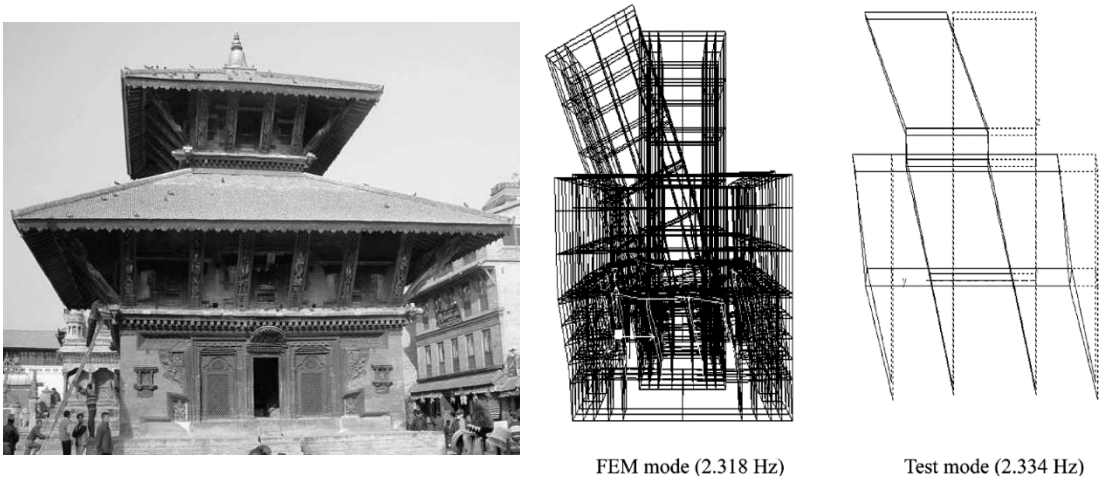

Figure 2.6. (a) Image of Yechheswor temple, Nepal and (b) First bending mode of Yechheswor temple from finite element modelling and ambient vibration tests (Jaishi et al. 2003)

Peña et al. (2010) carried out ambient vibration tests on an old masonry tower Qutb Minar, India for dynamic characterization of the structure. Two 3-D models, one using solid elements (Solid model) and the other with composite beams (Beam model), and one 2-D model with just in-plane elements (Rigid model) were considered to evaluate the structural behavior. Material properties were obtained by optimizing variables in GAMS software to minimize the error between experimental and analytical frequencies. Figure 2.7 shows the masonry tower and its experimental and analytical mode shapes.

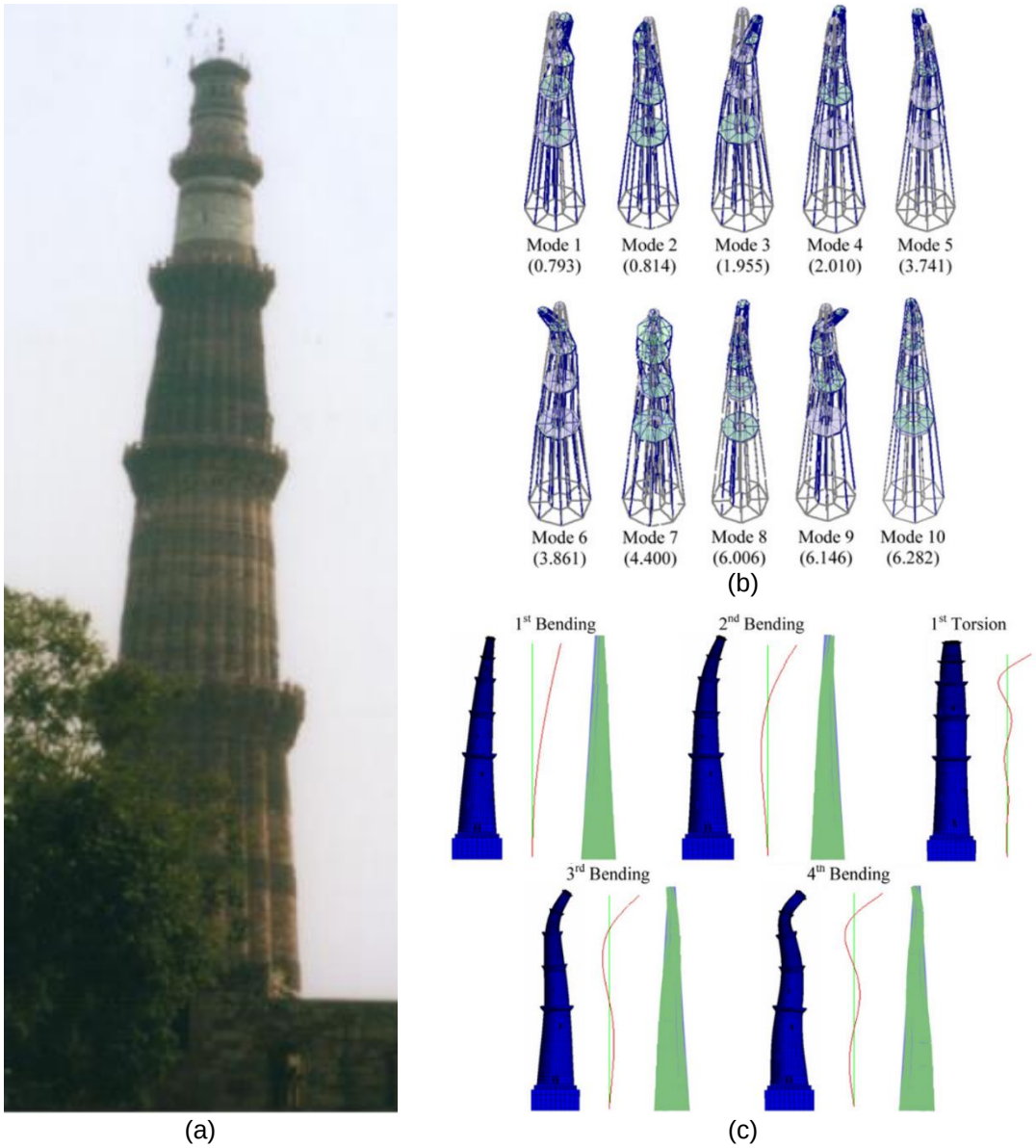

Figure 2.7. (a) Qutb Minar in Delhi, India, (b) Experimental mode shapes and associated frequencies and (c) Analytical mode shapes for different models, Solid (left), Beam (center) and Rigid (right) (Peña et al. 2010)

Ramos et al. (2010) carried out ambient dynamic characterization tests on Mogadouro Clock Tower, Portugal. The modal parameters were estimated by Stochastic Subspace Identification (SSI) method implemented in ARTeMIS software. A 3-D FE model with brick elements was made for structural assessment. Modulus of elasticity of different parts were chosen as updating parameters and optimization was carried out by minimizing the objective function comprising of residuals between experimental and analytical natural frequencies and mode shapes. A comparison of experimental and analytical results after FE model updating is shown in Figure 2.8. An average value of 0.98 for correlation between analytical and experimental mode shapes was achieved after updating the FE model.

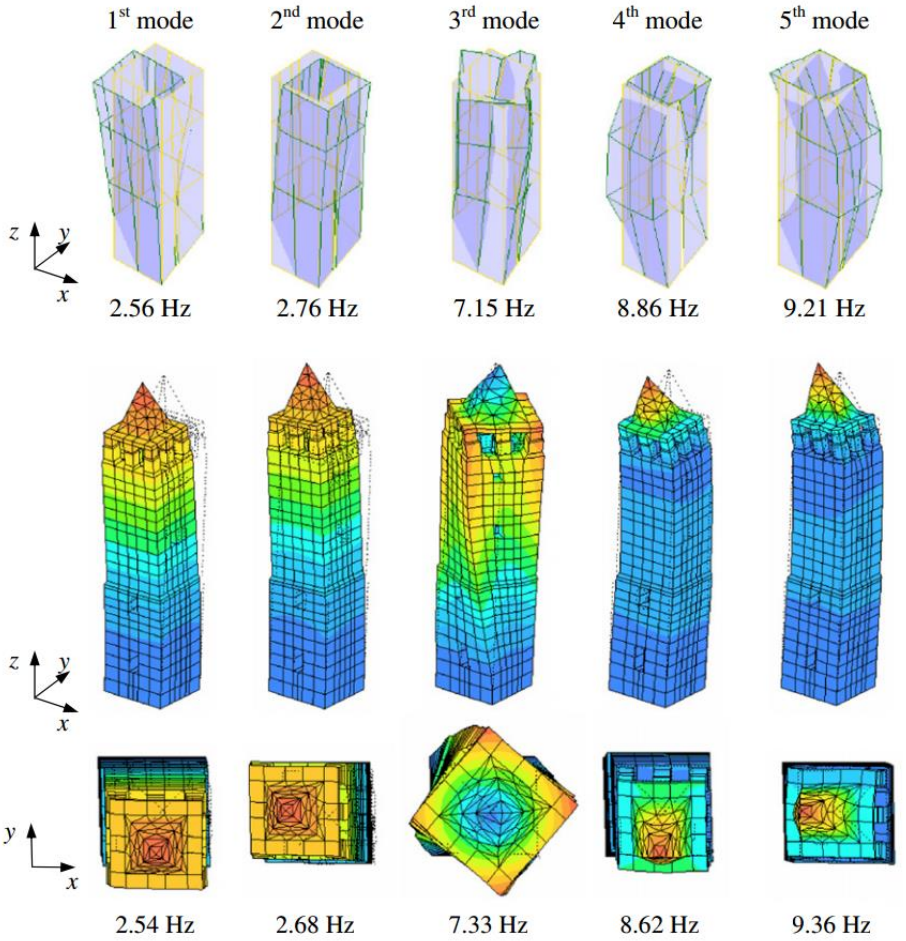

Figure 2.8. Comparison of experimental and analytical results after FE model updating (Ramos et al. 2010)

2.5 SEISMIC ASSESSMENT USING FINITE ELEMENT ANALYSES

Old monuments are large structures with complicated geometries and built with materials whose behaviour is not well understood. These problems make seismic assessment of monumental structures a difficult task. Finite element analyses provide a method for their structural analysis. Several models have been proposed in literature to predict the behaviour of masonry material adopting different strategies to account for the nonlinear behaviour in tension and in compression. However large number of degrees of freedom involved in defining the geometry and updating of mechanical properties after calibration largely limits their application for analysis of complex 3-D structures (Betti and Vignoli 2008). Linear elastic static and dynamic analysis of the 3-D structure provides valuable information about its global behaviour. Comparing strength capacity with the structural response prediction from FE models provides an indication of location and type of damage expected and gives an estimate of seismic safety of the structure, and suggest need for restoration interventions.

Three studies that are relevant to our research program are described in the following which use finite element techniques for seismic assessment. Taliercio and Binda (2007) developed a finite element model to analyze the Basilica of San Vitale in Ravenna, Italy. It is one of the most important surviving examples of Byzantine architecture and mosaic work from 6th century. It has an octagonal plan, with another concentric octagon inside that rises higher. The inner octagon rises and ends with a drum-dome system, supported by pillars. It is a masonry structure which is characterized by thick mortar joints made of lime and powdered bricks. The walls are pierced with many windows to allow more light to enter and reflect from the beautiful mosaics present inside. Figure 2.9 shows the strucure of Basilica and its finite element model developed in Abaqus using C3D10 ten-noded quadratic tetrahedral elements. The structure was analysed under its self weight and the compressive and tensile stress contours were analyzed. It was seen that, under dead load, the predicted compressive stresses were far below the material strength. However tensile stress computed around the vaults and crowns of exedras were seen to approach, and exceed in some locations, the expected ultimate tensile strength of masonry. The location of these high tensile stress regions explained the crack pattern observed in the Basilica.

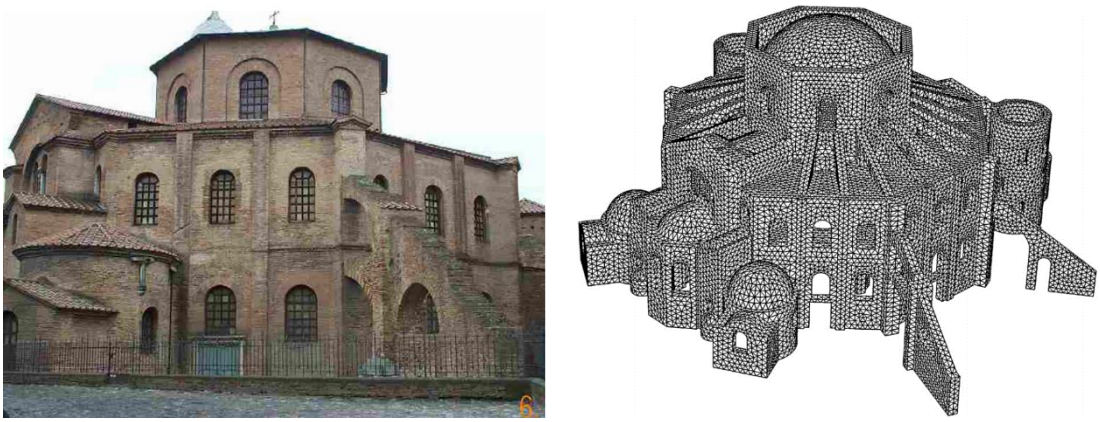

(a) (b)

Figure 2.9. (a) Basilica of San Vitale, Italy and (b) Finite element model of Basilica (Taliercio and Binda 2007)

Peña and Manzano (2015) carried out finite element analyses for seismic assessment of an old masonry church, St. Bartholomew the Apostle in Mexico built in the late 16th century. The church has suffered from several earthquakes of moderate and high intensity due to its location in a high seismicity region and has undergone repairs and modifications over time. Dynamic characterization of the structure was carried out using ambient vibration recordings. A FE model was developed and calibrated based on the experimental results with elastic modulus of different sections of the church as the updating parameters. The structure was analysed under self-weight first. Response spectrum analysis was carried out considering design spectrum proposed by Mexican building code. The analysis considerd combination of earthquake in two directions (100% for one direction plus 30% in the other). Under self weight, the induced stresses were below 10% of compressive strength of masonry. However response spectrum analysis revealed that the bell tower and roof as the critical elements of the structure. Jaishi et al. (2003) also performed response spectrum analysis on the multi-tiered temples of Nepal to get maximum displacements and member forces by summing modal response using the square root of sum of the squares (SRSS) summation rule. Analysis revealed that masonry piers close to openings failed in tension in most of the temples.

Betti and Vignoli (2008) carried out numerical analyses on finite element model developed for a Romanesque masonry church, Farneta abbey in Italy with the aim to

justify the observered damage in the structure and to understand its behaviour to propose different strengthening techniques. Static analysis under its self-weight showed that the compressive stresses were well within the strength of the material. Also, maximum displacement was observed at arch of the transept which was because of thrust due to half dome not being appropriately supported at top level of apse. This explained the cracking pattern observed in the structure. Further, non-linear properties for masonry were assumed and non-linear static analysis was carried out which revealed that the main cause of damage of transept and apse was due to modifications in hydraulic tenor of soil done during the last restoration. On the basis of crack patterns observed and finite element analyses, different strengthening techniques were proposed. Three different techniques with increasing level of strengthening were proposed which included filling of existing cracks with mortar, effectively connecting timber roof frame with the walls, providing post-tensioned horizontal steel chains at the top level, a new foundation, post-tensioned vertical steel tie bars inside masonry walls along the entire height, concrete ring beam along the sides of structure. FE models for the different strengthening techniques were developed and it was shown that the collapse load (as % of seismic weight) increased with increasing level of strengthening.

2.6 SUMMARY

Various methods adopted by researchers in the past for seismic assessment of vulnerable historic monuments have been described in this chapter. Different aspects of seismic assessment of monuments have been presented. Different researchers have carried out research for material characterization, dynamic characterization, and finite element modelling of monuments as deemed appropriate for their particular case. It can be seen that the seismic assessment of monuments poses a great challenge because of its inherent difficulties related to material modelling, restricted in-situ testing and restoration which respects the original existence. However, past studies show that through comprehensive modelling and analyses, suitable strengthening measures can be developed which will be effective in enhancing the earthquake resistance of these monuments.

CHAPTER 3

DYNAMIC CHARACTERIZATION

3.1 OVERVIEW

The importance of dynamic characterization as applied to structural engineering has increased steadily in the recent times. Modal parameters such as natural frequencies, mode shapes and damping ratios are important characteristics of a structure that are required for determining its dynamic performance. Prediction of structural response to environmental loading such as earthquakes or wind forces requires analytical modelling of the structure. Although the tools available for Finite Element modelling and analysis have seen tremendous growth, experimental validation of analytical models is necessary to increase confidence in the predicted results. The desire to achieve an accurate description of the structure to predict its response, to access its damage, and to finally propose structural intervention has motivated the application of system identification to structural engineering. It is the process of correlating the dynamic characteristics of a mathematical model with the characteristics of the physical model obtained from experimental measurements (Brincker and Ventura 2015). This chapter presents the results of the experimental testing conducted to obtain modal parameters of the historic structure of *Rumi Darwaza*.

3.2 DESCRIPTION OF BUILDING

Rumi Darwaza, shown in Figure 3.1, is a free standing circular Roman arch structure combined with a half-dome. This half-dome rests on a half-octagonal plan structure with three 8.8 m high arched gateways passing through it. The main structure is 26 m x 16 m in plan and 27 m high, and is flanked by two storied structures, 16 m x 12 m in plan and 10 m high, on each side along with two octagonal bastions 19.5 m high on their extreme ends. Although the diameter and thickness of the dome could not be measured directly, it is estimated that the dome has an internal diameter of 15.4 m and 0.5 m thickness. The structure has 5 landings at different levels which are accessible

from the rear side of the monument as shown in Figures 3.2 and 3.3. The direction convention used is also shown in Figure 3.2. Y-direction denotes the direction along the road, while X-direction denotes the direction across the road. Z-direction is for elevation direction.

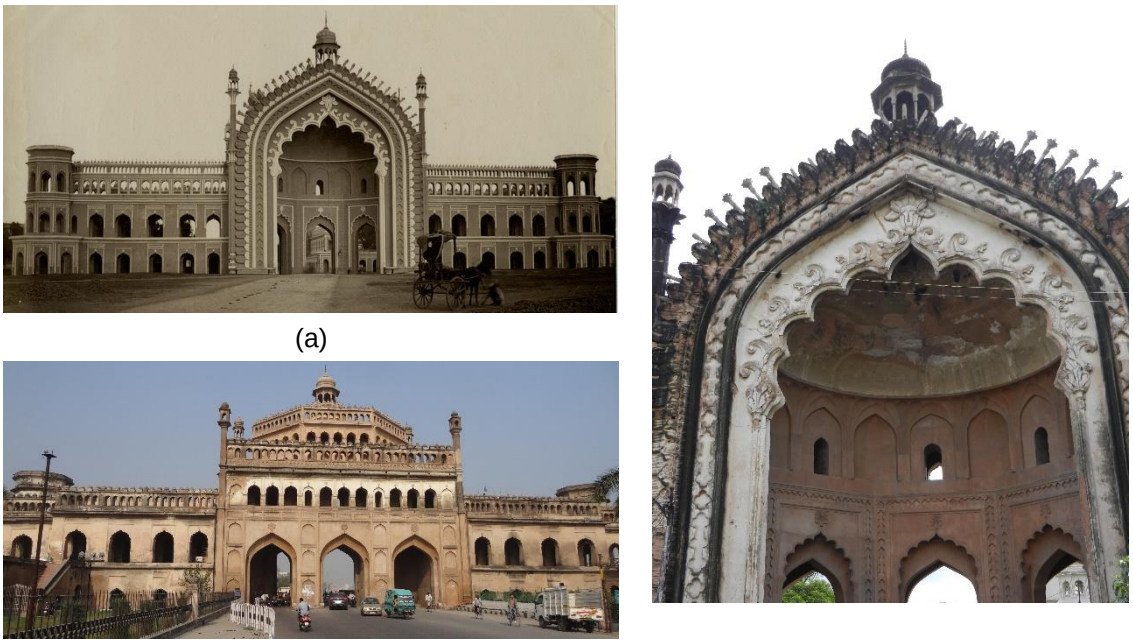

(a)

(b) (c)

Figure 3.1. Brick masonry arch in half-dome structure Rumi Darwaza at Lucknow, 1784 AD

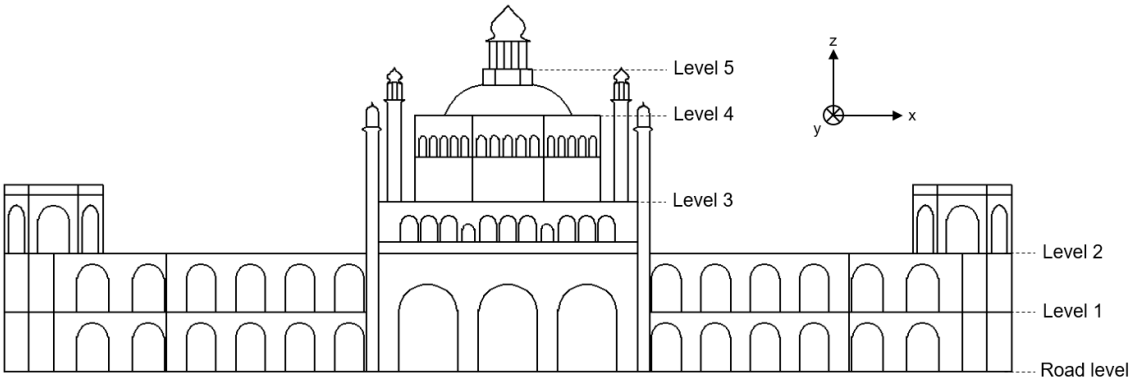

Figure 3.2. Elevation view of Rumi Darwaza from rear side

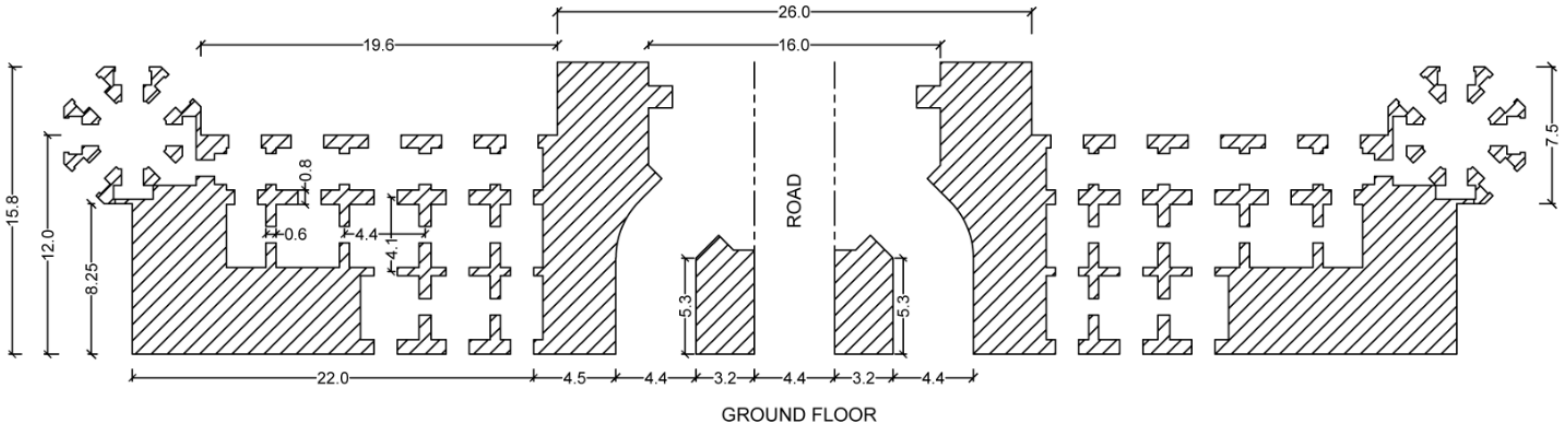

GROUND FLOOR

(a)

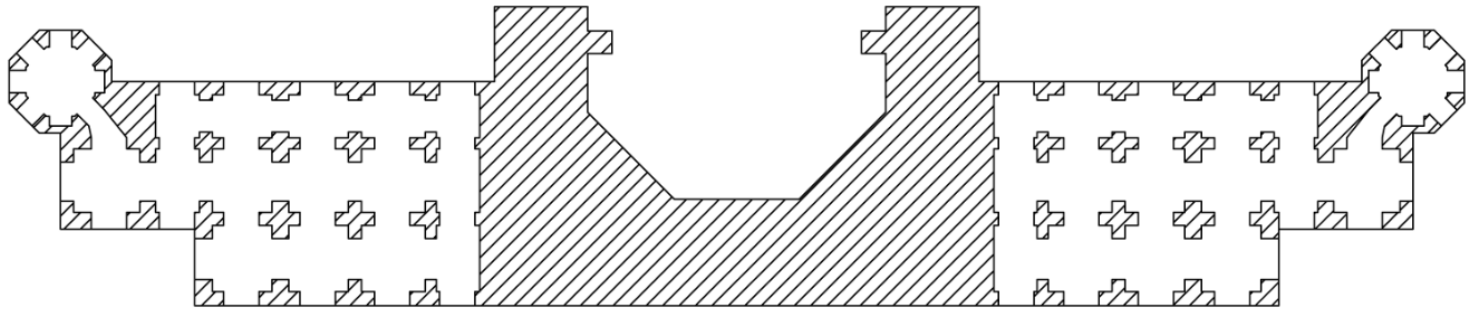

FIRST FLOOR

(b)

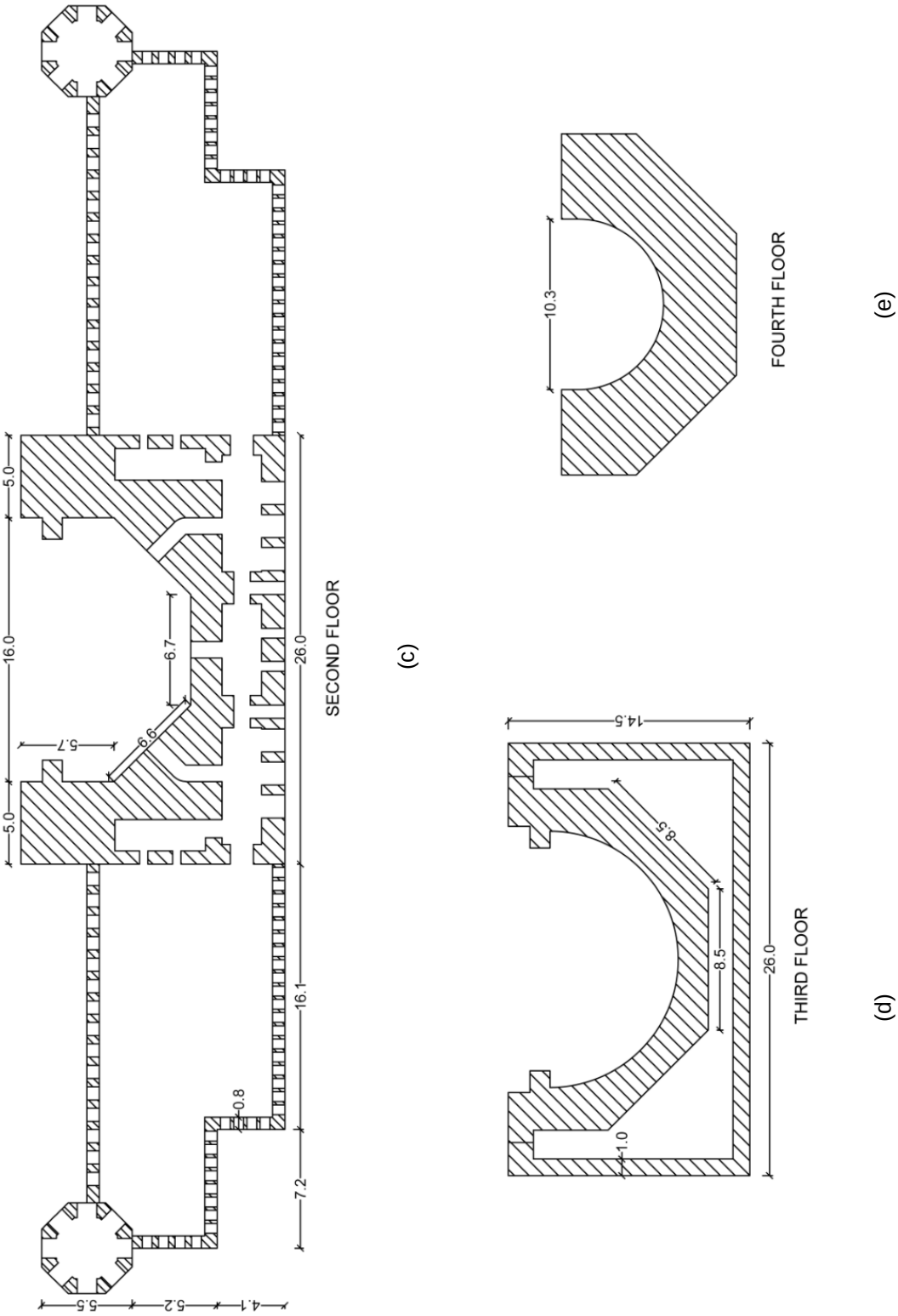

Figure 3.3. Floor plans of different landings of structure

3.3 FIELD VIBRATION TESTING

Dynamic characteristics of the structure can be measured by performing full-scale field testing. Dynamic characterization experiments can be carried out in two possible ways. The basis behind both the ways is to simultaneously measure the vibration response of a building at strategically determined set of locations. The first way is ambient vibration testing in which response of the structure to ambient excitations, such as wind, micro-tremors from ground and nearby vehicular movement, is measured and this data is used for identification. The other method is forced vibration testing which involves applying a force to the structure and measuring the response and applied force as well, if possible, to identify the system parameters. This force to be applied can be achieved by using shakers whose size will depend on the structure desired to be excited. These shakers can produce different types of vibrations depending on their mechanism of generating force. Eccentric mass shakers, which generate force through heavy masses rotating around a vertical axis, can be used to give sinusoidal input vibration. The frequency and amplitude of this vibration can be varied by changing the rotating speed of the masses and by changing the eccentricity between the masses, respectively. The downside of using eccentric mass shakers is that they can only produce harmonic force and hence, cannot be used to simulate ground motions. Another type of shaker is the linear mass shaker, which derives its force from linear motion of a moving mass. These type of shakers can be used to provide any type of input vibration to the structure, including broad range frequency sweeps and earthquake ground motions. Other methods such as Impact Hammer Test and Pull Back Test can also be used for forced vibration testing, but their uses are mostly confined to smaller systems or structural elements only as there are several difficulties involved in their application to large structures.

Although ambient vibration testing is easier to carry out at site as the setup time is less and the cost associated with shaker is also removed but there is no control on the input vibration. Also, at times, it is possible that ambient vibration may not be enough to excite to structure. In such situations, forced vibration may seem like the suitable option as the input vibration can be controlled and the structural response gets increased significantly. But forced vibration can induce significant damage to heritage structures

and monuments. It is also possible that the concerned authorities may not permit the use of heavy mass shakers for testing due to lack of knowledge or out of fear of damage. A middle way has to be found to avoid the two problems of low structural response and causing unintentional damage to structure. Rendon (2011) explored the possibility of using Ultra-Low level Forced Vibration Testing (UL-FVT), a procedure proposed by McDaniel and Archer (2010), to excite a large building to a measurable extent. The procedure utilized portable linear shaker which could input very low level vibrations into the structure that can not possibly damage the structure. They concluded that their testing procedure was capable of generating detectable accelerations throughout a massive building, with induced accelerations as much as 12 times the ambient acceleration readings. Since the procedure showed significant promise in its efficacy to excite a massive structure, it was decided that a similar procedure will be used for extracting the modal parameters of *Rumi Darwaza*. Since the procedure indicated no chance of damaging the structure while still amplifying the structural response, it was deemed appropriate for the current study.

3.3.1 Testing Equipment

Testing equipment used for low level forced vibration testing of *Rumi Darwaza* consisted of a small linear shaker, an amplifier, a signal generator, velocity meters and accelerometer, data acquisition board and a laptop equipped with data measurement and analysis software. The portable nature of the instrumentation makes it suitable for its application to any structure. The complete testing equipment is shown in Figure 3.4.

The APS 113 ELECTRO-SEIS shaker, shown in Figure 3.4a, is a long stroke, electrodynamic force generator which can be used to input sine waves, swept sine waves or random force waveforms. It can generate a peak force of 133 N within the 2-20 Hz frequency range which can be transferred directly through friction between its base and structure, and hence it does not require any special anchoring to the structure as can be the case with heavy eccentric mass shakers. A Honeywell accelerometer (Model MA331), shown in Figure 3.4e, attached to armature of shaker is used to monitor the vibration that is being input into the structure. The weight of shaker, including the lifting handles and reaction masses, comes to ~50 kg, which makes it easily portable.

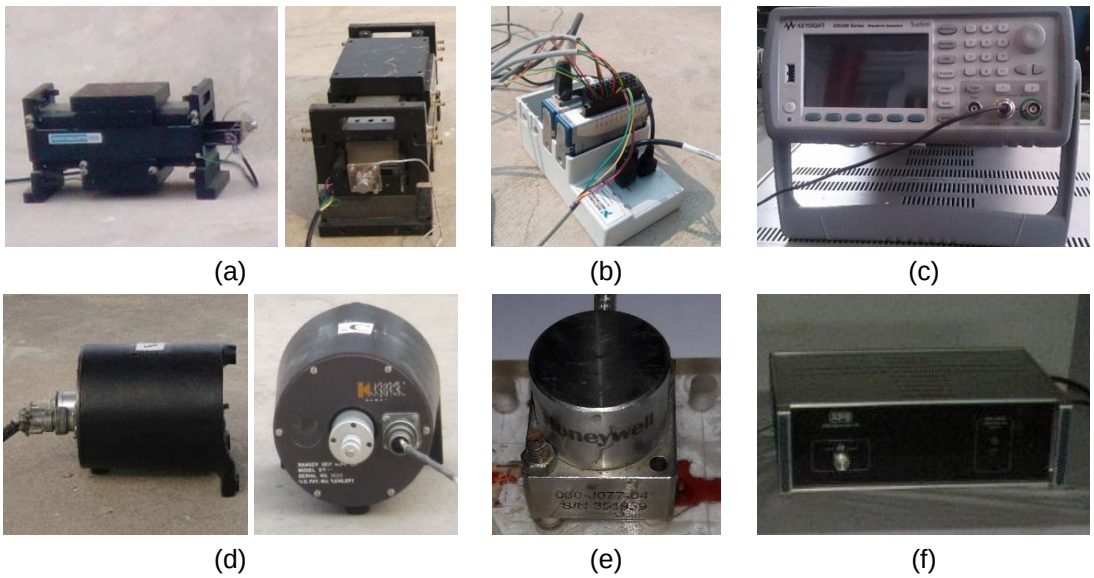

Figure 3.4. Testing Equipment: (a) Linear electromagnetic shaker, (b) Data acquisition board, (c) Function generator, (d) Velocity meter, (e) Accelerometer and (f) Amplifier

Four Kinemetrics SS-1 Ranger Seismometers, shown in Figure 3.4d, are used to measure the small vibrations induced in the structure. The SS-1 Ranger Seismometer is a moving coil style velocity meter. The coil remains stationary, while the strong permanent magnet acts as the seismic inertial mass. The mass remains supported and constrained by annular springs at the top and bottom of the moving magnet. The velocity meters are highly sensitive sensors having a sensitivity of 345 V/(m/s) and weighs only 5 kg which is why it has been used extensively for ambient and forced vibration measurements of buildings, bridges and offshore platforms. NI cDAQ-9174, shown in Figure 3.4b, a compact data acquisition board with 4-slot USB chassis by National Instruments, is a 32-bit analog to digital converter used for signal conditioning and processing of measurements made by velocity meters and accelerometer. A Function Generator (Keysight 33500B Series) and Amplifier (APS Model 124), shown in Figures 3.4c and 3.4f respectively, are used to give the desired force waveform to shaker. The measurements signals are further processed using LabVIEW software and stored on laptop's hard drive.

3.3.2 Low Forced Vibration Testing Principle and Basis

Low level forced vibration testing relies on the use of a small linear shaker to input significant levels of vibration into the structure. The use of small shaker can be supported by the argument of dynamic amplification of response of structure with low damping ζ subjected to harmonic excitation of frequency ω close to natural frequency ω_n of structure. The structure will be set into resonance if the shaker is set to input a force with frequency close to its natural frequency. The dynamic amplification factor, R_d is given by (Chopra 1995):

$$R_d = \frac{1}{\sqrt{[1-(\omega/\omega_n)^2]^2 + [2\zeta(\omega/\omega_n]^2}} \tag{3.1}$$

Substituting $\omega = \omega_n$ and $\zeta = 2.7\%$ (damping ratio for fundamental mode determined from vibration testing data) in Equation 3.1, amplification factor comes out as $R_d = 18.5$ The variation of amplification factor with ratio of forcing frequency and natural frequency of structure for this level of damping is shown in Figure 3.5. Even though the force generated by the shaker is small, amplifying the structural response by 18 times by setting the structure into resonance should provide measurable response levels.

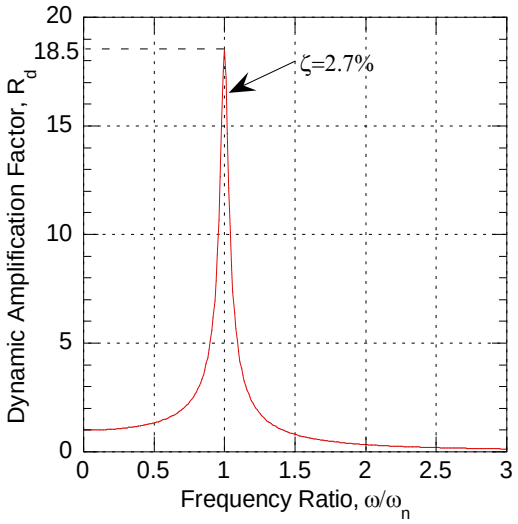

Figure 3.5. Dynamic Amplification Factor

Another argument in favour of the use of linear shaker lies in the comparison of Power Spectral Density (PSD) plots of sensor measurements for forced and ambient vibration recordings. Figure 3.6 shows the comparison of the two types of excitation recordings made at the same location, one due to ambient vibration and the other when the structure was excited at 2.41 Hz (fundamental frequency of structure determined from vibration testing). It can be seen that the peak observed at 2.41 Hz from forced vibration testing is more than 10 times greater than the same peak from ambient vibration recordings. A more direct comparison of the two recordings can be made by examining the time histories of the same sensor under the two different excitation types as shown in Table 3.1. Theoretical argument and experimental measurements show that the procedure can be suitably applied for a structure as massive as *Rumi Darwaza*.

Table 3.1. Comparison of ambient and forced excitations

	Ambient Excitation	**Forced Excitation**	**% Increase**
Absolute Maximum (mm/s)	34.95	50.52	44.5
Root Mean Square (mm/s)	4.56	7.78	70.6
Root Mean Square of Peaks (mm/s)	5.60	9.50	69.6

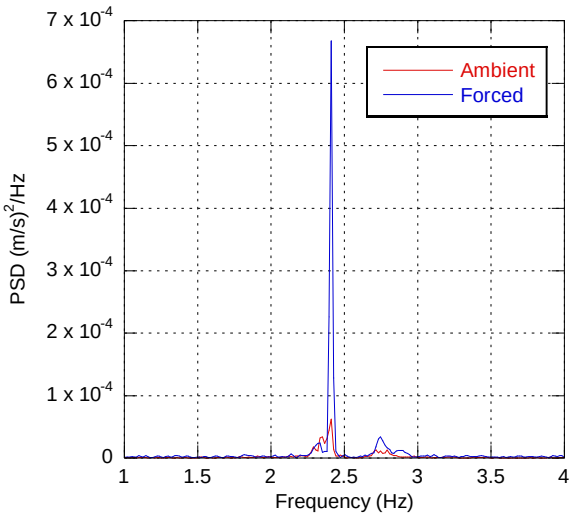

Figure 3.6. Comparison of PSD plots for ambient and forced vibration recordings

3.3.3 Testing Procedure

The testing procedure has two main components:

1. Ambient and broad sine sweep forced vibration tests for identification of natural frequencies of the structure.
2. Fixed frequency forced vibration tests at each identified frequency for mode shape.

Figure 3.7 shows the locations of points on the structure at which velocity meters and shaker were placed. As per the adopted coordinate system, X-direction denotes the in-plane direction of the monument, and Y-direction denotes the out-of-plane direction of the monument, along the road. The location and orientation of sensors for different test setups are listed in Table 3.2.

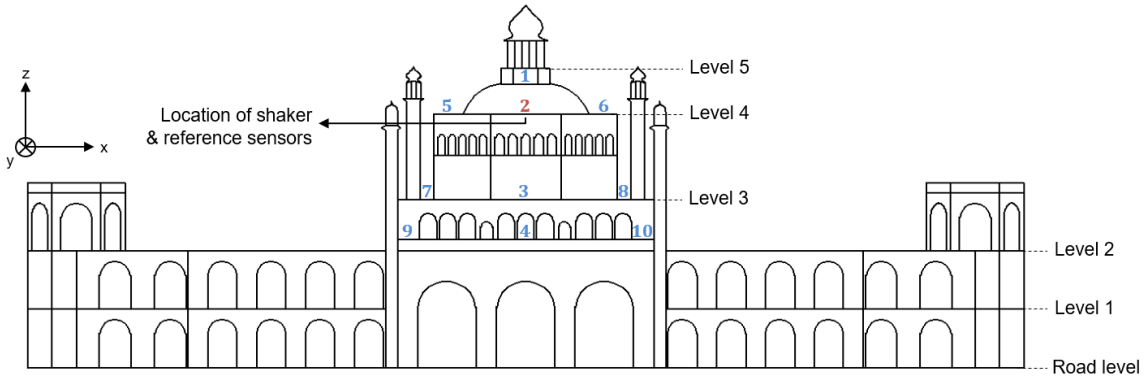

Figure 3.7. Location of sensors and shaker on monument

Table 3.2. Sensor locations in different test setups

Test Setup	Velocity Meter Locations and Orientation			
	A	B	C	D
T0	1	3	2 (*y*)	4
T1	1	3	2 (*y*)	2 (*x*)
T2	6	5	2 (*y*)	2 (*x*)
T3	7	8	2 (*y*)	2 (*x*)
T4	9	10	2 (*y*)	2 (*x*)

The sampling rate for the velocity meters and accelerometer was kept at 2000 samples/s. The shaker was kept at Location 2 throughout the testing. The location of shaker was

chosen on the basis that a structure should be most flexible at the top, and hence the shaker should be able to induce vibrations into the structure with most ease. The landing on Location 2 was the highest landing that was easily accessible and was chosen as the location of the shaker. The sensors were positioned as per test setup *T0* configuration for the first phase of testing. The identification of natural frequencies can be carried out based on just ambient vibration recordings, however forced vibration recordings are more suitable as they provide a clearer picture and better estimates can be obtained. First, the natural frequencies in the out-of-plane (y) direction were identified by ambient and forced vibrations exciting the structure over a broad range of frequencies, with the sensors and shaker oriented in the Y-direction. Next, the structure was excited over the same broad range of frequencies in the in-plane (x) direction by changing the orientation of shaker and sensors to estimate the natural frequencies of the structure in the in-plane direction. This broad range frequency sweep was multiple runs of sine sweep waveform from 0.1 to 9 Hz in 150 s duration. The number of runs required depends on the mode number that is being identified, with higher modes requiring more number of runs as they require more excitation, but 2-3 runs should be sufficient for the lower modes to show up. Broad range sine sweep may not be sufficient for identification of higher modes as it will only provide a rough estimate of the natural frequency. This broad sweep should be followed by a narrow range of sine sweep around the rough estimate to get a better idea of natural frequency for higher modes. The signal processing of the measured data was performed at the site using MATLAB. A simple Fast Fourier Transform (FFT) based procedure gave the natural frequency estimate for the first three modes. The measurements made during this phase can be later processed for damping ratios for each mode.

The second phase of testing involved measuring the structural response at strategically chosen locations on the structure to find the mode shape coordinates. As can be seen from Figure 3.7, the number of locations to be measured were greater than the number of sensors, and hence a number of test setups had to be performed to cover the entire structure. Before the beginning of this phase of testing, two sensors (Sensor C and D) were fixed as the reference sensors. These sensors were located at Location 2, close to the linear shaker, with their orientations as mentioned in Table 3.2 and were not

disturbed during the testing. The other sensors (Sensors A and B) were employed as the rover sensors which were moved to a different location in each test setup. During each test setup, the rover sensors were first oriented in Y-dir. The structure was excited at fixed frequencies, i.e., natural frequencies identified in the first phase of testing, one by one in both orthogonal directions. The input force waveform is a sine wave at the determined frequency for a duration of 180 s. Next, the orientation of the rover sensors were changed to X-dir and the whole procedure was repeated, before moving on to the next test setup. Since the number of natural frequencies identified was three, each test setup consisted of 12 measurements. No measurements on the two-storied structures flanking the main structure were made for a number of reasons. The measurement locations were too far away from the shaker and the height of these structures was too low for any considerable vibration to be induced externally or through ambient disturbances. Hence the measurement of their response was not considered necessary. As will be shown later through Finite Element analyses, these adjoining structures did not have any significant mass participation in the analytical modes either.

3.4 OPERATIONAL MODAL ANALYSIS

The study of modal properties of a system under ambient vibration or normal operational conditions is known as Operational Modal Analysis (OMA). It is the process of characterizing the dynamic properties of a structure, i.e., the natural modes of vibration which have a natural frequency and damping ratio associated with it and a mode shape which defines the spatial distribution of movement of the entire structure. The fundamental idea behind OMA is to do modal analysis without having the knowledge and/or control over the input excitation, which is why it is also known as *output-only* modal analysis. As mentioned before, OMA testing techniques are more attractive due to their relatively lower costs and speed of implementation when compared with the classical modal testing, also known as Experimental Modal Analysis (EMA). EMA methods are based on knowing and controlling the input vibration and using the measured excitation and response time histories to compute the Frequency Response Functions (FRFs) between the input point and the point of measurement to determine the modal properties. In OMA, since there is no measurement of input

vibration, FRFs cannot be calculated and hence, the analysis is based on spectral density functions calculated from the measured response.

A rather fast OMA technique for estimating the modal parameters is the Peak Picking (PP) frequency domain technique. The idea behind this technique is that a structure excited near its natural frequencies will show a strong response. These frequencies can be identified from the peaks in FFT or PSD plots of the measured recordings. This simple and fast technique has been used in the first phase of experimental testing to provide quick estimate at the site of the natural frequencies of *Rumi Darwaza*. However, this classical approach has limitations concerning the accuracy in the identification process. Additionally, the frequency estimates from this technique are limited by the frequency resolution of the spectral density estimate, and damping ratio estimation is not possible. Due to these reasons, Peak Picking technique is not used for signal processing of measurements done in the second phase of the experimental testing. Instead, another frequency domain approach known as Frequency Domain Decomposition (Brincker et al. 2000), which takes care of the problems associated with PP technique, has been used.

3.4.1 Data Processing and Identification Algorithm

Peak Picking (PP) and Frequency Domain Decomposition (FDD) are both output-only system identification techniques based on evaluation of spectral density matrix, i.e., the matrix of cross spectral densities

$$G(f) = E[y(f)y^H(f)] \tag{3.2}$$

where E denotes expected value, $y(f)$ contains the measured responses in frequency domain and superscript H denotes the complex conjugate transpose of matrix. The diagonal terms of the matrix $G(f)$ are the real valued auto-spectral densities (ASD) and the other terms are the complex valued cross-spectral densities (CSD). The first step in extraction of modal parameters is to estimate these ASDs and CSDs from the measured time-histories. This has been done using the modified periodogram method (Welch 1967). The method involves dividing the time history record into periodograms with

certain overlap between them and then averaging over each of them with windowing applied. The velocity time history records were sectioned into periodograms of 2^{17} points with 50% overlapping for spectral averaging. A Hanning window was applied to prevent the phenomenon known as spectral leakage in which the energy at one frequency leaks into adjacent frequencies when FFT over a non-integer number of cycles is performed. This occurs due to the inherent assumption that the signal is periodic over the chosen sampling interval, which may not be always true. Figure 3.8a shows the problem of leakage for a sinusoidal signal with sampling intervals which are integer and non-integer multiples of signal period. If the signal is sinusoidal, the FFT should be non-zero at just one frequency. But in the case of a non-integer multiple sampling interval, the power contained at that frequency can be seen to leak into adjacent frequencies. Windowing reduces the amplitude of discontinuities at the ends by multiplying the time series with a finite length window having an amplitude that varies smoothly and gradually becomes zero at the ends. The improvement in the FFT plot after the use of Hanning window can be seen in Figure 3.8b. The frequency resolution, for a sampling rate of 2000 samples/s, achieved was $2000/2^{17} = 0.0153\,Hz$.

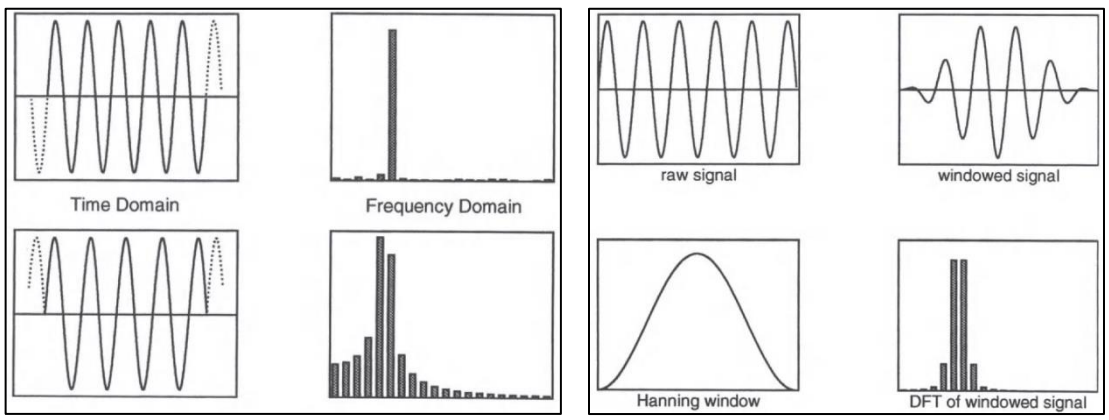

Figure 3.8. (a) The effect of sampling interval and leakage on the Fourier Transform of sinusoidal time signal, (b) The use of Hanning window to reduce leakage effects (Friswell and Mottershead 1995)

For data processing of measurements made in first phase of experimental testing, Peak Picking procedure was applied to identify the natural frequencies at the site. The natural frequencies are identified from resonant peaks in ASDs and from amplitude of CSDs,

for which the cross-spectral phases are either zero or π radians (Gentile and Saisi 2007). The cross-spectral phase between the DOFs becomes zero (in-phase) or π (out-of-phase) radians when the DOFs reach their maximum amplitude, as it should be in the mode shapes. The natural frequencies so obtained were used in the second phase of testing, as has been explained before. Although it is not necessary, but it is a good idea to repeat this procedure for the measurements made in the second phase also, before the extraction of modal parameters, as a method for sensors measurement quality and consistency check.

Data processing of measurements made in second phase of experimental testing was done using the FDD technique to extract the modal parameters. The FDD procedure also starts with the estimation of spectral density matrix using the modified periodogram method. The estimate of output SD matrix $G(f)$ known at discrete frequencies is then decomposed by taking the Singular Value Decomposition (SVD) of the matrix

$$G(f) = U(f)S(f)U^H(f) \tag{3.3}$$

where the diagonal matrix S holds the real positive singular values in descending order and U is a complex matrix containing the singular vectors as columns. The rank of G is estimated at each frequency by SVD, with the number of non-zero singular values $s_i(f)$ being equal to the rank. If the modes are well separated, then close to a peak, only one mode should dominate, and hence spectral matrix G should be rank one matrix as

$$G(f) \cong u_1(f)s_1(f)u_1^H(f) \tag{3.4}$$

and it can be shown that the first singular vector $u_1(f)$ is an estimate of the mode shape.

$$\psi = u_1(f) \tag{3.5}$$

Since the first singular value $s_1(f)$ represents the strength of dominating mode, it can be used as a modal indication function. The curves representing the singular values can be inspected to yield the natural frequency as local maxima. Additionally, this singular value is the auto spectral density function of the corresponding single degree of freedom

(SDOF) system which is identified around the peak by comparing the mode shape estimate ψ with the singular values for frequency lines around the peak. Modal Assurance Criterion (MAC) is generally used as a measure for comparing mode shapes. If a singular vector is found to have high MAC value with ψ, the corresponding singular value also belongs to SDOF density function. This piece of SDOF density function around the peak of PSD is then taken back into time domain by inverse FFT and damping is estimated from logarithmic decrement of the corresponding SDOF auto correlation function. A MAC value of 0.9 was targeted for the current application. Allemang and Brown (1982) defined MAC value between vectors ϕ_1 and ϕ_2, as shown in Equation 3.6.

$$MAC(\phi_1, \phi_2) = \frac{\left|\phi_1^{*t} \phi_2\right|^2}{\left(\phi_1^{*t} \phi_1\right)\left(\phi_2^{*t} \phi_2\right)} \tag{3.6}$$

where superscript *t denotes complex conjugate transpose of a vector. A MATLAB implementation of the complete data processing and identification procedure has been added in Appendix A.

3.4.2 Mode Shape Rescaling for Multi-Patch Data

Mode shape rescaling is required when the experimental testing involves measurements of greater number of points as compared to the number of sensors available for instrumentation, and hence requires multiple test setups to cover all the measurement points. The mode shape estimations from the data, collected in different test setups or patches, have to be combined together. Combining the mode shape estimates from different patches requires them to be rescaled to the same level first. This rescaling to the same level is carried out through the Post Global Estimation Rescaling (PoGER) approach (Parloo 2003) which has been described here.

Consider a system for which N_o is the total number of locations where the structural response has to be measured. These N_o points are the experimental degrees of freedom (DOF), which have to be covered in N_{pat} number of test setups or patches for the

structural response in N_m number of modes. Each patch or test setup will have N_{ref} and N_{rov} number of reference and rover measurements respectively, where reference measurements are the ones which are common to all patches. For each patch, system identification can be carried out by transforming the time domain data into frequency domain, estimating the auto and cross spectral densities, resulting in a mode shape estimate from the SVD of spectral matrix. This estimated mode shape vector for patch *i* and mode *r* can be represented as:

$$\psi_{[:,r]}|_i = \begin{bmatrix} \psi^{rov}_{[:,r]}|_i \\ \psi^{ref}_{[:,r]}|_i \end{bmatrix} \tag{3.7}$$

where $\psi^{ref}_{[:,r]}|_i$ is a $\left(N_{ref} \times 1\right)$ vector containing the mode shape coordinates obtained from the reference measurements and $\psi^{rov}_{[:,r]}|_i$ is a $\left(N_{rov} \times 1\right)$ vector containing the mode shape coordinates obtained from the rover measurements. If the reference DOFs are the same across all patches, the mode shape vectors $\psi^{rov}_{[:,r]}|_j$ of patch j $\left(j = 1,\ldots,N_{pat}\right)$ and mode r $\left(r = 1,\ldots,N_m\right)$ can be rescaled to a common level as dictated by patch $k \in \left\{1,\ldots,N_{pat}\right\}$.

$$\psi^{rov}_{[:,r]}|_{i\to k} = \left(\alpha_{[r]_{i\to k}}\right).\left(\psi^{rov}_{[:,r]}|_i\right) \tag{3.8}$$

where,

$$\alpha_{[r]_{i\to k}} = \frac{\left(\psi^{ref}_{[:,r]}|_i\right)^H.\left(\psi^{ref}_{[:,r]}|_k\right)}{\left(\psi^{ref}_{[:,r]}|_i\right)^H.\left(\psi^{ref}_{[:,r]}|_i\right)} \tag{3.9}$$

For each mode *r*, the rescaled mode shape vectors are organized in the $\left(N_o \times 1\right)$ vector Ψ

$$\Psi_{[:,r]} = \begin{bmatrix} \psi^{rov}_{[:,r]}|_{1\to k} \\ \psi^{rov}_{[:,r]}|_{2\to k} \\ \vdots \\ \psi^{rov}_{[:,r]}|_{N_{pat}\to k} \\ \psi^{ref}_{[:,r]}|_{k} \end{bmatrix} \tag{3.10}$$

3.4.3 Realization of Complex Modes

With proportional viscous damping, the mode shapes of classically damped system will be the same as that of an undamped system. However, the actual damping of a structure is mostly never represented by proportional viscous damping. Such a system is known as a non-classically damped system. Due to this, mathematically, the damping matrix is not diagonalizable by the undamped mode shapes and hence, the mode shape estimates derived from the experimental data are complex valued vibration modes. The complex mode shape vector can be further realized by (Niedbal 1984)

$$\Psi_R = \mathrm{Re}(\Psi_C) + \mathrm{Im}(\Psi_C)\left(\mathrm{Re}(\Psi_C)^T\,\mathrm{Re}(\Psi_C)\right)^{-1}\mathrm{Re}(\Psi_C)^T\,\mathrm{Im}(\Psi_C) \tag{3.11}$$

where Re and Im denote the real and imaginary parts of a complex number, respectively. The equation holds good for systems having low damping.

3.5 RESULTS AND DISCUSSION

The first phase of experimental testing involved using the Peak Picking technique for identification of natural frequencies from the broad range frequency sweep measurements in the *T0* test setup for the two orthogonal directions. The natural frequencies are identified from peaks in ASD and CSD plots where the cross-spectral phases are either zero or π radians. Additionally, if the broad sweeps are not sufficient for identification of higher modes, frequency sweeps of a narrow range around the expected natural frequency should be performed. In the present study, broad range frequency sweeps in the out-of-plane (y) direction were able to excite two modes of the structure in that direction. Figure 3.9 show the results of frequency sweep test in Y-dir. The two modes of the structure in Y-dir have a natural frequency of 2.41 Hz and 2.78 Hz.

The ASD and CSD plots (where *Vel* denotes Velocity meter), shown in Figures 3.9a and 3.9b respectively, show peaks at these frequencies and the cross-spectral phases, shown in Figures 3.9c and 3.9d, are close to zero radians, implying that they are in phase with each other.

However, the mode which was dominantly in the in-plane direction, could not be excited suitably by the broad range sweep in X-dir, as shown in Figure 3.10. Only a rough idea of the natural frequency could be gained, and the test had to be followed by frequency sweep of narrow range. It can be seen that in-plane mode of the structure has natural frequency between 3.0 Hz and 3.2 Hz. A frequency sweep of narrow range, 3.0-3.5 Hz was performed to get a better estimate of natural frequency of this mode. But even this frequency sweep could not provide a good estimate and could only narrow down the location of natural frequency between 3.05 Hz and 3.15 Hz. Finally, fixed frequency test at 3.06 Hz was performed to excite the structure and to see its structural response. The ASD and CSD plots, shown in Figures 3.11a and 3.11b respectively, demonstrate that the structure could be suitably excited with cross spectral phase, shown in Figure 3.11c, close to zero radians. This implies that even though 3.06 Hz may not be exact natural frequency of the third mode, it should be within 2% of the true value.

The fundamental natural frequency shows that the structure is stiff and lies in the acceleration sensitive region of response spectrum of IS 1893 (BIS 2002), and therefore the structure can be expected to attract large forces and experience high base shear in event of an earthquake.

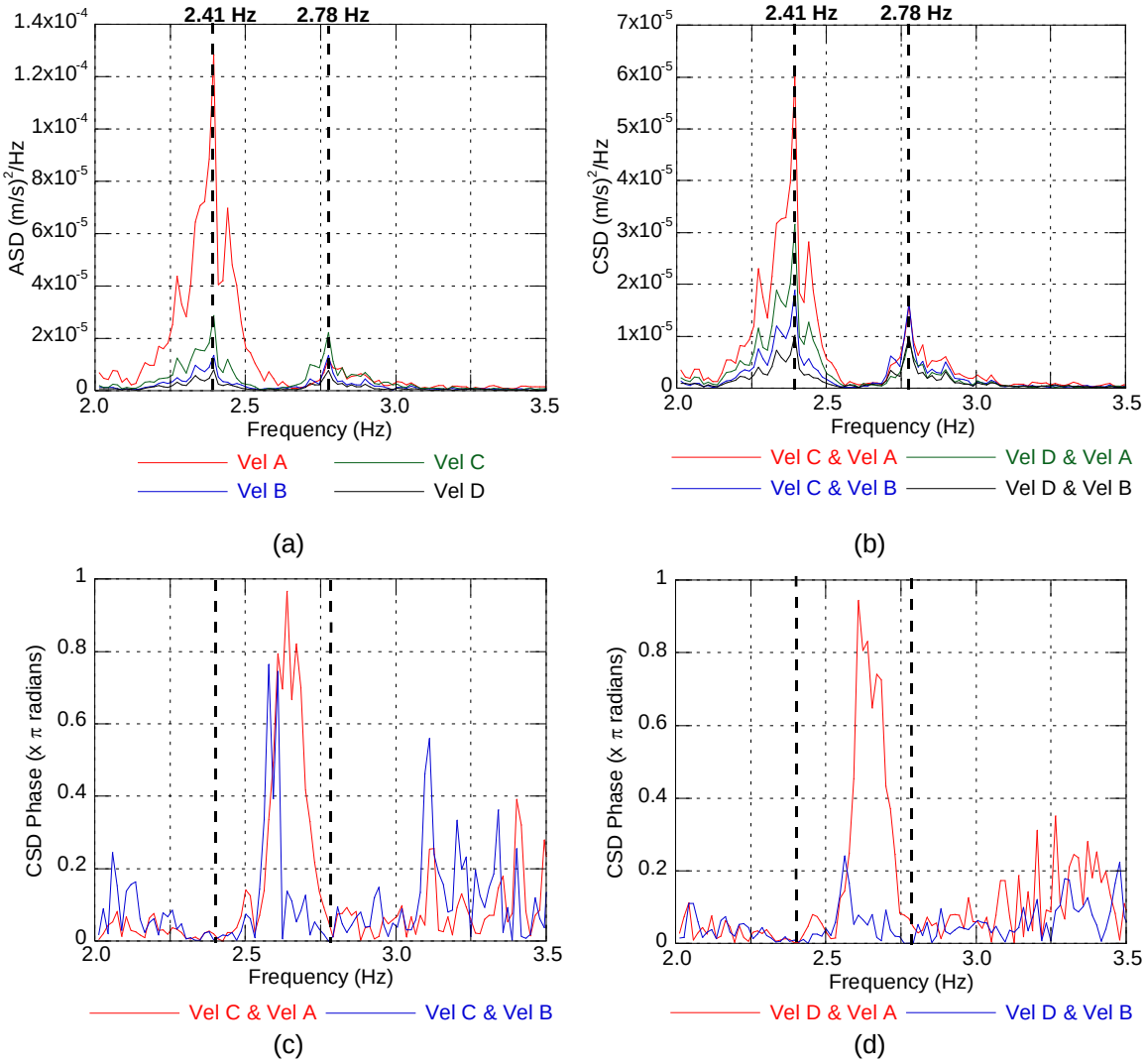

Figure 3.9. Frequency sweep test for identification of modes in Y-direction

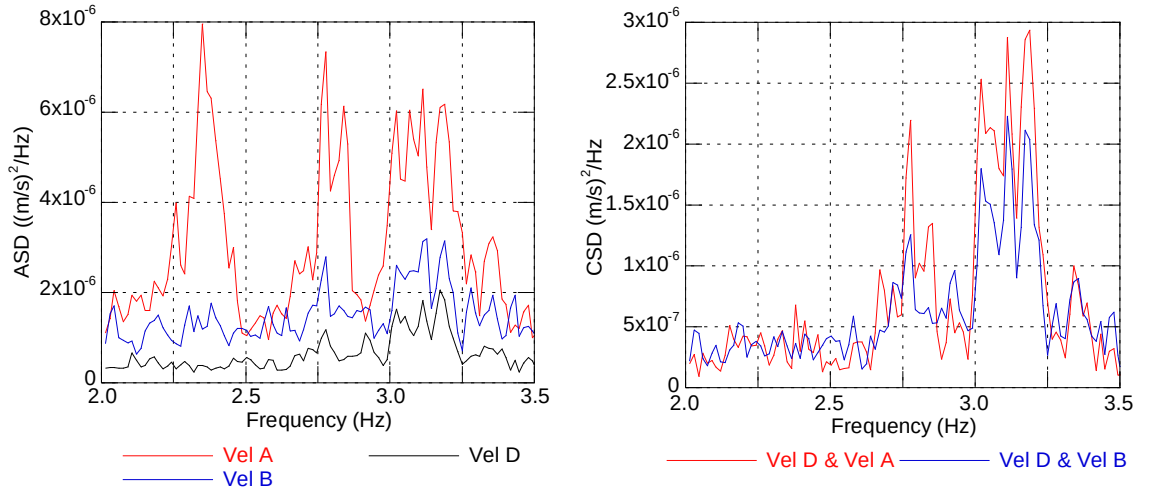

Figure 3.10. Frequency sweep test in X-direction

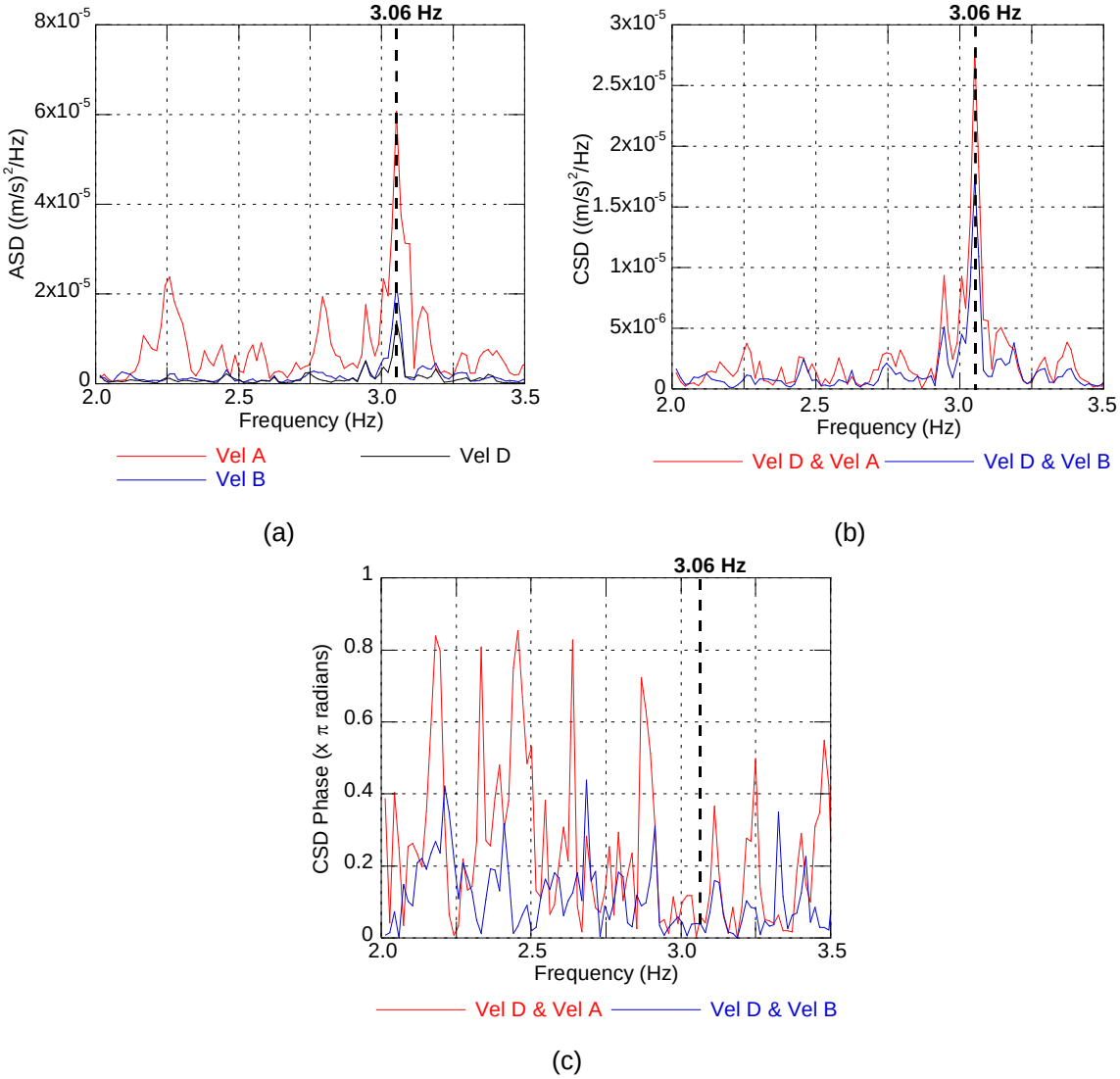

Figure 3.11. Fixed frequency test at 3.06 Hz for identification of mode in X-direction

Second phase of experimental testing involved exciting the structure at the three identified natural frequencies, 2.41 Hz, 2.78 Hz and 3.06 Hz for extracting the mode shape coordinates by measuring the structural response at different locations using the rover sensors. However, before proceeding to the mode shape estimation, as a check for quality of sensor measurements, it is a good idea to examine the ASD plots from different tests to gain confidence in the mode shape results. Figure 3.12 shows the ASD plots of some select sensors from different test setups. The ASD plots show dominant response at identified frequencies of different modes, which demonstrates the good quality of sensor measurements.

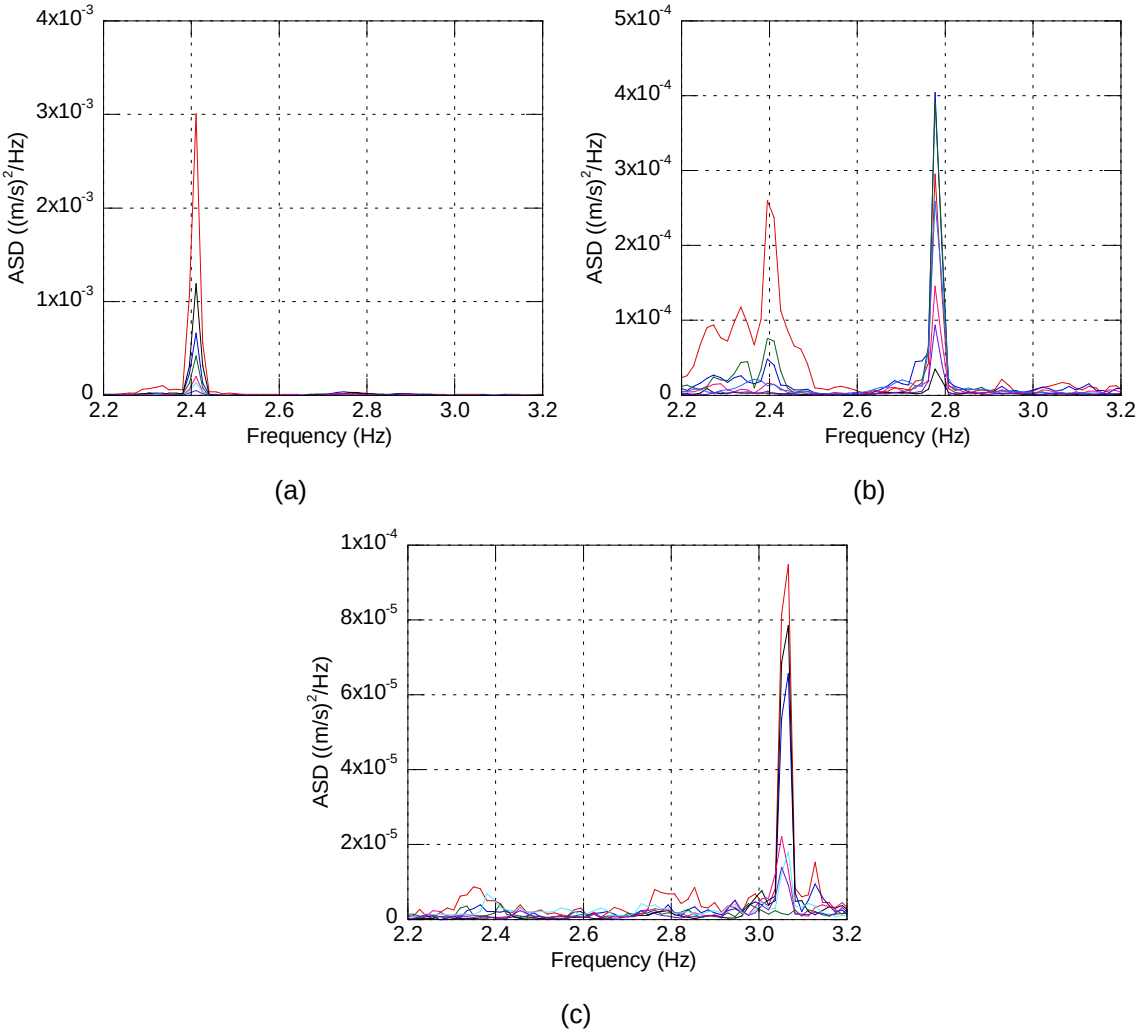

Figure 3.12. ASD plots from fixed frequency tests for (a) Mode A, (b) Mode B and (c) Mode C

Another observation that can be made from Figure 3.12b is that although the linear shaker is set to input vibration at 2.78 Hz, the location and/or orientation of the shaker is not ideal to excite the structure in Mode B only. The shaker is not able to isolate the mode and the structural response is a combination of Modes A and B. However, that does not affect the mode shape estimation. This quality check procedure also revealed the sensor measurements which were incorrect as they did not show any response at the natural frequencies of the structure. This can be attributed to the incorrect balancing of the sensors or due to disturbance from other equipments being used nearby. Due to these problems, the mode shape coordinates at locations 10 (both X and Y directions) and 9 (X-direction) as shown in Figure 3.7, could not be estimated. As no measurements

were available in the X-dir for that level, the vibration measurement made at location 4 during the first phase of testing has been used for mode shape estimation. Additionally, although measurements were taken, mode shape coordinates at some other locations could not be estimated due to low signal to noise ratio. The mode shape coordinates are extracted by SVD of SD matrix at spectral lines corresponding to the identified frequencies. Figure 3.13 shows the singular value plots of fixed frequency tests for the three modes.

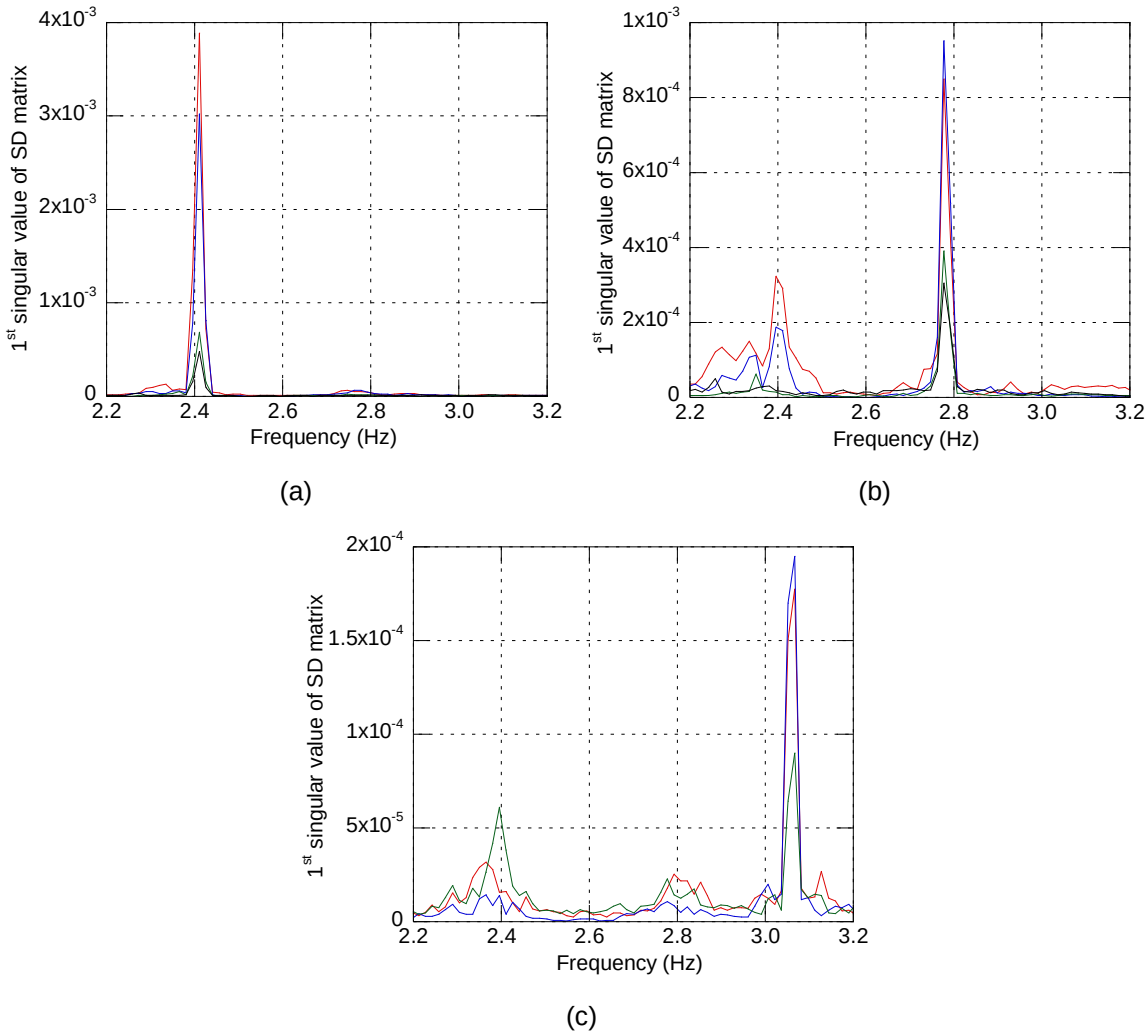

Figure 3.13. First singular value of SD matrix from fixed frequency tests for (a) Mode A, (b) Mode B and (c) Mode C

In the present study, there were two rover and two reference sensors, and hence the mode shape for every test setup is a 4×1 complex valued vector. Table 3.3 presents the mode shape estimates from different test setups for the Mode A. Mode shape rescaling is done as dictated by the estimate from test setup *T1* in Y-dir taken as the reference. The modal scaling factor is calculated as per Equation 3.9 for scaling the estimates to a common level. The different patches are joined together as described in Equation 3.10 and realized as per Equation 3.11. The mode shape vector is then rearranged in an order of DOFs and normalized by the mode shape coordinate of DOF with the greatest value. Table 3.4 shows the mode shape vector for Mode A.

Table 3.3. Mode shape estimates and modal scaling factors for different patches of Mode A

Test Setup	Y-direction		X-direction	
	Mode shape estimate $\psi_{[:,r]}\|_i$	**Modal scaling factor** $\alpha_{[r]_{i\to k}}$	**Mode shape estimate** $\psi_{[:,r]}\|_i$	**Modal scaling factor** $\alpha_{[r]_{i\to k}}$
T1	$\begin{bmatrix} 0.88+0.00i \\ 0.22+0.01i \\ 0.41+0.02i \\ -0.06-0.00i \end{bmatrix}$	$1.00+0.00i$	$\begin{bmatrix} 0.40+0.00i \\ 0.04-0.01i \\ 0.91+0.05i \\ -0.11-0.02i \end{bmatrix}$	$0.46+0.00i$
T2	$\begin{bmatrix} 0.63+0.00i \\ 0.52-0.01i \\ 0.57+0.02i \\ -0.08-0.03i \end{bmatrix}$	$0.72+0.03i$	–	–
T3	$\begin{bmatrix} 0.44+0.00i \\ 0.31+0.04i \\ 0.83+0.07i \\ -0.12-0.03i \end{bmatrix}$	$0.50-0.01i$	$\begin{bmatrix} 0.05+0.00i \\ -0.03-0.17i \\ -0.52-0.82i \\ 0.11+0.14i \end{bmatrix}$	$-0.25+0.34i$
T4	$\begin{bmatrix} 0.32+0.00i \\ – \\ 0.94-0.01i \\ -0.11-0.01i \end{bmatrix}$	$0.44+0.03i$	–	–

Table 3.4. Mode shape vector for Mode A

DOF location and direction	Complex valued mode shape vector	Realized mode shape vector	Normalized mode shape vector
1y	$0.88 + 0.00i$	0.88	1.00
1x	$0.18 + 0.00i$	0.18	0.21
5y	$0.38 + 0.01i$	0.38	0.43
5x	–	–	–
2y	$0.41 + 0.03i$	0.41	0.47
2x	$-0.06 - 0.00i$	–0.06	–0.07
6y	$0.45 + 0.02i$	0.46	0.52
6x	–	–	–
7y	$0.22 - 0.00i$	0.22	0.25
7x	$-0.01 + 0.02i$	–0.01	–0.01
3y	$0.22 + 0.01i$	0.22	0.26
3x	$0.02 - 0.01i$	0.02	0.02
8y	$0.15 + 0.02i$	0.15	0.18
8x	$0.07 + 0.03i$	0.07	0.08
9y	$0.14 + 0.01i$	0.14	0.16
9x	–	–	–
10y	–	–	–
10x	–	–	–

Following the same procedure, mode shape vectors for Modes B and C were evaluated. Mode shapes for the three identified modes are shown in Figure 3.14 and the vectors are presented in Table 3.5. Figures 3.14a and 3.14b use modal coordinates corresponding to DOFs 1y, 2y, 3y and 9y. Figure 3.14c uses modal coordinates corresponding to DOFs 1x, 2x, 3x and 4x. Modes A and B are in the out-of-plane direction. The complete structure is seen to move in the out-of-plane direction with the dome deflecting greater than the rest of structure. Mode B also shows similar deflection, however the dome is seen to deflect lesser in comparison to rest of the structure. Mode C is the in-plane movement of the main structure. Physical description of these mode shapes has also been provided in Chapter 5, where these mode shapes have been used for validation of Finite Element model of the monument.

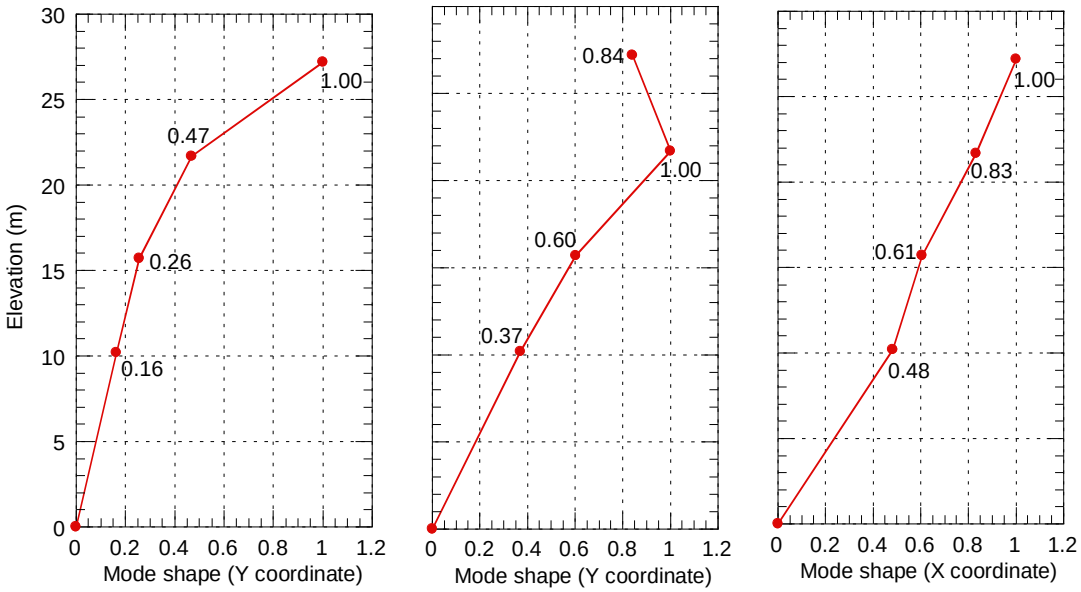

Figure 3.14. Normalized mode shapes for (a) Mode A, (b) Mode B and (c) Mode C

Table 3.5. Normalized mode shape vectors for all identified modes

DOF location and direction	Mode shape vector Mode A	Mode shape vector Mode B	Mode shape vector Mode C
1y	1.00	0.84	–0.10
1x	0.21	0.27	1.00
5y	0.43	0.92	–
5x	–	–	1.11
2y	0.47	1.00	0.03
2x	–0.07	–0.05	0.83
6y	0.52	1.14	–
6x	–	–	1.14
7y	0.25	0.63	–
7x	–0.01	0.04	0.45
3y	0.26	0.60	0.02
3x	0.02	0.09	0.61
8y	0.18	0.40	–
8x	0.08	–0.01	0.40
9y	0.16	0.37	–
9x	–	–	–
4x	–	–	0.48
10y	–	–	–
10x	–	–	–

From Table 3.5, it can also be observed that the modal coordinates at DOFs on the same level are almost the same. Modal coordinates at DOFs 2y, 5y, 6y on Level 4 for Modes A and B are very close to each other. Similarly modal coordinates at DOFs 3y, 7y on Level 3 are also close, with the coordinates at 8y being slightly lower for Modes A and B indicating some differential movement at that level. Modal coordinates at DOFs 2x, 5x, 6x on Level 4 and DOFs 3x, 7x, 8x on Level 3 for Mode C are also seen to be similar to each other.

Damping ratio estimations have been done from the broad frequency sweep measurements made in the first phase of testing. The first step is the calculation of MAC value of mode shape estimate ϕ_1 with the singular vectors ϕ_2 around the natural frequencies. Here, a MAC acceptance criteria has been kept at 0.9 as it is seen that this value is sufficient to capture all the energy content related to any particular mode. The piece of SDOF density function around the natural frequency, within which the singular vector at each spectral line has a MAC value greater than 0.9 with mode shape estimate, is taken back into time domain by inverse FFT. Damping is estimated from logarithmic decrement of the corresponding SDOF auto correlation function. Figure 3.15 shows the damping ratio estimation for Mode A. Table 3.6 presents a brief summary of results of field vibration testing of *Rumi Darwaza*. From Table 3.6, it can be observed that the damping ratio goes down for higher modes.

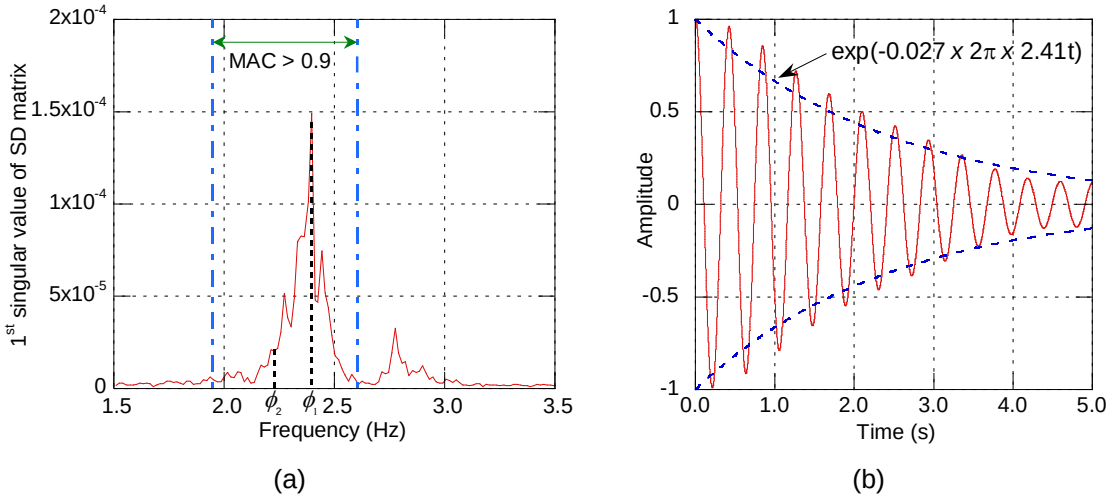

Figure 3.15. Damping ratio estimation for Mode A: (a) Singular vectors ϕ_2 with MAC > 0.9 with mode shape estimate ϕ_1 and (b) Auto correlation function after inverse FFT

Table 3.6. Summary of results of forced vibration testing

Mode Number	Natural Frequency (Hz)		Damping Ratio	Nature of Mode
	Ambient	Forced		
Mode A	2.41	2.41	2.7%	Out-of-Plane (*y*)
Mode B	2.82	2.78	2.3%	Out-of-Plane (*y*)
Mode C	3.14	3.06	1.8%	In-Plane (*x*)

3.6 SUMMARY

Forced vibration testing for extracting the modal parameters – natural frequencies, mode shapes and damping ratios of the monument *Rumi Darwaza* was conducted. The testing procedure involved the use of a small linear shaker which showed that it can be used successfully for this application even though the maximum force output of the shaker is very low (133 N). Theoretical arguments and experimental data show the suitability of the procedure for dynamic characterization of such structures. Operational Modal Analysis of the experimental data showed three modes of the structure identified at 2.41 Hz, 2.78 Hz and 3.06 Hz. The mode shapes and mode shape vectors have been estimated from SVD of spectral matrix. Damping ratios of three modes have been estimated at 2.7%, 2.3% and 1.8% by taking a piece of SDOF density function around the natural frequency back into time domain by Inverse Fast Fourier Transform. These extracted modal parameters have been later on used for validation of Finite Element model of *Rumi Darwaza*.

CHAPTER 4

MATERIAL CHARACTERIZATION

4.1 OVERVIEW

Any structural intervention for a monument requires detailed material characterization of the existing materials of the monument. This includes site investigations followed by comprehensive laboratory testing of mortar, brick and any other previous intervention material samples, aiming at characterizing the original material composition from mineralogical, chemical and mechanical perspectives. Interventions for heritage structures and historic monuments are generally guided by the concept of reversibility, however achieving a reversible intervention is not always possible. Therefore, it is guided by the concept of compatibility with retreatability/repairability, which implies that the intervention material should not have negative consequences on the existing material, in short or long term, and that it will not prevent or hinder any future repairs, if needed (Rai and Dhanapal 2013). Material characterization is necessary to achieve this compatibility between proposed intervention materials with the existing materials.

Rai and Dhanapal (2015b) performed a comprehensive set of laboratory tests to check the compatibility of lime-surkhi mortar used in Lucknow monuments of Nawabi era with the intervention material used in their renovation work by Archaelogical Survey of India (ASI). The study concluded that the renovation plaster was different in several aspects from the existing mortar such as binder-aggregate ratio, particle size distribution and hydraulicity based on analytical methods including Microwave Acid Digestion and Thermo-Gravimetric Analysis with Differential Thermal Analysis (TGA-DTA). This chapter builds on the results of that study and discusses the tests conducted for the mechanical characterization of the materials used in 18th century Lucknow monuments – bricks, mortar and masonry. An overview of various tests performed has been provided in Figure 4.1.

<table>
<tr><td rowspan="2">Unit Properties</td><td>Lakhauri Bricks</td><td>Compressive strength</td></tr>
<tr><td>Lime-Surkhi Mortar</td><td>Compressive strength</td></tr>
<tr><td rowspan="3">Masonry Properties</td><td>Compressive strength</td><td>Stack bonded prism
Multi-wythe prism</td></tr>
<tr><td>Elastic modulus</td><td></td></tr>
<tr><td>Diagonal tensile strength</td><td></td></tr>
</table>

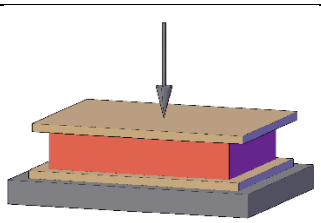

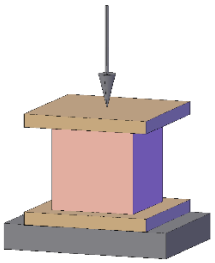

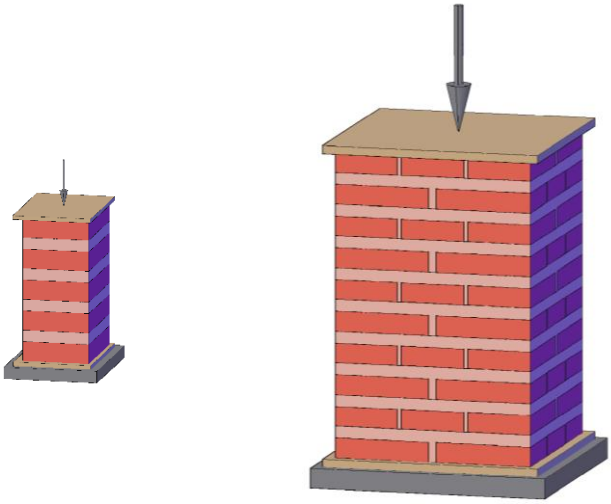

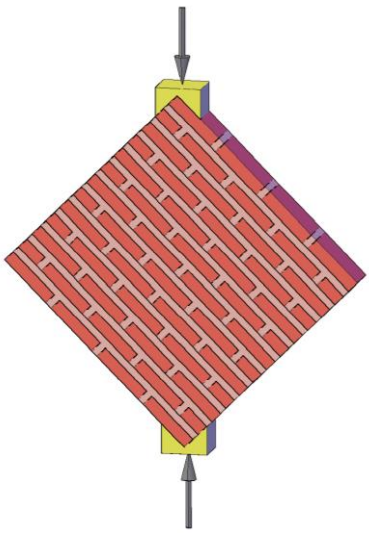

Figure 4.1. Tests conducted on brick units and assemblages

4.2 LIME-SURKHI MORTAR FORMULATION

Lime-surkhi mortar refers to mortar composed of lime as the binder with crushed brick (surkhi) and sand constituting the aggregate content. Use of surkhi content of particles finer than 300 μm in mortar is known to add hydraulicity to an otherwise non-hydraulic lime-sand mortar, by acting as a pozzolana which reacts with the lime. Surkhi content of higher particle size (>300 μm) acts as a porous particulate or air-entraining additive which aids the carbonation of lime (Teutonico et al. 1993). Apart from being used as structural mortar, in the past, lime-surkhi mortar has also been used as a protective surface render because it is impermeable to water (Verhosek 2006). Hence, lime-surkhi mortar has the dual nature of being porous and yet being impermeable to water.

Various samples of mortar from different sites of Lucknow monuments under the care of ASI were collected and characterized for their various properties by Rai and Dhanapal (2013). These included samples from Imambara complex, Naubatkhana, Moosa Bagh and *Rumi Darwaza*, which are shown in Figure 4.2.

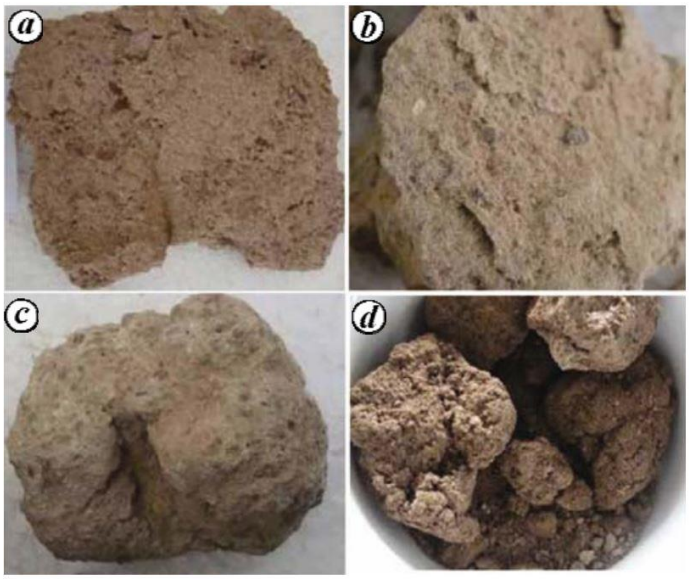

Figure 4.2. Representative mortar samples: (a) Imambara Comlpex, (b) Naubatkhana, (c) Moosa Bagh and (d) Rumi Darwaza (Rai and Dhanapal 2013)

Out of the collected samples, the sample collected from Naubatkhana (Figure 4.2b) was the only masonry mortar sample, while the rest were either plaster samples (Figures

4.2a and 4.2c) or renovation mortar samples (Figure 4.2d). An ASI protected heritage structure, Naubatkhana is part of the Bara Imambara complex which was also built by Nawab Asaf-uf-Daula and designed by Kifayatullah at about the same time as *Rumi Darwaza* (1780-90 AD). Therefore, it can be fairly assumed that the same masonry mortar would have been used for the construction of *Rumi Darwaza*. Hence, the formulation of lime-surkhi mortar for laboratory simulation was based on mortar proportion and aggregate fraction used in Naubatkhana.

4.2.1 Binder-Aggregate Ratio and Particle Size Distribution

Lime and crushed brick mortar has been used for different purposes such as joint mortar for structural masonry, as lining material in wells, baths and duct drains, as plaster on internal and external walls, and as supporting materials for frescoes (Moropoulou et al. 2005). Different proportions of lime, surkhi and sand have been used in historical and contemporary mortars, some of which have been presented in Table 4.1.

Table 4.1. Lime-crushed brick mortar proportions used in historical and contemporary mortars

Location/Reference	Historic Period	Mortar Proportion	Binder	Aggregate	
				Crushed Brick	Sand
Hagia Sophia (Moropoulou 2002)	Middle Byzantine 7th century	1:2.8	1	1	1.8
Central Basilica of Dion (Stefanidou 2014)	Roman 2nd century	1:2			
Cretan ancient mortar (Maravelaki-Kalaitzaki 2003)	Classical to Byzantine	1:2 to 1:3			
Greek ancient pozzolana mortar	Classical	1:3	1	1	2
IS: 2250 - 1981		1:2 to 1:3	1	1	1-2
Maharashtra Engineering Research Institute (MERI 1964)		1:2.5 to 1:4			
CE handbook		1:2	1	1	1

Mortars using lime and crushed bricks as constituents have mostly had a binder to aggregate ratio between 1:2 and 1:3, as can be seen from Table 4.1. Lime-surkhi mortar, used in Lucknow monuments, also used similar proportions. The binder aggregate ratio

for Naubatkhana mortar sample was evaluated by Dhanapal (2009) as 1:2.5 by volume proportion of lime:(surkhi+sand) with an aggregate size distribution as shown in Figures 4.3 and 4.4. Based on the chemical analyses of mortar samples from Lucknow monuments and other historical monuments, a mortar proportion of 1:1:1.5 (lime:surkhi:sand) by volume has been used for simulating the lime-surkhi mortar in laboratory experiments. The aggregate size distribution of surkhi and sand used in the formulated mortar has been arrived at based on the distribution evaluated for Naubatkhana mortar sample. The contribution at each grain size from surkhi and sand is such that the combination is close to the original size distribution of mortar used in the monument. The particle size distribution of surkhi and sand used in the formulated mortar are shown in Figures 4.3 and 4.4. Locally available lime was used in the formulated mortar. From the grain size distribution, coefficients of uniformity and curvature can be calculated according to Equation 4.1.

$$C_u = \frac{D_{60}}{D_{10}}$$
$$C_c = \frac{\left(D_{30}\right)^2}{D_{10} \times D_{60}} \qquad (4.1)$$

where D_{60} is the grain diameter at 60% passing, D_{30} is the grain diameter at 30% passing, and D_{10} is the grain diameter at 10% passing, which can be obtained from Figure 4.3. Coefficients of uniformity C_u and curvature C_c are evaluated as 12.2 and 2.95 respectively. Comparing with the gradation criteria, surkhi sand aggregate combination can be classified as being well graded.

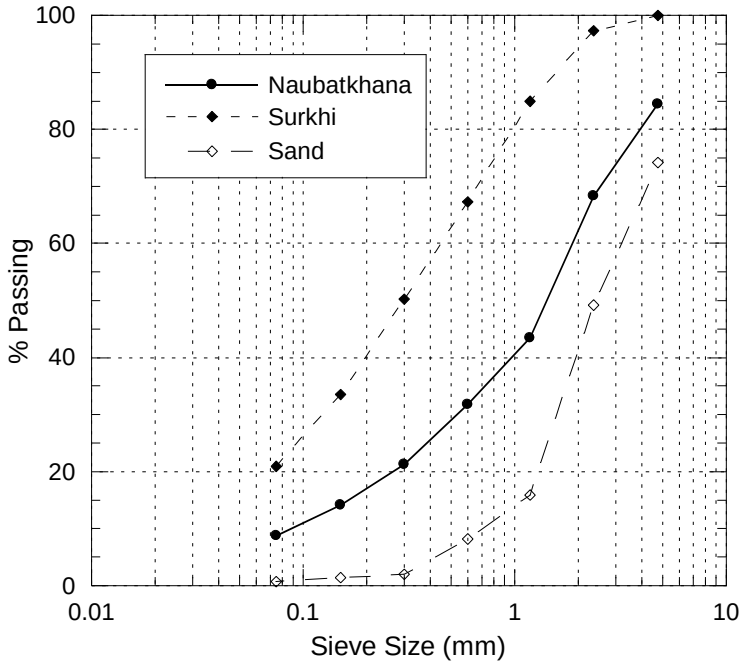

Figure 4.3. Aggregate size distribution

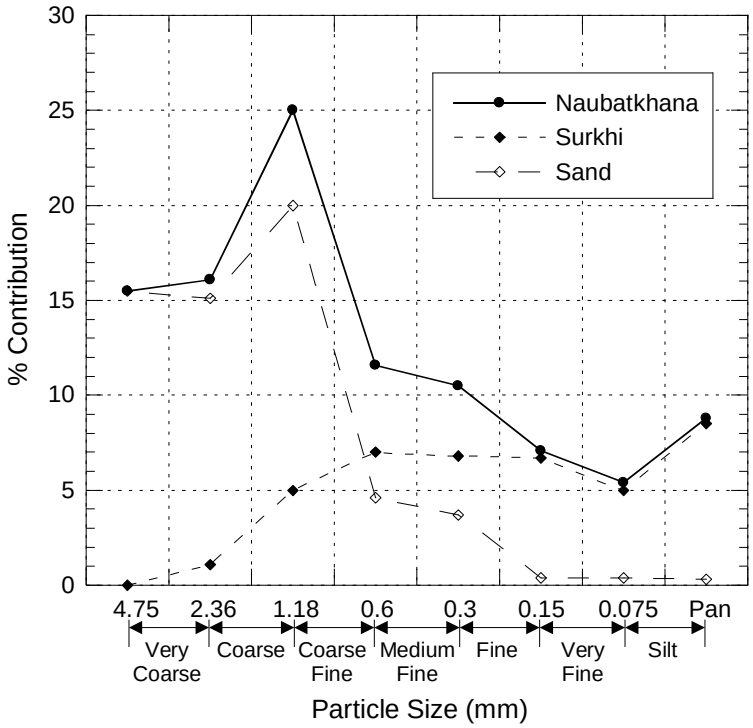

Figure 4.4. Aggregate size contributions of surkhi and sand in formulated mortar

4.3 DETERMINATION OF MECHANICAL PROPERTIES

Mechanical properties such as compressive strength and modulus of elasticity of bricks, mortar and masonry were determined. Additionally, the tensile strength of masonry wall was determined from the diagonal tension test.

4.3.1 Lakhauri Bricks

The uni-axial compressive test for bricks was performed on six fully baked (red) and partially baked (pale yellow) bricks each, shown in Figure 4.5. Because of the irregular shape, the bricks had to be cut with a tile cutter to an approximately same size of 120 mm × 80 mm × 20 mm. The surfaces were further leveled using a grinder and capped as per ASTM C67-14 with plaster of paris. The failure pattern of Lakhauri bricks has been shown in Figure 4.6. As expected, the bricks failed by crushing and vertical tensile splitting. Average compressive strength for fully baked bricks was found to be 36.2 MPa with 15% COV. Similarly, average compressive strength for partially baked bricks was found to be 19.0 MPa with 13% COV. Fully baked bricks were seen to have almost double compressive strength as compared to partially baked bricks.

(a) (b)

Figure 4.5. Lakhauri bricks: (a) Fully baked brick and (b) Partially baked brick

Figure 4.6. Failure pattern of Lakhauri bricks

4.3.2 Formulated Lime-Surkhi Mortar

The lime-surkhi mortar simulated in laboratory, based on mortar proportion and aggregate fraction evaluated through chemical analyses by Dhanapal (2009), was tested for its mechanical properties. Lime-surkhi mortar cubes of 50 mm size with volume proportion 1:1:1.5 (lime:surkhi:sand) were prepared to perform the compressive strength test at an age of 28 days as per ASTM C109. The water-binder ratio required for preparation of mortar was left up to the judgement of mason. Although, it was observed that a ratio of 1.0-1.1 by weight was required for obtaining a workable mortar. The compressive strength test was performed using 3000 kN Instron Compression Testing Machine with displacement controlled loading at a rate of 1 mm/min. The failure pattern of the mortar cubes is shown in Figure 4.7. In total 8 number of cubes were tested and average results and COV of the tests are summarized in Table 4.2. The stress-strain curve for mortar cubes, presented in Figure 4.8, remain linear almost up to 90% of its compressive strength. Stress strain curves also show that lime-surkhi mortar behave in a highly ductile manner, reaching 12-15% strain before losing 50% of its strength.

Figure 4.7. Failure pattern of lime-surkhi mortar cubes

Table 4.2. Summary of test results for lime-surkhi mortar cubes

Mortar	Compressive Strength f_j, (MPa)	Strain at peak stress	Modulus of Elasticity E_j, (MPa)	E_j / f_j
Lime-Surkhi Mortar (1:1:1.5)	1.06 [0.13]	0.0197 [0.21]	81.4 [0.22]	79.7 [0.32]

* Figure in [ ] indicates COV

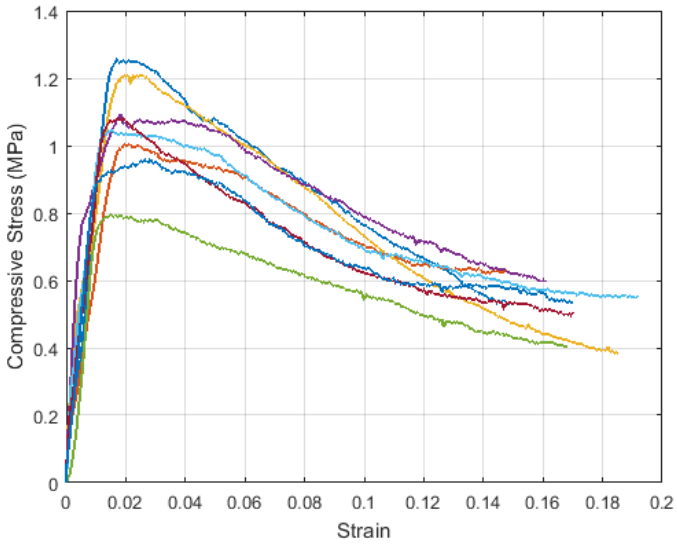

Figure 4.8. Stress-strain curve for lime-surkhi mortar cubes

Kaushik et al. (2007) showed that modulus of elasticity E_j varies between 100 to 400 times compressive strength f_j for cement lime sand mortar, with an average value of 200 times f_j. The lime-surkhi mortar formulated in laboratory had E_j value varying between 50 to 130, which is on the lower side. This can be attributed to the very low strength of lime mortar and also that the relation is defined for cement based mortars. Various researchers (Lanas et al. 2003, Binda et al. 1999) have evaluated the effect of curing time on strength gain in lime based mortars and reported that mortars gained only up to 50% of their maximum compressive strength in 28 days and continued to gain strength even till a period of 365 days. This is because lime mortars can take many years to reach total carbonation. The long term properties of lime-surkhi mortar will have to be evaluated to investigate the relationship between modulus of elasticity and compressive strength for such mortars.

4.3.3 Masonry

Masonry prisms made using Lakhauri bricks and formulated lime-surkhi mortar were tested for their uni-axial compressive strength and modulus of elasticity. Also, tensile strength of masonry prism was evaluated from diagonal tension test. The masonry prisms were prepared with a mortar course thickness almost 3/4th of brick thickness

similar to what has been seen in Lucknow monuments. Masonry specimens were prepared using fully baked bricks only. Even though the monument may have used partially baked bricks as well, but their effect on the global behaviour may not be significant as they should only constitute an small percentage. However, in masonry test specimens, their effect can be significantly larger, as they would constitute a greater proportion of the bricks in specimens. Due to this reason, only fully baked bricks have been used in the construction of the specimens.

Stack Bond Prism

Three specimens of standard five brick prisms with a size 120 mm × 80 mm × 180 mm, made of fully baked bricks and formulated lime-surkhi mortar, were prepared according to ASTM C1314-16 and cured for 28 days. The specimens were tested using Instron CTM under displacement controlled loading at a rate of 1 mm/min. An extensometer was attached to the surface of prism to measure the axial strain induced in the specimen. Additionally, the in-built load cell and displacement transducer provided the values for stress-strain calculations. As the cracks propagated, the extensometer readings got distorted, due to which they were not available for the post-peak behaviour. However, for the post-peak behaviour, strain can be calculated using the CTM displacement measurements. This has been done by applying a suitable correction factor on strain calculated from CTM displacement values to account for the difference in stiffness measured by extensometer and CTM. Strain measurements are combined together with the initial linear portion from extensometer and the rest from CTM displacement. The compressive strength of stack bond prisms were corrected for their aspect ratio by applying the correction as described in ASTM C1314-16. Modulus of elasticity is calculated from stress-strain curves by measuring the slope of a secant between ordinates corresponding to 5% and 33% of compressive strength of specimens as per the requirements of MSJC (2002). The experimental setup and failure pattern for stack bond prism compression test are shown in Figure 4.9. The prisms showed vertical splitting failure with the cracks propagating through the mortar joints and bricks vertically. Results of stack bond prism tests are summarized in Table 4.3 and stress-strain curves are shown in Figure 4.10.

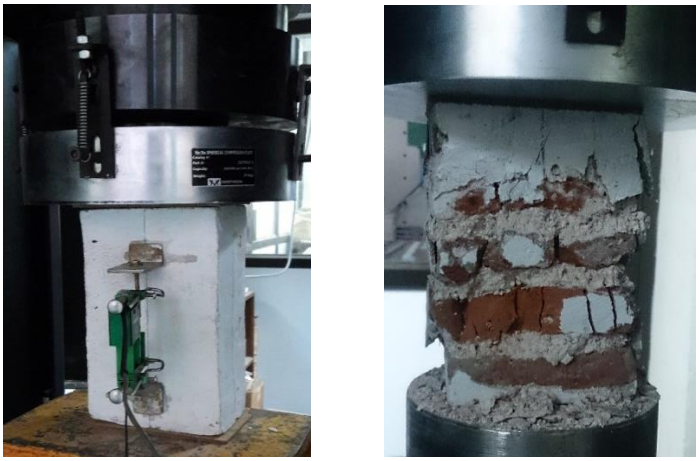

(a) (b)

Figure 4.9. Stack bond prism test: (a) Experimental setup and (b) Failure pattern

Table 4.3. Summary of stack bond prism compressive strength test results

Specimen	Peak load (kN)	Compressive strength, f'_m (MPa)	Strain at peak stress	Modulus of elasticity, E_m (MPa)	E_m / f'_m
1*	25.27	2.66	0.0246	2382.9	894.2
2	27.51	2.74	0.0374	916.8	335.2
3	25.29	2.78	0.0307	1011.7	363.9
Average [COV]	26.40 [0.04]	2.76 [0.01]	0.0341 [0.10]	964.3 [0.05]	349.5 [0.04]

Note: * outlier, Figure in [ ] indicates COV

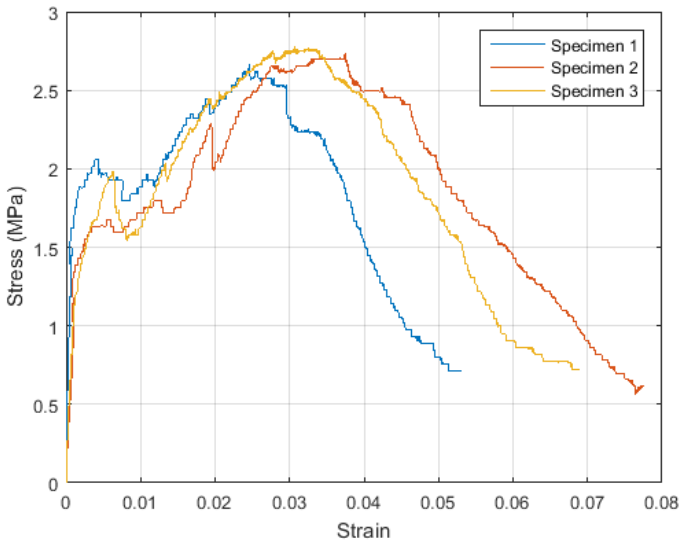

Figure 4.10. Stress-strain curve for stack bond prism compressive strength test

The obtained compressive strength can be compared with those predicted by different relations proposed by researchers relating masonry strength with compressive strength of mortar and brick as given below:

Kaushik et al. (2007):

$$f_m^{'} = 0.63 f_b^{0.49} f_j^{0.32} \tag{4.2}$$

Eurocode 6 (BEN 1996):

$$f_m^{'} = 0.6 f_b^{0.65} f_j^{0.32} \tag{4.3}$$

Dayaratnam (1987):

$$f_m^{'} = 0.275 f_b^{0.5} f_j^{0.5} \tag{4.4}$$

Bennet et al. (1997):

$$f_m^{'} = \frac{3}{10} f_b \tag{4.5}$$

where $f_m^{'}$ is the compressive strength of masonry, f_b is the compressive strength of brick and f_j is the compressive strength of mortar. The comparison of experimental results with different predictive relations is presented in Table 4.4. It can be observed from Table 4.4 that the relations proposed by Kaushik et al. (Equation 4.2) and Dayaratnam (Equation 4.4) predict compressive strength comparatively better for such masonry.

Table 4.4. Comparison of experimental compressive strength with predictive relations

	Experiment	**Kaushik et al. (2007)**	**Eurocode 6 (1996)**	**Dayaratnam (1987)**	**Bennet et al. (1997)**
Compressive Strength (MPa)	2.76	3.73	6.30	1.70	10.86

Multi-Wythe Prism

Stack bond prisms may not simulate the actual conditions of masonry material present in the structure as the actual masonry has many more interactions between brick and mortar along the bed joints, head joints and collar joints. To simulate the actual field

interaction, multi-wythe masonry specimens were prepared. Four specimens made of fully baked bricks and formulated lime-surkhi mortar were prepared having a size of 250 mm × 250 mm × 410 mm. The multi-wythe prisms were tested using the Instron CTM with a displacement controlled loading at a rate of 1 mm/min. Two extensometers were attached to the surface of the prisms to measure the compressive deformation. Additionally, the in-built load cell and displacement transducer provided the values for stress-strain calculations. The experimental setup and the failure pattern are shown in Figure 4.11.

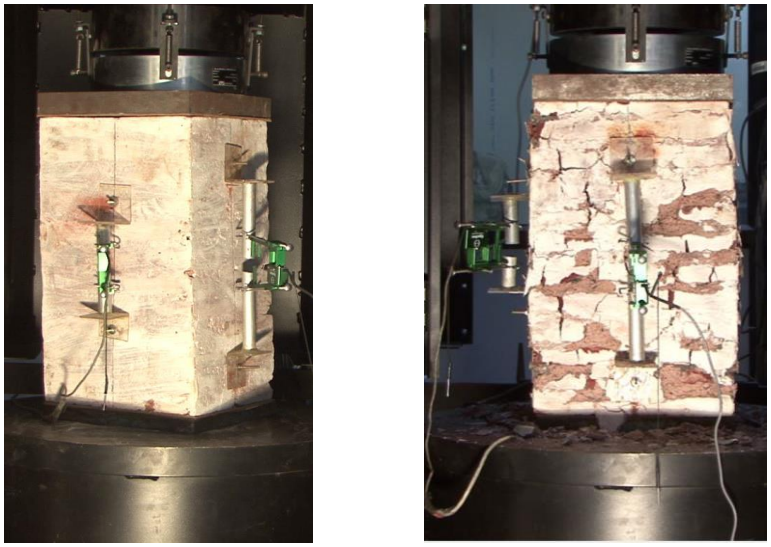

(a) (b)

Figure 4.11. Multi-wythe masonry prism test: (a) Experimental setup and (b) Failure pattern

Multi-wythe prisms also showed the classical vertical splitting failure, where the cracks propagated through the bricks. The stress-strain curves for the specimens are shown in Figure 4.12 where the in-built load cell and displacement transducer were used to calculate the stress and strain, respectively. However, the extensometers also closely followed the same stress-strain curves, but the post-peak behaviour was not always available, which is why the CTM displacement has been used for stress-strain curves. Results of multi-wythe compression tests are summarized in Table 4.5.

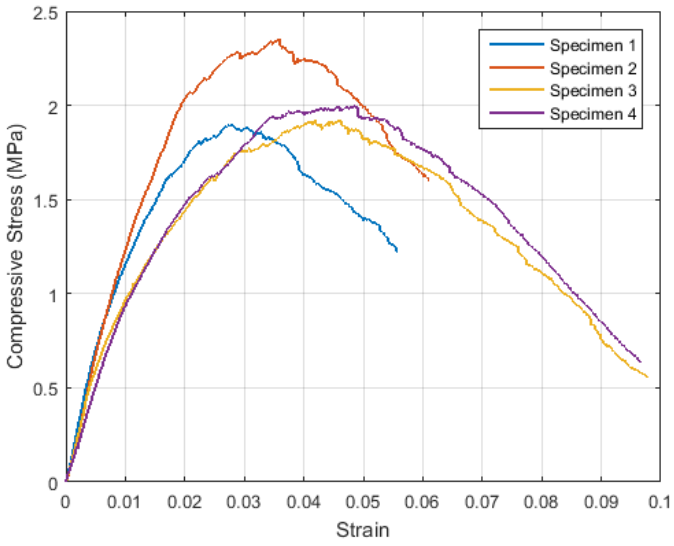

Figure 4.12. Stress-strain curves for multi-wythe prism compressive strength test

The average compressive strength of multi-wythe prisms was about 75% of compressive strength of stack bond prisms. The increased mortar bonds along the head joints and collar joints cause the reduction in compressive strength and also causes the stress-strain behaviour to be much more non-linear as compared to stack bond prisms. Since the stress-strain behaviour is non-linear, secant modulus was calculated using the ordinates at 0.33 $f_m^{'}$ and 0.75 $f_m^{'}$ for modulus of elasticity with extensometer recordings being used for strain calculations, similar to stack bonded masonry.

Table 4.5. Summary of multi-wythe prism compressive strength test results

Specimen	**Peak load (kN)**	**Compressive strength, $f_m^{'}$ (MPa)**	**Strain at peak stress**	**Modulus of Elasticity, E (MPa)**	$E/f_m^{'}$
1	115.97	1.89	0.0292	60.3	31.8
2	146.11	2.35	0.0371	81.5	34.6
3	117.23	1.92	0.0357	60.9	31.7
4	125.02	2.00	0.0463	57.7	28.9
Average [COV]	126.08 [0.10]	2.04 [0.09]	0.0371 [0.16]	65.08 [0.15]	31.76 [0.06]

* Figure in [ ] indicates COV

Diagonal Tension Test

The shear strength of masonry can be determined through the diagonal tension test. ASTM E519-15 recommends a nominal size of specimen as 1.2 m× 1.2 m, assuming standard modular bricks. However, since Lakhauri bricks are very thin, such a large specimen will be too slender. RILEM standard LUM B6 (1991) lays the guidelines for diagonal tension testing of smaller wall specimens. The standard suggests the preparation of specimen such that the length of specimen is at least four brick unit long. Two masonry specimens made using fully baked bricks and formulated mortar with a size 520 mm × 520 mm× 85 mm were prepared and cured for 28 days. The specimens were tested by applying load along the diagonal direction till failure. Extensometers were attached to the surface of the wall to measure the vertical shortening and horizontal expansion of the specimen. The specimens were tested using Universal Testing Machine (UTM) of 2000 kN capacity at an approximate loading rate of 1 kN/min. Figure 4.13 shows the experimental setup and failure pattern for diagonal tension test. Wall panels failed by cracking occurring along the diagonal.

Shear stress according to ASTM E519-15, which assumes the stress state at the center of diagonal specimen to be of pure shear and value of average diagonal shear stress to be equal to principal tensile stress, is calculated as:

$$S_s = \frac{0.707P}{A_n} \tag{4.6}$$

where S_s is shear stress, P is the applied load and A_n is the net area of the specimen which is given by

$$A_n = \left(\frac{w+h}{2}\right)tn \tag{4.7}$$

where w, h, t and n are width, height, thickness and the percent gross area of the unit that is solid expressed as a decimal of the specimen respectively.

Shear strain is calculated from extensometer readings as:

$$\gamma = \left(\Delta V + \Delta H\right)/l \tag{4.8}$$

where, ΔV is the vertical shortening, ΔH is the horizontal extension and l is the gauge length.

Using the shear stress and strain, modulus of rigidity is calculated as

$$G = S_s / \gamma \tag{4.9}$$

The results of the diagonal tensile test are summarized in Table 4.6. The tensile strength of masonry is evaluated to be 4.7% of the compressive strength of masonry.

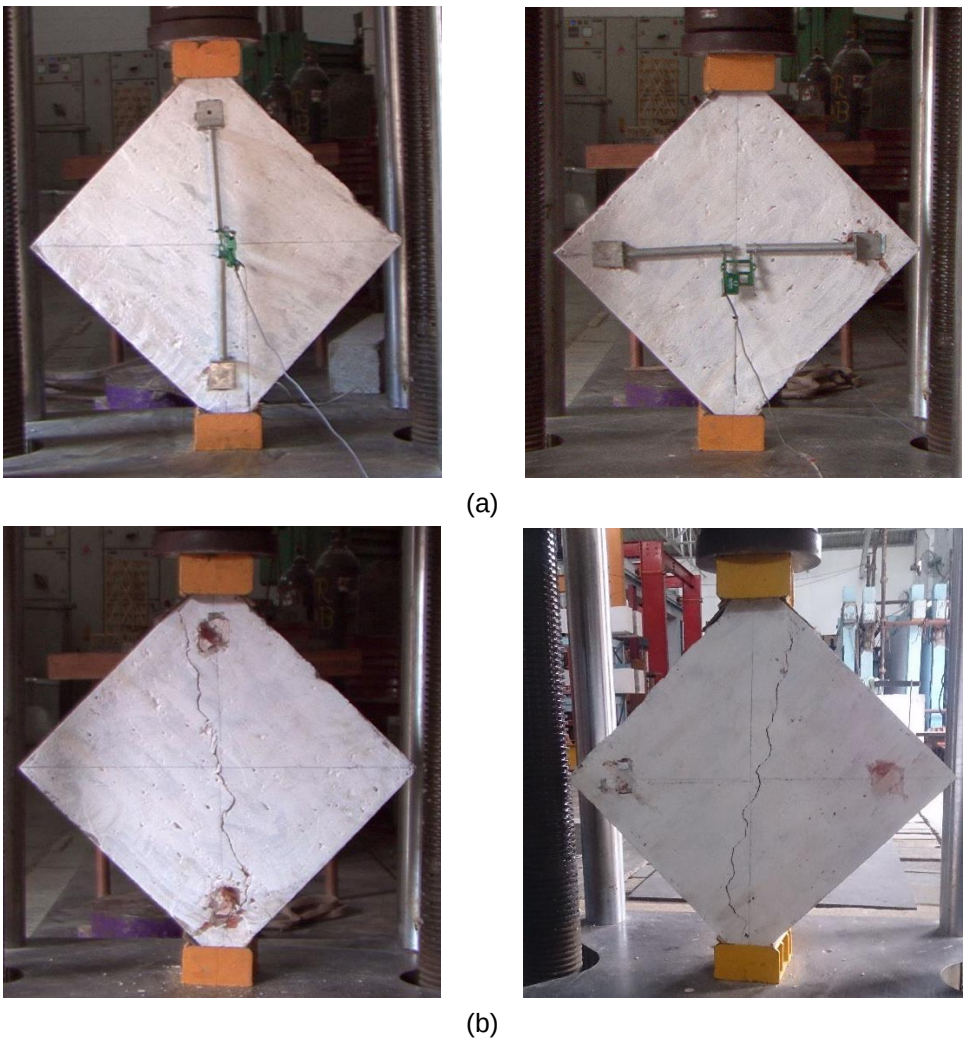

Figure 4.13. Diagonal tension test: (a) Experimental setup and (b) Failure pattern

Table 4.6. Summary of diagonal tensile test results

Specimen	Peak load (kN)	Shear stress s_s (MPa)	Shear strain γ	Modulus of Rigidity G (MPa)
1	8.35	0.133	0.00090	148.0
2	6.61	0.121	0.00063	192.6
Average [COV]	7.48 [0.12]	0.127 [0.05]	0.00076 [0.18]	170.3 [0.13]

* Figure in [ ] indicates COV

4.4 SUMMARY

Various experiments for mechanical characterization of Lakhauri bricks, lime-surkhi mortar and masonry prisms were performed and the results have been presented. Lime-surkhi mortar formulation was based on grain size distribution and binder-aggregate ratio evaluated for Lucknow monuments and other historical monuments.

Average compressive strength for fully baked and partially baked bricks was 36.2 MPa and 19.0 MPa respectively. Fully baked bricks were seen to have almost twice the compressive strength of partially baked bricks. Due to the significant difference in strength, only fully baked bricks were used for preparing masonry prisms. Formulated lime-surkhi mortar was seen to have a very low compressive strength of 1.06 MPa. The low strength is attributed to incomplete carbonation reaction which takes much longer to complete in such lime-surkhi mortar. However the mortar displayed highly deformable nature reaching 12-15% strain before losing 50% of its strength.

Standard stack bond prisms were prepared and tested for their compressive strength, which was found to be 2.76 MPa. Relations proposed by Kaushik et al. (Equation 4.2) and Dayaratnam (Equation 4.4) were seen to predict compressive strength better than other relations for this kind of masonry. To simulate the actual field interaction present in the structure with many more interaction surfaces between brick and mortar other than bed joint, multi-wythe masonry prisms were prepared and tested for compressive strength. Average compressive strength for multi-wythe prisms was evaluated as 2.04 MPa, which is about 75% of compressive strength of stack bonded prisms. This decrease

is expected due to the enhanced number of brick mortar interaction surfaces which present planes of weakness. To evaluate the tensile strength, diagonal tension tests were performed on prisms. The tensile strength of masonry is evaluated to be a low value of 4.7% of the compressive strength of masonry.

CHAPTER 5

SEISMIC ASSESSMENT USING FINITE ELEMENT ANALYSES

5.1 OVERVIEW

Seismic response of a structure can be predicted through Finite Element (FE) modelling of the structure. This chapter describes the different steps involved in FE modelling of the monument, *Rumi Darwaza*. Various analyses carried out in Abaqus, a general purpose FE software, to predict the structural response have been explained and the results of the same have been presented. A comparison between experimental and analytical results has also been drawn to validate the analytical FE model. Finally, strengthening techniques have been proposed based on the evaluated structural behaviour and their effect on the structural response of *Rumi Darwaza* has been evaluated through finite element analyses.

5.2 MODELLING STRATEGY

Masonry is a composite material consisting of bricks joined together by layers of mortar. As a material, it exhibits anisotropic and non-linear behaviour due to the presence of mortar joints, which act as planes of weakness. Numerical modelling of masonry can be done in two main frameworks, micro-modelling and macro-modelling. In micro-modelling, the focus is on individual components, i.e., units (bricks, blocks etc.) and mortar. Each unit-mortar interface is defined individually and constitutive relationships are defined for each material type to simulate the non-linear behaviour. In macro-modelling, masonry is considered as a homogeneous material, defined by constitutive relations for the overall behaviour (Singhal 2014). The different modelling strategies that can be used for masonry are shown in Figure 5.1. Depending on the level of accuracy and simplicity desired, it is possible to use the following modelling strategies (Roca et al. 1998):

- *Detailed micro-modeling*: Masonry units and mortar in header and bed joints are represented by continuum elements while the unit-mortar interface is characterized by discontinuous elements as shown in Figure 5.1a. Detailed micro-modeling provides most realistic representation of masonry composites and better understanding about the local behaviour of masonry.
- *Simplified micro-modeling*: In this strategy, joint thickness is included in the brick unit, which is referred to as "expanded units", as shown in Figure 5.1b. These expanded units are represented as continuum elements while the combined behaviour of mortar joint and unit-mortar interface is defined through discontinuous elements.
- *Macro-modeling*: This strategy assumes that units, mortar, and unit-mortar interface are smeared out in the continuum, as shown in Figure 5.1c. This strategy is generally adopted for analyzing large structures where stresses along and across the length can be considered to be uniformly distributed.

For large structures, such as monuments, macro modelling yields sufficiently accurate results about the global behaviour. In the current study, macro-modelling approach has been adopted for FE modelling of *Rumi Darwaza*.

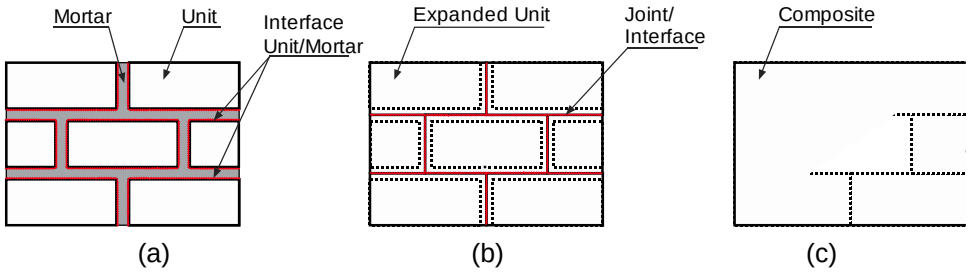

Figure 5.1. Modelling strategies for masonry structures: (a) Detailed Micro-modelling, (b) Simplified Micro-modelling, and (c) Macro-modelling (Singhal 2014)

5.2.1 Geometrical and Material Modelling

The structure of *Rumi Darwaza* presents a very complex geometry with several features that mandate the use of a sophisticated software which has the capabilities to define the complex geometry as close as possible to the actual shape. Rough sketches of floor plans of the monument were available from Archaeological Survey of India, and other dimensions which were required for modelling of the structure were measured. A

complete 3-D model of the monument prepared in AutoCAD software is shown in Figure 5.2. Some simplifying assumptions such as modelling the curved arches as semi-circles were made. Additionally, wherever a direct measurement of a feature's dimension was not available, a suitable value was arrived at based on available dimensions of other features in its vicinity. The ornamentation around the main arch gate and *Guldastas* on the parapet walls were not considered to be important owing to their insignificant mass and have not been modelled. The material properties obtained from laboratory experiments on masonry prisms were used as material modelling input in FE analysis and have been shown in Table 5.1.

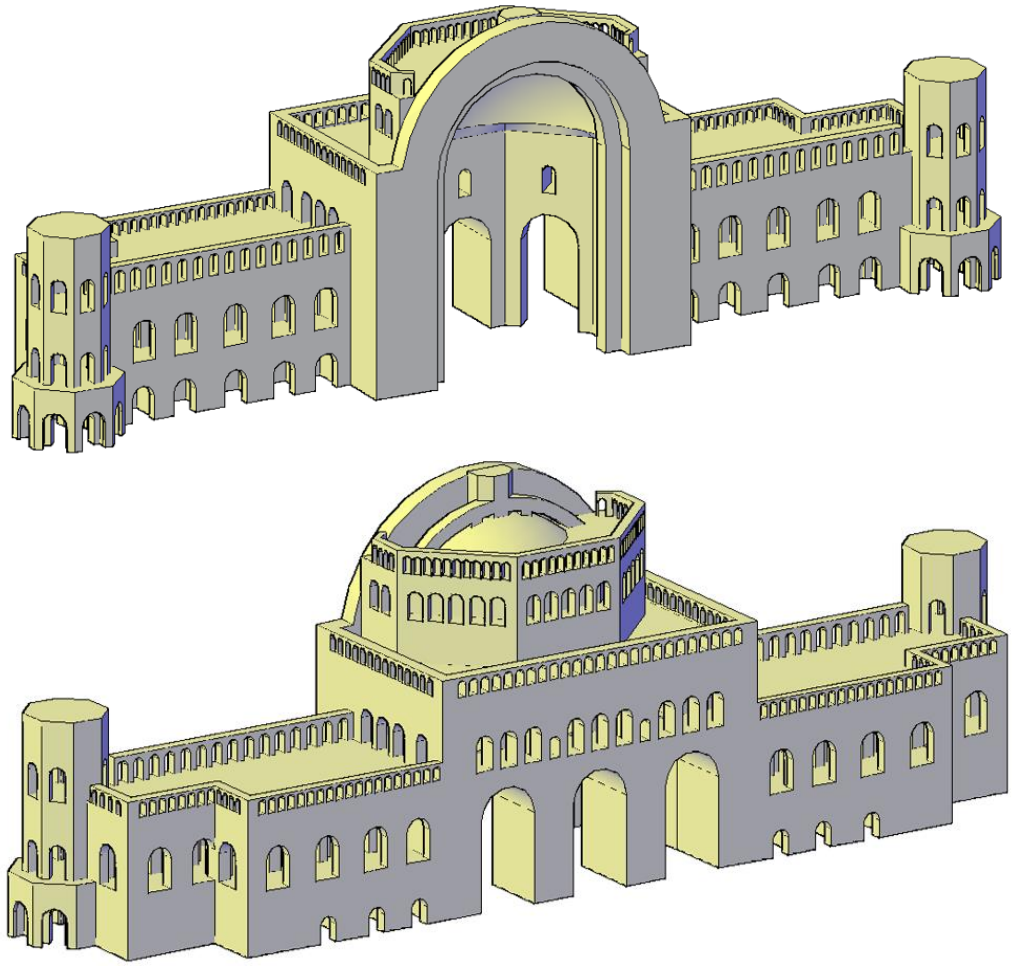

Figure 5.2. 3-D model of Rumi Darwaza monument in AutoCAD

Table 5.1. Material modelling data

Property	Density	Modulus of Elasticity	Poisson's Ratio
Value	1790 kg/m^3	964.3 MPa	0.2

5.2.2 Meshing using FEM pre-processor HyperMesh

The 3-D AutoCAD geometry can be directly imported into Abaqus for carrying out any analysis by meshing the geometry using the techniques present along with defining other parameters involved in different steps. However, when the geometry presents complexity due to several curved surfaces and additional features, it is better to use an advanced software such as HyperMesh as a pre-processor to Abaqus. HyperMesh offers better tools for meshing a geometry. The Volume Tetra meshing utility present in HyperMesh can quickly and automatically create a tetrahedral mesh within an enclosed volume with a few user inputs. 4 node tetrahedral element C3D4 for the volume with triangular faces at the surface was used for meshing the geometry imported from AutoCAD. *Element size* and *minimum element size* for the elements were defined based on the fineness level of meshing required. Default value of 30.0^{o} for *feature angle* was used. Additionally, the features of *Surface Curvature* and *Proximity* were used to obtain refined meshing on curved surfaces and in regions around the openings. *Proximity* refines the mesh by placing more elements in areas where features are small and close together. The *Surface Curvature* feature option creates finer mesh in areas with high curvature (HyperWorks 2014). Figure 5.3 shows the effect of *Surface Curvature* and *Proximity* on mesh quality.

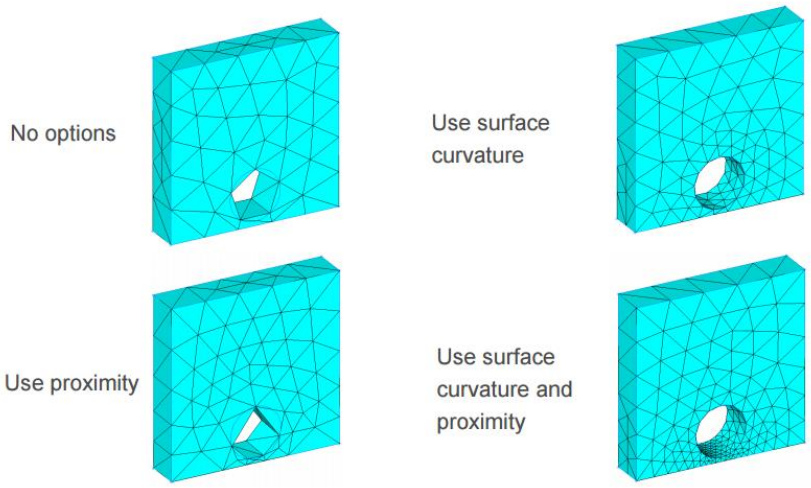

Figure 5.3. Effect of Proximity and Surface Curvature on mesh quality (HyperWorks 2014)

Cleanup elements option was enabled to apply an additional stage of calculation to improve the mesh quality by removing some nodes and combining some elements. Mesh of the complete geometry had a total of 211,087 nodes and 843,359 elements. The total mass of the monument is estimated at 120×10^3 kN. This mesh information was imported into Abaqus for performing the subsequent FE analyses. The complete mesh of 3-D geometry is shown in Figure 5.4.

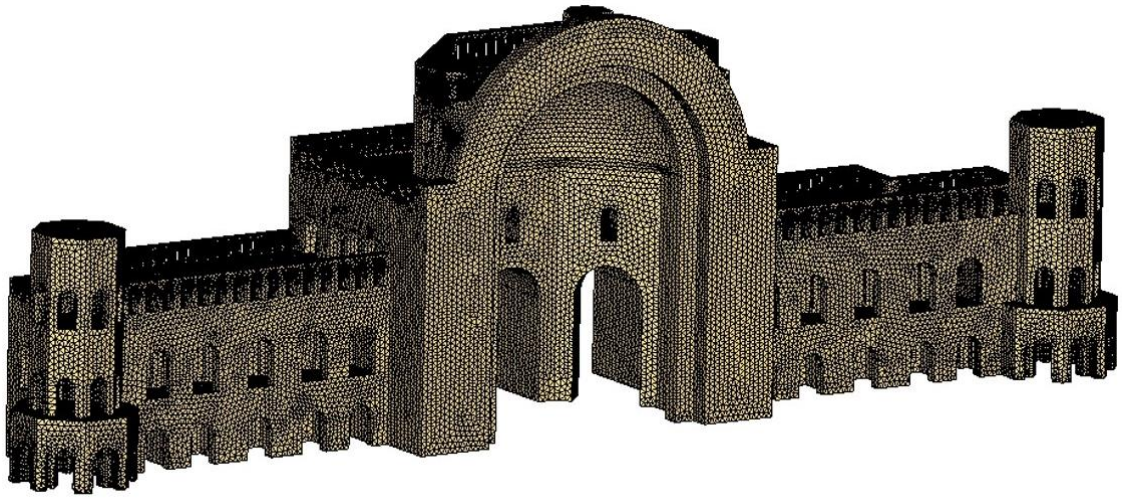

Figure 5.4. Complete mesh of 3-D geometry of Rumi Darwaza

5.3 MODAL ANALYSIS

Modal analysis of FE model is performed to obtain modal parameters such as natural frequencies, mode shapes and associated parameters of modal and mass participation factors. These modal parameters can be compared with those obtained from dynamic characterization and can be used for calibration of FE model. Fixed boundary conditions were assumed for the FE model by providing translational and rotational constraints to all the nodes on boundary surfaces. A Frequency step is defined as a linear perturbation procedure which performs eigenvalue extraction to calculate natural frequencies and corresponding mode shapes of the system. The iterative *Lanczos* eigenvalue extraction method in Abaqus has been used with the eigenvectors output to be normalized with respect to model's mass matrix. The eigenvalue problem for natural frequencies is given by (Chopra 1995):

$$\left[\mathbf{k} - \omega_n^2 \mathbf{m}\right]\phi_n = 0 \tag{5.1}$$

where $\mathbf{k}$ is the stiffness matrix, $\mathbf{m}$ is the mass matrix, ω_n is the natural frequency and ϕ_n is the eigenvector (mode of vibration). Normalizing the eigenvectors with respect to mass matrix implies normalizing them such that:

$$\phi_n^T \mathbf{m} \phi_n = 1 \tag{5.2}$$

The results of modal analysis have been presented in Table 5.2 and have been compared with the results obtained from experiments conducted for dynamic characterization.

Table 5.2. Results of modal analysis of FE model

Mode	Mass participation (% of total mass)		Natural frequency (Hz)	
	X-direction	Y-direction	FE Model	Experimental
Mode A	0.0	31.4	2.74	2.41
Mode B	0.0	7.4	3.36	2.78
Mode C	33.2	0.0	2.92	3.06

The results obtained from dynamic characterization can be used to update the material properties to calibrate the FE model to get more accurate estimate of global stiffness of structure. Previous studies have shown that natural frequencies depend on the material properties such as modulus of elasticity, however the associated mode shapes and mass participation factors are more dependent on geometry and boundary conditions and not as much on material properties (Erdogmus et al. 2007). The modulus of elasticity can be corrected as:

$$E_{updated} = E_{old} \times \left(\frac{f_{updated}}{f_{old}}\right)^2 = 964.3 \times \left(\frac{2.41}{2.74}\right)^2 = 744.7 MPa \tag{5.3}$$

Using the updated modulus of elasticity, while keeping the other properties same, modal analysis of the updated FE model was performed. As expected, the mode shapes and mass participation factors remained the same, while the natural frequencies changed. Mode shapes for the three analytical modes have been shown in Figures 5.5, 5.6 and 5.7. A scaled up displacement contour of the main structure, without wing structures flanking the main structure for the analytical Mode B, has been shown in

Figure 5.7b. It can be seen from the mode shapes that these wing structures do not have any significant movement/deformation in these modes. This is why measurement of their response was not considered necessary and no measurement points were defined on them for the forced vibration tests. The results of the updated FE model are presented in Table 5.3.

Table 5.3. Results of modal analysis of updated FE model

Mode	Mass participation (% of total mass)		Natural frequency (Hz)		
	X-direction	Y-direction	Old FE Model	Updated FE Model	Experimental
Mode A	0.0	31.2	2.74	2.41	2.41
Mode B	0.0	7.4	3.36	2.95	2.78
Mode C	33.2	0.0	2.92	2.56	3.06

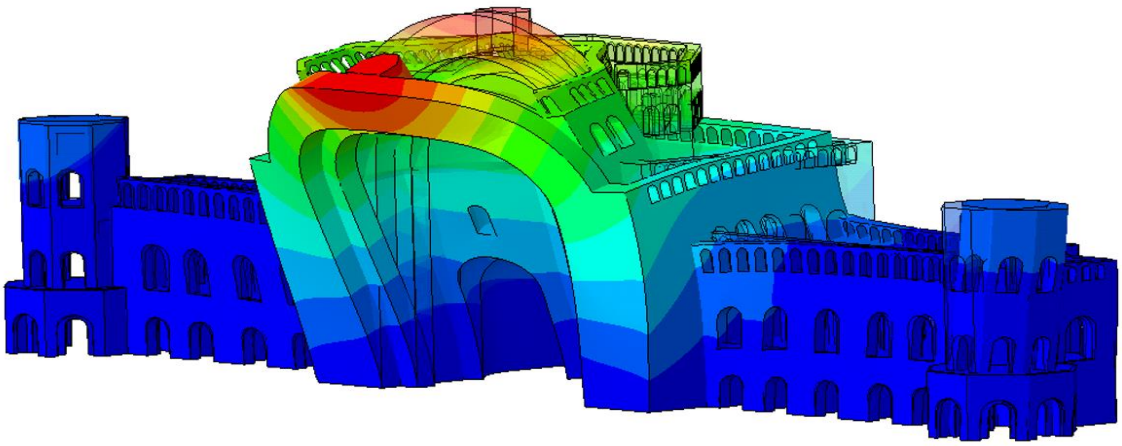

Figure 5.5. Analytical mode shape for Mode A

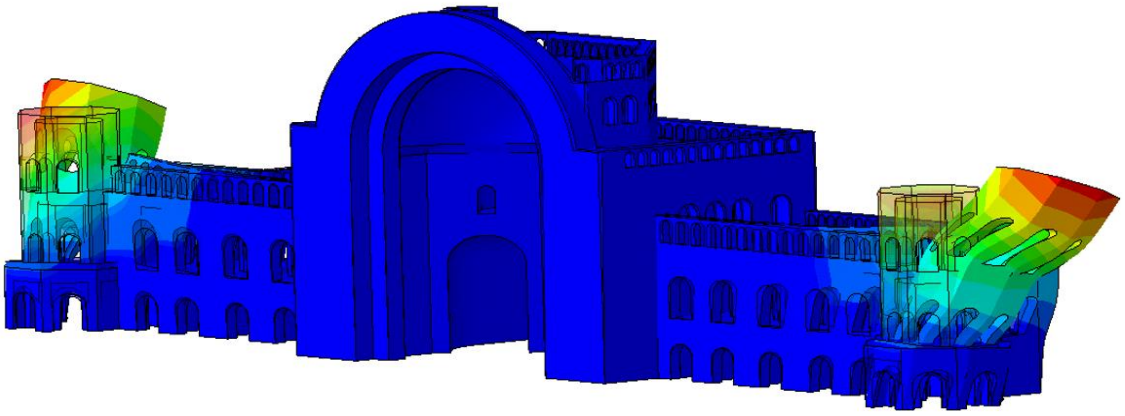

(a)

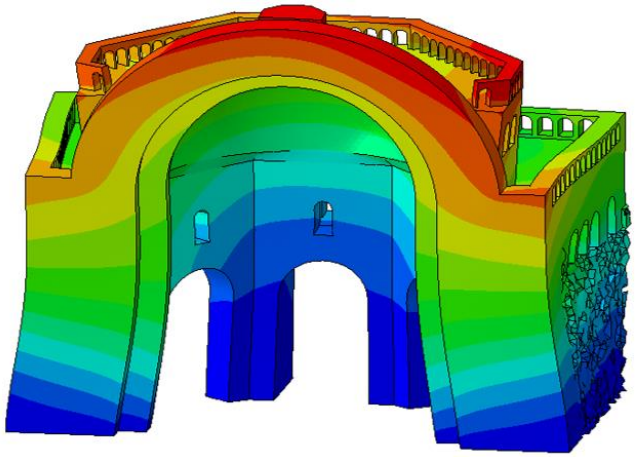

(b)

Figure 5.6. Analytical mode shape for Mode B: (a) Displacement contour of complete structure and (b) Displacement contour of main structure

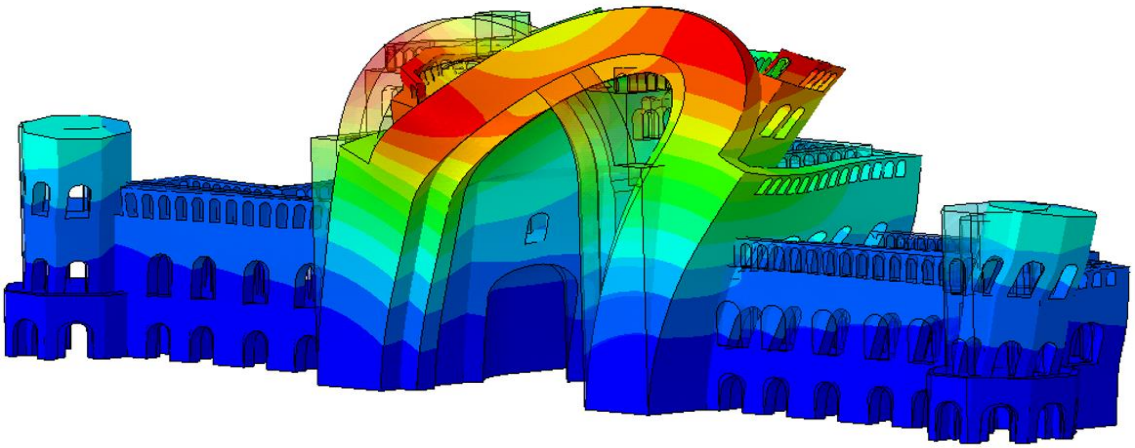

Figure 5.7. Analytical mode shape for Mode C

5.3.1 Comparison of Analytical and Experimental Mode Shapes

Prediction of structural response to earthquakes forces requires accurate analytical modelling of the monument. This accuracy can be achieved through validation of analytical model with experimental results of dynamic characterization. Greater accuracy leads to increased confidence in the predicted analytical results. The degree of closeness between experimental mode shapes and analytical mode shapes can be used for validation of FE model. Modal Assurance Criterion (MAC) has been used as a Mode Shape Correlation Constant (Pastor et al. 2012) to quantify the closeness of experimental and analytical mode shapes. MAC value, evaluated as per Equation 3.6, lies between zero and 1.0, with a value close to 1.0 representing high correlation, while a value close to zero representing no correlation.

The mode shape coordinates for analytical modes can be extracted from Abaqus by defining Field Output Request for displacement at nodes in the Frequency step for all the required modes. This nodes should represent the spatial location at which sensors were placed in forced vibration tests. The extracted mass normalized coordinates for analytical modes have to be arranged in a vector in the same order of DOFs as for experimental mode shapes. The number of elements in both the vectors for experimental and analytical mode shape must be same for MAC calculation, although their scaling does not have to be same (Friswell and Mottershead 1995). Since there were some DOFs for which the experimental mode shape coordinate could not be evaluated, coordinate corresponding to these DOFs were dropped from the analytical mode shape vector in order to make the two vectors of the same length.

A comparison of experimental and analytical mode shapes has been shown in Figure 5.8. Table 5.4 shows the comparison between experimental results and FE modal analysis results. MAC values between the experimental and analytical mode shapes are also presented in Table 5.4. % error has been calculated as:

$$\%\ error = \left| \frac{f_{Exp} - f_{FE}}{f_{Exp}} \right| \times 100 \tag{5.4}$$

Table 5.4. Comparison between dynamic characterization results and FE modal analysis

Mode	Frequency (Hz)		% Error	MAC
	Experimental	Analytical		
A	2.41	2.41	0.0	0.94
B	2.78	2.95	6.1	0.83
C	3.06	2.56	16.3	0.98

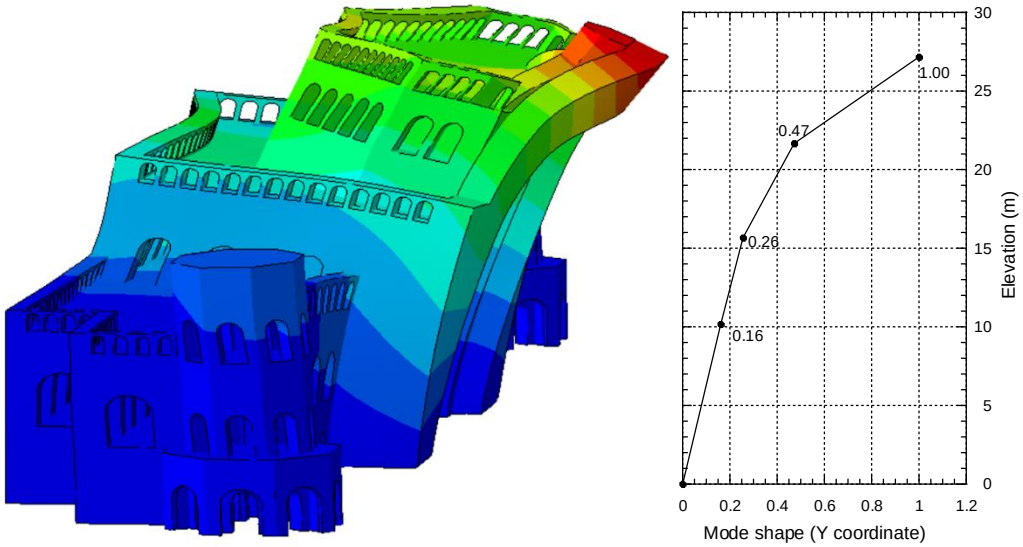

(a) Mode A: Analytical (2.41 Hz) and Experimental (2.41 Hz); MAC = 0.94

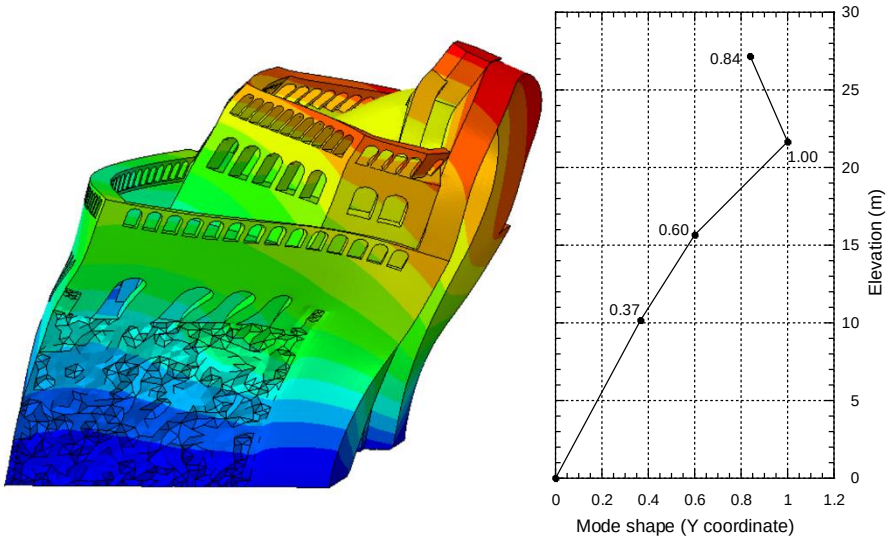

(b) Mode B: Analytical (2.95 Hz) and Experimental (2.78 Hz); MAC = 0.83

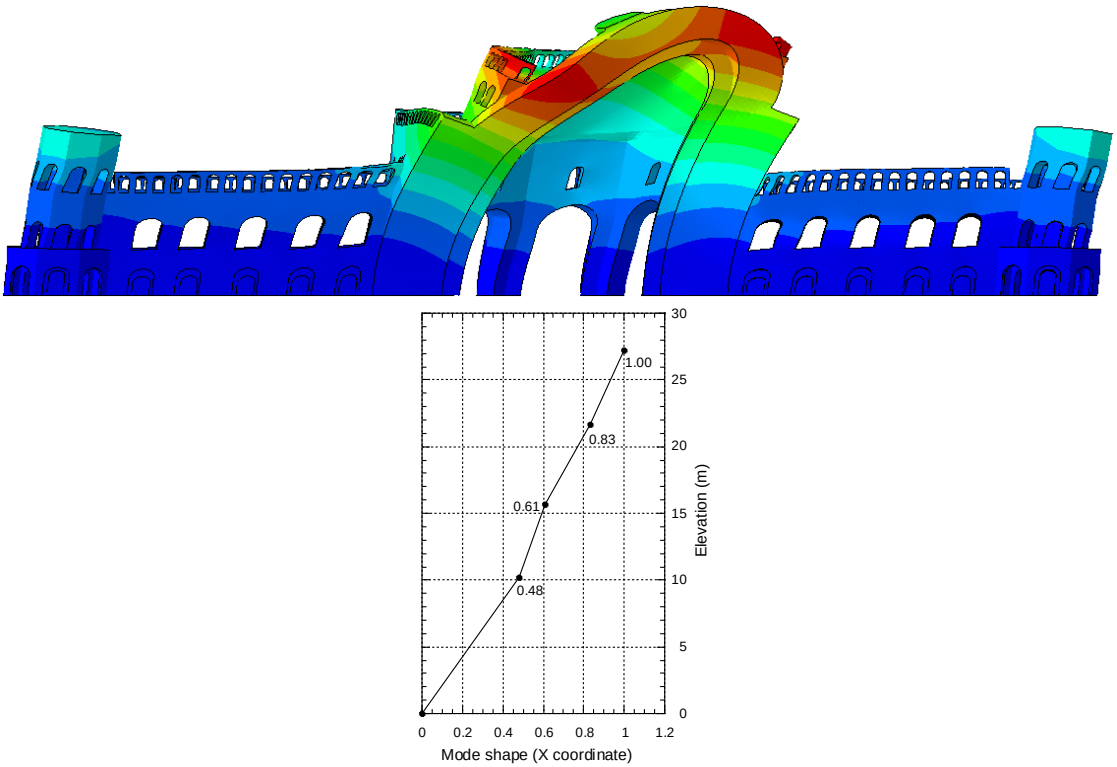

(c) Mode C: Analytical (2.56 Hz) and Experimental (3.06 Hz); MAC = 0.98

Figure 5.8. Comparison of experimental and analytical mode shapes

Figure 5.7 shows that the analytical mode shapes match very closely with experimental mode shapes, especially for Modes A and C where the MAC value is greater than 0.9. Even for Mode B, MAC value greater than 0.8 is obtained, which shows that the testing procedure as well as the equipments can be used successfully for dynamic characterization of such massive structures. Additionally, the FE model can be said to be fairly accurate as it is geometrically very close to the actual structure and closely captures all the modes obtained from experiments, with a minimum MAC value of 0.83. Further updating of FE model is not done, since that would require knowledge of local stress conditions and material properties at different locations in the monument through in-situ tests such as flat jack test etc. The difference between analytical and experimental results can be attributed to the simplifying assumptions made during modelling of the structure and the uncertainties in geometric properties and boundary conditions.

From Figure 5.8, it can be seen that Modes A and B are in the out-of-plane direction of the structure, with the first mode showing the excessive deflection of half-dome and arch in out-of-plane direction. The structure looks most vulnerable in the out-of-plane direction due to the instability of half-dome and arch in that direction. Mode B also shows deflection in the out-of-plane direction, however the deflection of structure is greater than the deflection of dome. Mode C is a translational mode in the in-plane direction of the structure. The physical description of the modes can be verified from the mass participation factors obtained from FE modal analysis also. The short structures flanking the main structure do not show any significant response, which is why response parameters of the main structure only are presented henceforth.

5.4 RESPONSE SPECTRUM ANALYSIS

The seismic demand on a structure can be evaluated using linear static analyses. This calculation can be done considering only the fundamental mode, which is justifiable for normal structures that can be idealized as lumped mass system shear building. Such structures typically have translational fundamental mode in one of their orthogonal directions and have >90% mass participation in that direction for the fundamental mode itself. However for structures, such as *Rumi Darwaza*, which are continuous mass systems, calculation based on fundamental mode will underestimate the seismic demand as higher modes will also have significant contribution. IS:1893 (BIS 2002) suggests considering significant number of modes such that the mass participation in both orthogonal directions is at least 90%. Hence, response spectrum analysis, considering all modes with natural frequency below 25 Hz, was performed to predict the seismic demand on the structure.

Response spectrum analysis gives the maximum magnitude of structural response quantities and their locations which can be compared with the locations of actual damage on the monument due to past earthquakes or natural ageing. To include the effects of self-weight, a static general step prior to frequency step is defined and gravity load is defined in this step. The 'NLGEOM' option must be enabled to include the effect of geometric non-linearity, even if non-linearity is not being modelled, to allow the

subsequent frequency and response spectrum steps to assume the state after self-weight step as their initial/base state. The response spectrum step is defined in Abaqus following the frequency step, which is the eigen-frequency extraction step. The analysis is used to obtain an approximate upper bound of peak significant response of a system to a user provided input spectrum as a function of frequency. Since *Rumi Darwaza* is situated near Gomati river basin, the response spectrum given in IS:1893 for soft soil, shown in Figure 5.9, is scaled for Zone III for Lucknow city. Dynamic characterization showed the damping ratio of fundamental mode as 3%, however this damping ratio was derived from low amplitude vibrations, and researchers (Rivera et al. 2008, Peña et al. 2010) have reported that historical masonry structures can present a damping of 8-10% when subjected to seismic excitation. Due to this reason 3% damping cannot be considered to represent the damping the structure may present in a seismic event and hence a damping ratio of 5% was considered in the analysis. Spectral acceleration was provided in terms of g with a scale factor of $0.16 \times 1.5 = 0.24$ corresponding to Zone III (ZPA = 0.16g) and Importance Factor of 1.5 for heritage structures. The structural response was evaluated for different load combinations involving dead load and earthquake loads with load factor taken as unity, and are mentioned in Table 5.5. The responses were summed as per SRSS summation rule.

Table 5.5. Load combinations considered for response spectrum analysis

	Load Combinations
LC1	$1.0DL$
LC2	$1.0\left(DL + E_y\right)$
LC3	$1.0\left(DL + E_x\right)$
LC4	$1.0\left(DL + \sqrt{E_x^2 + E_y^2}\right)$

DL: Dead Load; E_y: Excitation along Y-Direction; E_x: Excitation along X-Direction

The maximum stress and displacement and their locations are monitored during the analysis. Displacement and tensile stress (S_{11}) contours are shown in Figures 5.10 and 5.11. Maximum response values for all load combinations are summarized in Table 5.6. The base shear results for all load combinations except LC1 are mentioned in Table 5.7 which is calculated to predict the seismic demand on the structure.

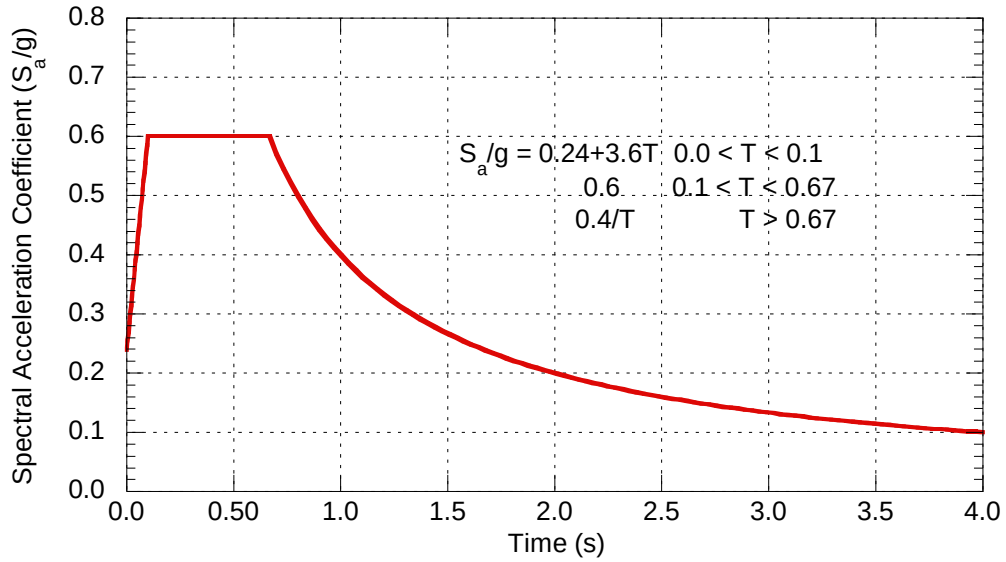

Figure 5.9. IS:1893 design response spectrum for soft soil

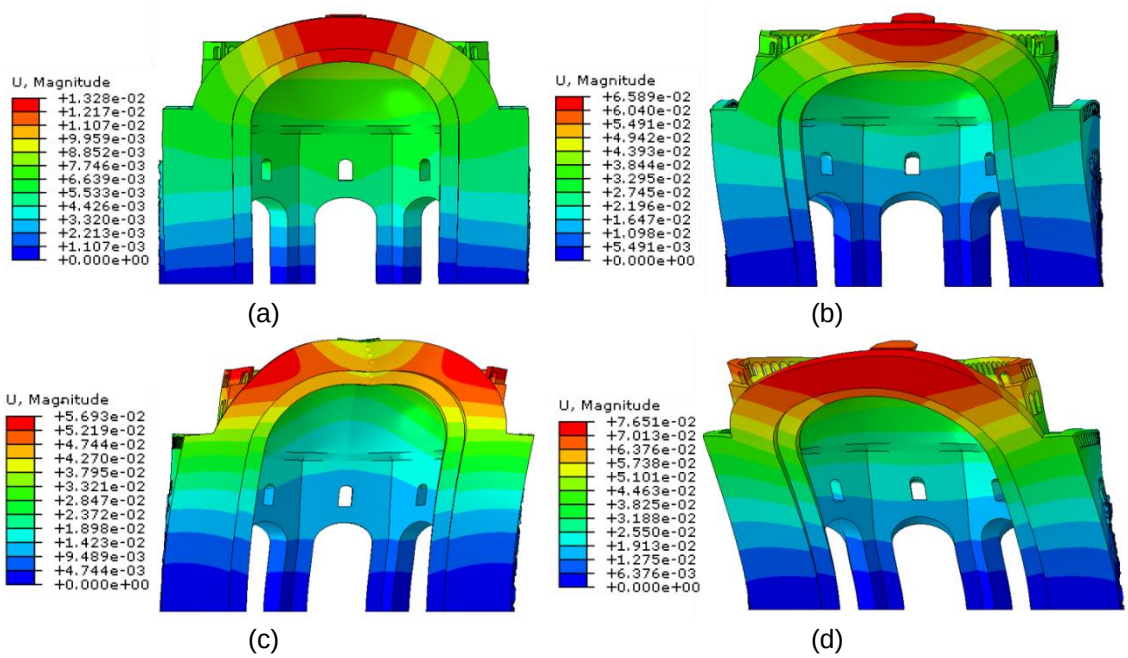

Figure 5.10. Displacement contour for load combination: (a) LC1, (b) LC2, (c) LC3 and (d) LC4 (as-is model)

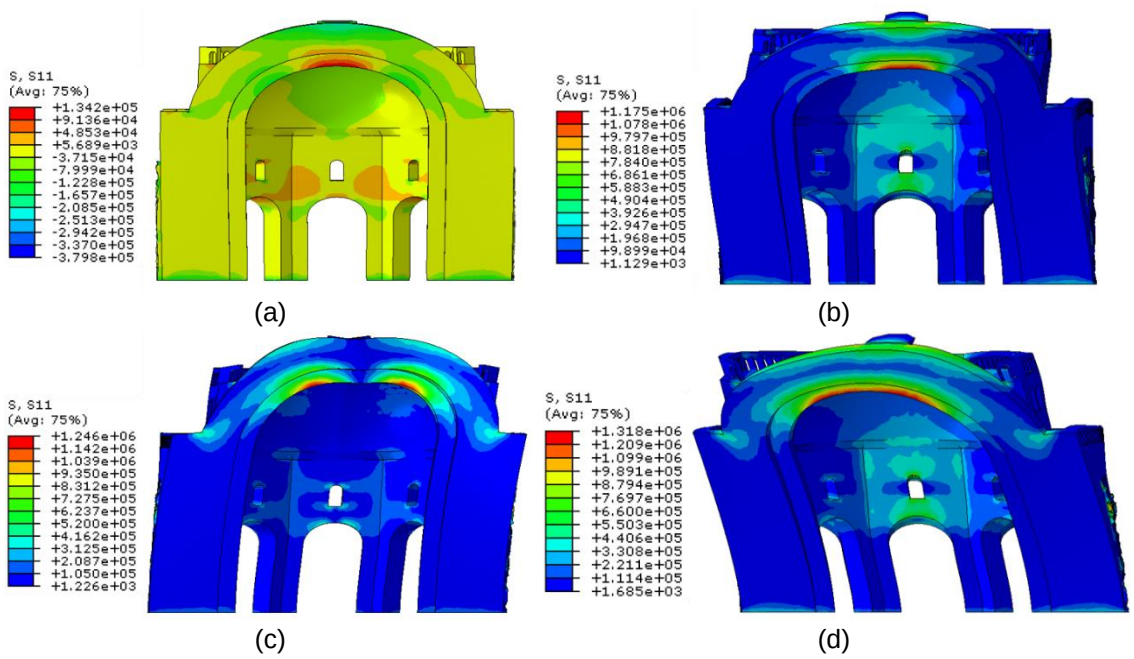

Figure 5.11. Principle tensile stress (S_{11}) contour for load combination: (a) LC1, (b) LC2, (c) LC3 and (d) LC4 (as-is model)

Table 5.6. Summary of response spectrum analysis results (as-is model)

Load Combination	Principal Stress (Compressive) (MPa)	Principal Stress (Tensile) (MPa)		Displacement (mm)		
	S_{33}	S_{11}	S_{22}	U_1	U_2	U_3
LC1	0.75	0.13	0.15	1.8	5.8	12.0
LC2	1.75	1.17	0.61	14.3	59.2	29.7
LC3	2.78	1.25	1.00	47.0	36.3	17.7
LC4	2.90	1.32	1.06	47.3	59.5	29.7

Table 5.7. Summary of response spectrum analysis base shear results (as-is model)

Load Combination	Base Shear (kN)		F_x/W	F_y/W
	F_x	F_y		
LC2	22.1×10^3	36.6×10^3	18.3	30.2
LC3	36.5×10^3	26.9×10^3	30.1	22.2
LC4	44.3×10^3	46.5×10^3	36.5	38.4

From Table 5.6, it can be seen that predicted tensile stresses exceeds the tensile capacity of masonry evaluated through experiments for all combinations with seismic loads, while the compressive stress is only slightly higher than the compressive strength for LC4. Displacement and stress contours shown in Figures 5.10 and 5.11 indicate that

half-dome and arch at the open face edge are the vulnerable elements of the structure. Damages can be observed in the same locations of high tensile stress in the actual structure also, as shown in Figure 5.12.

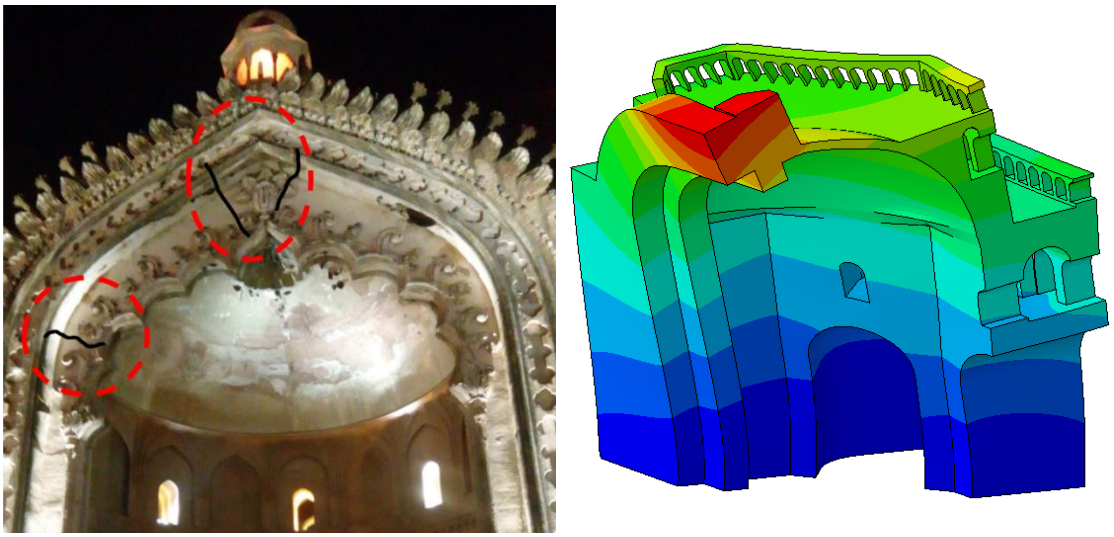

(a) (b)

Figure 5.12. (a) Cracks at dome crown and arch of Rumi Darwaza and (b) Outward bending of dome due to lack of restrain

5.5 STRENGTHENING TECHNIQUES

Response spectrum analyses showed that the stiffening arch at the open face of half-dome to be the critical structural element with high tensile stresses. Due to its instability, the half-dome is seen to deform excessively in the out-of-plane direction. Additionally, the arch-pier junction is seen to be pushed laterally outward due to local bending of half-dome as there is no lateral restraint from the missing other half. The same behaviour is seen under gravity loads (LC1) also. Based on the developed understanding of structural response, two strengthening techniques have been proposed to support and strengthen the dome/arch portion of the monument. The aim of these techniques is to restrict the movement of dome crown, to relieve the stress in the structure under its own load and to diffuse the high tensile stress in critical locations by adding structural elements increasing the structures' stiffness. Both the techniques employ latticed structure of concrete filled steel tubes (CFT). The properties of concrete and steel used in FE model are mentioned in Table 5.8.

Table 5.8. Material properties in FE modelling

Material	Density	Modulus of Elasticity	Poisson's Ratio
Steel	7850 kg/m^3	200 GPa	0.3
Concrete	2400 kg/m^3	35 GPa	0.2

5.5.1 Strengthening using Relieving Arch

First strengthening technique employs concrete filled steel tubes of 25 mm thickness. Figure 5.13 shows the frame and its position inside the structure. It is composed of a relieving arch supported by cantilever beams through truss-like members. The weight of the frame is supported by the thick masonry walls by anchoring using threaded rods grouted into the walls of structure.

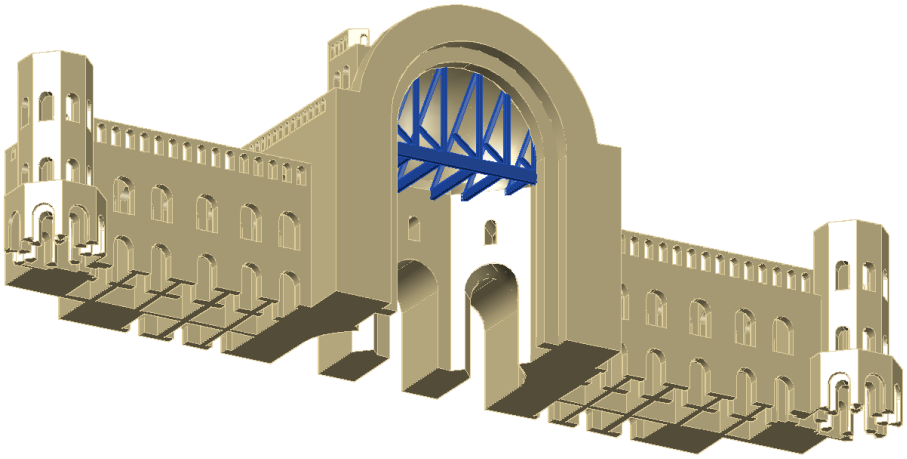

(a)

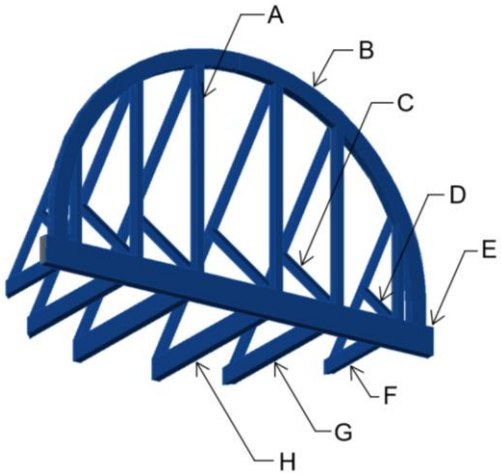

Section	Dimensions
A	300 x 350
B	350 x 600
C	250 x 300
D	250 x 250
E	350 x 1000
F	250 x 500
G	300 x 600
H	300 x 750

(b)

Figure 5.13. Strengthening using Relieving Arch (RA): (a) Position of frame inside the structure and (b) Dimensions of different members (mm)

The aim of this strengthening technique is to prop the arch/dome portion and reduce the high tensile stress concentration. Maximum response values for all load combinations are summarized in Table 5.9. The value in the bracket is the percent change (increase or decrease) in that response value as compared with the as-is structure response (Table 5.6). Displacement and principal tensile stress (S_{11}) contours are shown in Figures 5.14 and 5.15.

Table 5.9. Summary of response spectrum analysis results (strengthening model - RA)

Load Combination	Principle Compressive Stress (MPa)	Principle Tensile Stress (MPa)		Displacement (mm)		
	S_{33}	S_{11}	S_{22}	U_1	U_2	U_3
LC1	0.85 [13.3 ↑]	0.13 [0.0 ↓]	0.16 [6.7 ↑]	1.0 [44.4 ↓]	5.4 [6.9 ↓]	9.8 [18.3 ↓]
LC2	1.71 [2.3 ↓]	0.96 [17.9 ↓]	0.59 [3.3 ↓]	4.7 [67.1 ↓]	52.9 [10.6 ↓]	21.7 [26.9 ↓]
LC3	2.68 [3.6 ↓]	0.77 [38.4 ↓]	0.81 [19.0 ↓]	40.9 [13.0 ↓]	30.3 [16.5 ↓]	13.7 [22.6 ↓]
LC4	2.80 [3.4 ↓]	1.12 [15.2 ↓]	1.00 [5.7 ↓]	41.0 [13.3 ↓]	53.2 [10.6 ↓]	22.2 [25.3 ↓]

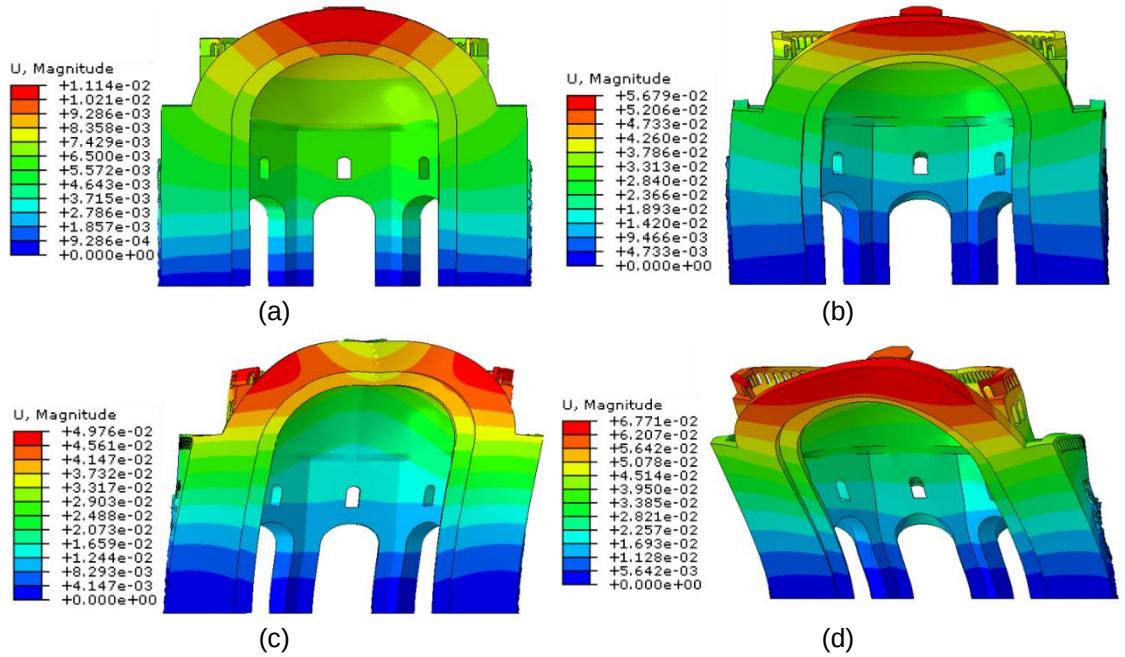

Figure 5.14. Displacement contour for load combination: (a) LC1, (b) LC2, (c) LC3 and (d) LC4 (strengthening model - RA)

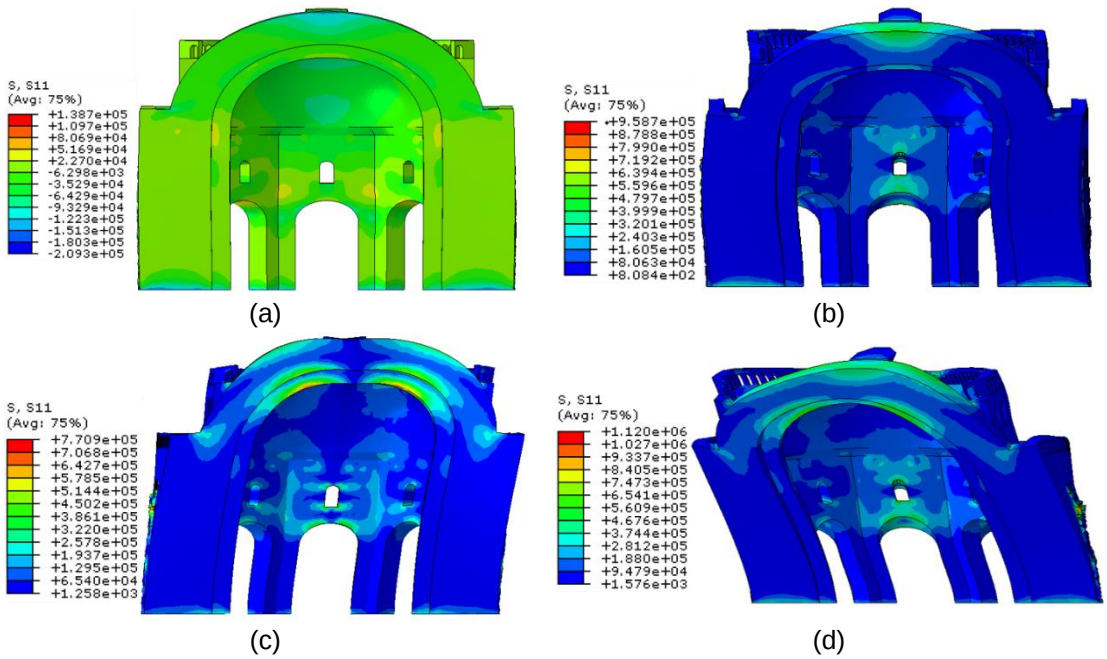

Figure 5.15. Principle tensile stress (S_{11}) contour for load combination: (a) LC1, (b) LC2, (c) LC3 and (d) LC4 (strengthening model - RA)

Efficacy of the strengthening technique can be summarized in the following points:

1. The fundamental frequency of structure increased from 2.41 Hz to 2.51 Hz.
2. The movement of dome crown and arch was reduced by 11.5%.
3. The arch-pier junctions which were seen to be pushed laterally outward due to local bending of dome in absence of lateral restraint under dead load (LC1) was considerably reduced by 44%.
4. The tensile stress concentration at the arch intrados and dome crown was significantly reduced, as can be seen by comparing Figures 5.11 and 5.15. The same is also shown in Figure 5.16. The high tensile stress was effectively reduced by ~50%.
5. All structural response values were seen to reduce, except compressive stress (S_{33}) for load combination LC1 which has increased by about 13%. However, it was still far below the compressive strength of masonry.

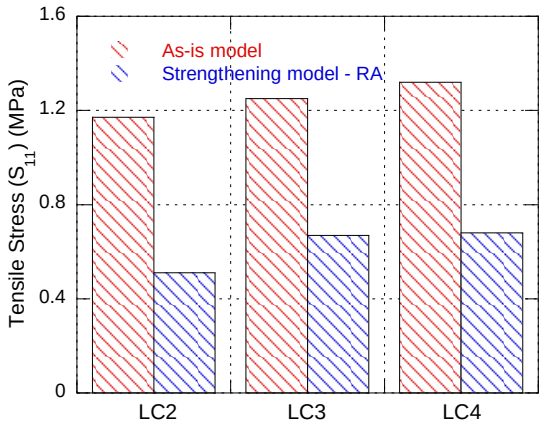

Figure 5.16. Comparison of principle tensile stress (S_{11}) between as-is model and strengthening model - RA

5.5.2 Strengthening using Relieving Half-Dome

This strengthening technique employs concrete filled steel tubes of 50 mm thickness. Figure 5.17 shows the frame and its position inside the structure. It is composed of arch beams travelling along the curvature of the dome. These arches rest on a curved beam which is tied by a horizontal member. The arches are connected with each other by cross-ribs which curve along the curvature of dome. The frame is supported by columns of composite section of 50 mm thick concrete filled steel tube. Location of columns are chosen such that traffic flow is not hindered.

The aim of this strengthening technique is to provide support to half-dome. The frame is supported by columns and hence no additional dead load is added to the structure. Maximum response values for all load combinations are summarized in Table 5.10 with the value in bracket as the percent change (increase or decrease) in that response value as compared with the as-is structure response (Table 5.6). Displacement and principle tensile stress (S_{11}) contours are shown in Figures 5.18 and 5.19.

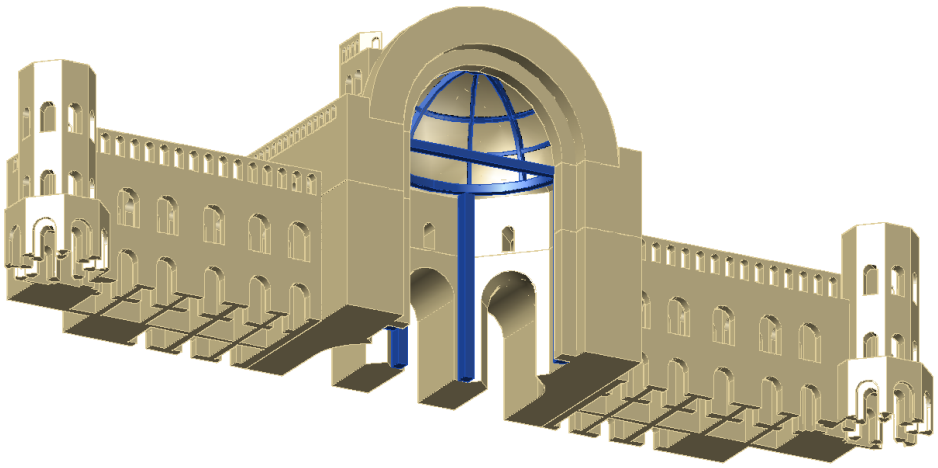

(a)

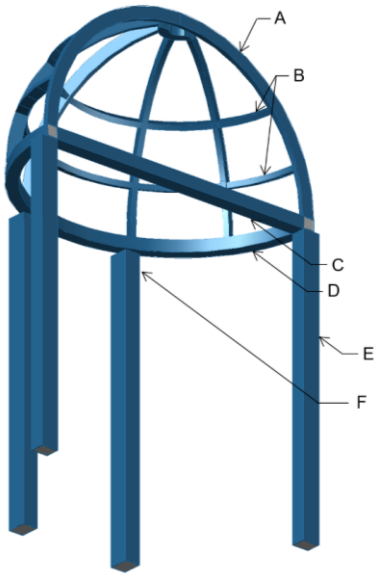

Section	Dimensions
A	250 x 600
B	250 x 550
C	600 x 750
D	600 x 600
E	750 x 900
F	800 x 1000

(b)

Figure 5.17. Strengthening using Relieving Half-Dome (RH): (a) Position of frame inside the structure and (b) Dimensions of different members (mm)

Table 5.10. Summary of response spectrum analysis results (strengthening model - RH)

Load Combination	Principle Compressive Stress (MPa)	Principle Tensile Stress (MPa)		Displacement (mm)		
	S_{33}	S_{11}	S_{22}	U_1	U_2	U_3
LC1	1.11 [48.0 ↑]	0.19 [46.2 ↑]	0.27 [80.0 ↑]	0.1 [95.0 ↓]	1.4 [75.9 ↓]	5.6 [53.3 ↓]
LC2	1.43 [18.3 ↓]	0.93 [20.5 ↓]	0.56 [8.2 ↓]	3.3 [76.9 ↓]	38.9 [34.3 ↓]	12.7 [57.2 ↓]
LC3	0.99 [64.4 ↓]	0.62 [50.4 ↓]	0.48 [52.0 ↓]	26.8 [43.0 ↓]	14.8 [59.2 ↓]	5.9 [66.7 ↓]
LC4	1.52 [47.6 ↓]	0.94 [28.8 ↓]	0.73 [31.1 ↓]	26.9 [43.1 ↓]	39.4 [33.8 ↓]	12.7 [57.2 ↓]

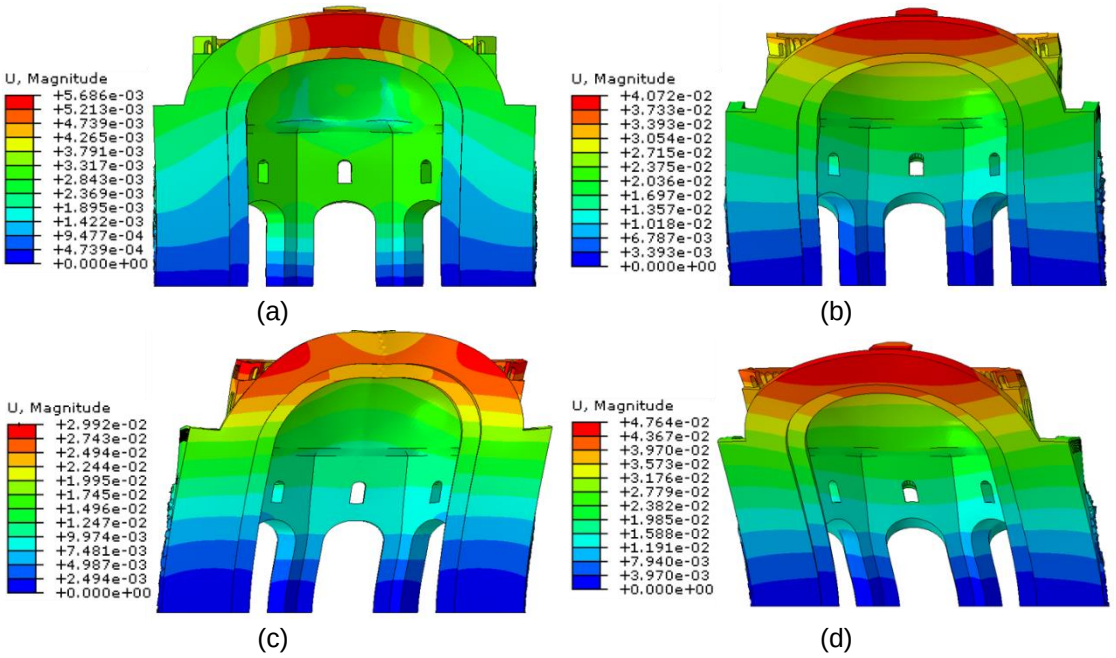

Figure 5.18. Displacement contour for load combination: (a) LC1, (b) LC2, (c) LC3 and (d) LC4 (strengthening model - RH)

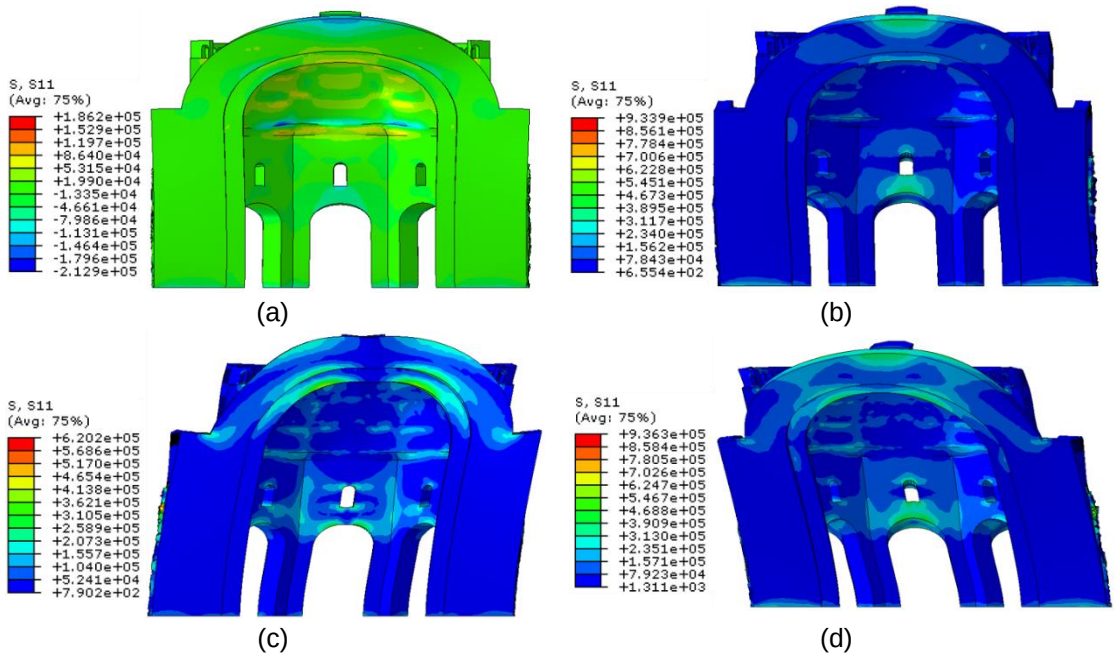

Figure 5.19. Principle tensile stress (S_{11}) contour for load combination: (a) LC1, (b) LC2, (c) LC3 and (d) LC4 (strengthening model - RH)

Efficacy of the strengthening technique can be summarized in the following points:

1. The fundamental frequency of structure increased from 2.41 Hz to 2.78 Hz, adding considerable stiffness in the out-of-plane direction.
2. The average movement of dome crown and arch was reduced by 40%.
3. The arch was now effectively tied against laterally outward thrust due to local bending of dome (LC1) with 95% reduction in outward deflection.
4. The tensile stress concentration at the arch intrados and dome crown was seen to be reduced, as can be seen by comparing Figures 5.11 and 5.19. The same is shown in Figure 5.20. The high tensile stress concentration was effectively reduced by 67%.

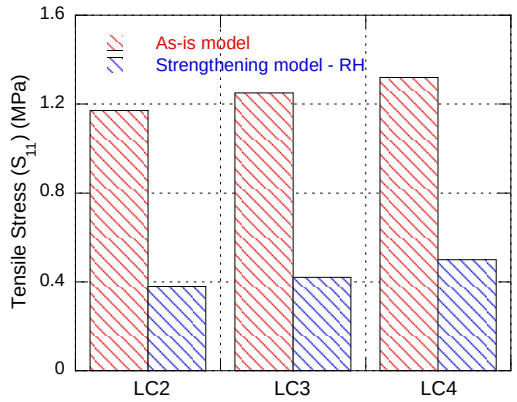

Figure 5.20. Comparison of principle tensile stress (S_{11}) between as-is model and strengthening model - RH

5. Maximum compressive stress at the base of structure was seen to reduce for all load combinations, and has been shown in Figure 5.21. This indicated that the frame was bearing some part of the weight of monument, effectively relieving the stress in the masonry walls due to structure's weight.

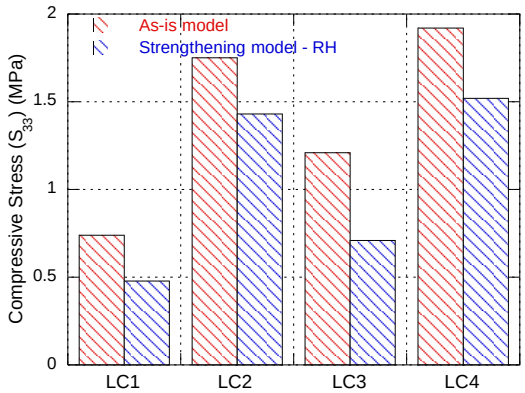

Figure 5.21. Comparison of principle compressive stress (S_{33}) between as-is model and strengthening model - RH

6. All structural response values were significantly reduced, especially deformation of dome and arch. Only stresses in load combination LC1 were seen to increase, however they were still below the strength of masonry.

5.5.3 Comparison of strengthening techniques

Both the strengthening techniques proposed are seen to serve the purpose of their application, however, there are considerable differences between the two. Comparing Tables 5.9 and 5.10, it can be clearly seen that the strengthening technique using Relieving Half-Dome has considerable advantages in terms of reduction of structural response. The movement of dome and arch is reduced 4 times more as compared to strengthening technique using Relieving Arch. The tensile stresses are also half for strengthening model RH as compared with model RA. Additionally, the frame in Model-RH is self-supported which instead of adding more load, as seen for frame in Model-RA, is seen to relieve the structure from its own load. On the other hand, strengthening technique RA offers advantages in terms of lesser cost of materials and fabrication. The amount of steel and concrete used and fabrication of greater number of curved beams in Model-RH will lead to higher costs. Both these strengthening techniques should be accompanied by sealing of major cracks by injecting mortar of suitable composition compatible with original mortar.

5.6 SUMMARY

The steps involved in FE modelling of structure of *Rumi Darwaza* have been explained. Mode shapes obtained from modal analysis were seen to closely match with the mode shapes obtained from dynamic characterization with the lowest MAC value of 0.83. The FE model was updated based on the experimental results to get a better estimate of global stiffness. Seismic analysis of the structure revealed that the dome crown and stiffening arch at the front face are the critical structural elements with high tensile stress concentration on the inside of the arch, even under dead loads. Compressive stresses were seen to marginally exceed the masonry compressive strength. However, tensile stresses were seen to be significantly higher than tensile strength of masonry. Two strengthening techniques based on the understanding of structural response have been

proposed. Their impact on the structural behaviour is seen through FE modelling. Strengthening technique RA was seen to prop the arch/dome portion and reduce the high tensile stress. Strengthening technique RH aimed to provide support to half-dome and restrict its movements under seismic loads. Both the techniques were seen to effectively serve their purpose. However, strengthening technique RH offers several advantages over the RA in terms of lower tensile stress, reduced displacement of dome and arch, bearing some part of structure's weight and adding considerable stiffness in out-of-plane direction.

CHAPTER 6

SUMMARY AND CONCLUSIONS

6.1 SUMMARY

Historical monuments are cultural assets worth preserving. They portray the architectural heritage and cultural wealth of a civilization. It is of paramount importance that these monuments be preserved and protected for future generations. Seismic assessment of historic monuments is very challenging task and requires considerable expertise because each monument presents its own unique problems. Past earthquakes in India has highlighted the deficient performance of our heritage structures. In the current study, the historic masonry structure of a monument *Rumi Darwaza* of Lucknow, a hallmark of 18th century Awadhi architecture, is assessed for its seismic performance.

First, the dynamic characteristics, such as natural frequencies, mode shapes and damping ratios, are extracted through ambient and forced vibration experiments. These modal parameters are required for the realistic numerical simulation. Additionally, laboratory experiments were conducted to characterize the mechanical properties of Lakhauri bricks and lime surkhi mortar, as well as masonry assemblages which have been used in *Rumi Darwaza* and other monuments in Lucknow of that era.

A detailed Finite Element (FE) model, closely resembling the original structure, was developed to understand the structural behaviour under gravity and seismic loads. Dynamic characterization results were used for validating the FE model. Response Spectrum analyses were performed to identify the critical structural elements. Based on the developed understanding, two strengthening techniques to mitigate the risk posed to the structure by seismic events were proposed which use concrete filled hollow steel tubes to support the dome-arch from the inside.

6.2 RESULTS AND CONCLUSIONS

Salient results and conclusions which can be drawn from the present study are briefly discussed below:

- Ambient and forced vibration testing for extracting the modal parameters of *Rumi Darwaza* showed three modes of the structure identified at 2.41 Hz, 2.78 Hz and 3.06 Hz. Damping ratios of the three modes were estimated at 2.7%, 2.3% and 1.8%.
- Field vibration testing involved the use of a small linear shaker which showed that it can be used successfully for this application even though the maximum force output of the shaker is very low (133 N).
- Average compressive strength for fully baked and partially baked bricks was evaluated as 36.2 MPa and 19.0 MPa respectively.
- Formulated lime-surkhi mortar was seen to have a very low compressive strength of 1.06 MPa. This low strength was due to incomplete carbonation reaction which takes much longer than 28 days to complete for such lime-surkhi mortars. However the mortar displayed highly deformable nature.
- Compressive strength of standard stack bond and multi-wythe masonry prisms were found to be 2.76 MPa and 2.04 MPa, respectively. Compressive strength for multi-wythe prisms was about 75% of compressive strength of stack bond prisms.
- The tensile strength of masonry was evaluated to be a low value of 4.7% of the compressive strength of masonry.
- Mode shapes obtained from modal analysis of FE idealization were seen to closely match with the mode shapes obtained from field vibration measurements.
- Seismic analysis of the structure revealed the dome crown and stiffening arch at the front face to be the critical structural elements. Tensile stress concentration on the inside of the arch was predicted even under dead loads.
- For the different load combinations considered, compressive stresses was seen to exceed slightly the masonry compressive strength only in the biaxial seismic load combination. However, tensile stresses greatly exceeded the material's tensile strength.

- Strengthening technique using Relieving Arch composed of arch supported by cantilever beams through truss-like members aimed to prop the arch/dome portion and reduce the high tensile stress. The high tensile stresses were effectively reduced by ~50%.
- Strengthening technique using Relieving Half-Dome composed of arch beams travelling along the curvature of the dome aimed to provide support to half-dome and restrict its movements under seismic loads. The high tensile stress concentration was effectively reduced by 67% and the movement of dome crown and arch was reduced by 40%.
- Strengthening technique RH offered several advantages over technique RA in terms of lower tensile stress, reduced displacement of dome and arch, bearing some part of structure's weight and adding considerable stiffness in out of plane direction.

6.3 RECOMMENDATIONS FOR FUTURE WORK

Based on the experience gained during this research work, following recommendations, as future extensions of this work, can be made:

- In-situ flat jack testing, which is only a slightly destructive technique, should be conducted to obtain the stress-strain characteristics and compressive strength of masonry. It can also be used to find the masonry mortar joint shear strength. The slight damage caused can be easily repaired after testing by filling the joints with mortar.
- Formulated lime surkhi mortar used in preparing the masonry assemblages should be further tested for its chemical, mechanical and aesthetical compatibility with original material. Additionally, the binder-aggregate ratio and grain size distribution of formulated mortar should be chemically evaluated to cross-check and compare with that used in monument masonry mortar.
- The stress-strain curve obtained from flat-jack testing should be incorporated in FE modelling to carry out static and dynamic non-linear analyses to predict the load carrying capacity and compare it with the seismic demand imposed on the structure according to IS 1893, Zone III design response spectrum for Lucknow.

- The impact of strengthening techniques on supporting the dome-arch portion can be more accurately understood through non-linear analyses. Based on that analysis, sections of concrete filled hollow steel tubes can be designed. A comprehensive strengthening plan can be recommended to safeguard the structure against potential future earthquakes.

LIST OF REFERENCES

A Glimpse of the Monumental Heritage of Lucknow. (n.d.). Retreived August, 2016 from http://asilucknowcircle.nic.in.

Ahmed, F. (1998, September 28). "Crumbling history." *India Today*, Retreived August, 2016 from http://indiatoday.intoday.in.

Allemang, R. J., and Brown, D. L. (1982). "A correlation coefficient for modal vector analysis." *Proceedings of the 1st International Modal Analysis Conference*, SEM, Orlando, 1, 110-116.

American Society for Testing and Materials (ASTM). (2014). *Standard Test Methods for Sampling and Testing Brick and Structural Clay Tile*, ASTM C67-14, West Conshohocken, PA.

American Society for Testing and Materials (ASTM). (2015). *Standard Test Method for Diagonal Tension (Shear) in Masonry Assemblages*, ASTM E519/E519M-15, West Conshohocken, PA.

American Society for Testing and Materials (ASTM). (2016). *Standard Test Method for Compressive Strength of Hydraulic Cement Mortars (Using 2-in. or [50-mm] Cube Specimens)*, ASTM C109/C109M-16a, West Conshohocken, PA.

American Society for Testing and Materials (ASTM). (2016). *Standard Test Method for Compressive Strength of Masonry Prisms*, ASTM C1314-16, West Conshohocken, PA.

Baronio, G., Binda, L., and Lombardini, N. (1997). "The role of brick pebbles and dust in conglomerates based on hydrated lime and crushed bricks." *Construction and Building Materials*, 11(1), 33-40.

Betti, M., and Vignoli, A. (2008). "Modelling and analysis of a Romanesque church under earthquake loading: Assessment of seismic resistance." *Engineering Structures*, 30(2), 352-367.

Binda, L., Baronio, G., and Tedeschi, C. (2000). "Experimental study on the mechanical role of thick mortar joints in reproduced byzantine masonry." *Historic Mortars: Characteristics and Tests*, 227-247.

Binda, L., Tedeschi, C., and Baronio, G. (1999). "Mechanical behaviour at different ages, of masonry prisms with thick mortar joints reproducing a Byzantine masonry." *Proceedings of the 8th North American Masonry Conference*, University of Austin, TX, USA.

Bose, A. (2012, October 8). "14 years hence, Rumi Darwaza inching towards sunset point.", Retreived August, 2016 from http://taurian123.blogspot.in.

Brincker, R., and Ventura, C. (2015). *Introduction to Operational Modal Analysis.* John Wiley & Sons, West Sussex, United Kingdom.

Brincker, R., Zhang, L., and Andersen, P. (2000). "Modal identification from ambient responses using frequency domain decomposition." *Proc. of the 18th International Modal Analysis Conference (IMAC)*, San Antonio, Texas.

Bureau of Indian Standards (BIS). (1981). *Indian Standard Code of Practice for preparation and use of Masonry Mortars*, IS 2250, 1st Rev., New Delhi, India.

Bureau of Indian Standards (BIS). (2002). *Indian Standard Criteria for Earthquake Resistant Design of Structures – Part 1: General provisions and buildings*, IS 1893, 5th Rev., New Delhi, India.

Chandra, S. (2003). *History of architecture and ancient building materials in India: Part I & Part II.* Tech Books International, New Delhi, India.

Chopra, A. K. (1995). *Dynamics of structures* (Vol. 3). Prentice Hall, New Jersey.

Dhanpal, S. (2009). "Evaluation of masonry materials and half-dome structure of lucknow monuments for seismic resistance." *Masters' Thesis*, Dept. of Civil Engineering, Indian Institute of Technology Kanpur, Kanpur, India.

Erdogmus, E., Boothby, T. E., and Smith, E. B. (2007). "Structural appraisal of the Florentine Gothic construction system." *Journal of Architectural Engineering*, 13(1), 9-17.

Friswell, M., and Mottershead, J. E. (1995). *Finite element model updating in structural dynamics* (Vol. 38). Springer Science & Business Media, Netherlands.

Gentile, C., and Saisi, A. (2007). "Ambient vibration testing of historic masonry towers for structural identification and damage assessment." *Construction and Building Materials*, 21(6), 1311-1321.

Güngör, I. H. (1988). "The dome in Sinan's works." *Proceedings of the IASS-MSU International Symposium*, 61-92.

Gupta, D. (2001). "INTACH Field Report: 26th January 2001 Gujarat (India) Earthquake", Retreived August, 2016 from http://conservationtech.com.

HyperWorks. (2014). "HyperMesh User's Guide.", Retreived August, 2016 from http://www.altairhyperworks.com.

Jaishi, B., Ren, W.-X., Zong, Z.-H., and Maskey, P. N. (2003). "Dynamic and seismic performance of old multi-tiered temples in Nepal." *Engineering Structures*, 25(14), 1827-1839.

Kaushik, H. B., Rai, D. C., and Jain, S. K. (2007). "Stress-strain characteristics of clay brick masonry under uniaxial compression." *Journal of Materials in Civil Engineering*, 19(9), 728-739.

Lagomarsino, S., and Cattari, S. (2015). "PERPETUATE guidelines for seismic performance-based assessment of cultural heritage masonry structures." *Bulletin of Earthquake Engineering*, 13(1), 13-47.

Lanas, J., and Alvarez-Galindo, J. I. (2003). "Masonry repair lime-based mortars: factors affecting the mechanical behavior." *Cement and Concrete Research*, 33(11), 1867-1876.

Malhotra, A. (2013, February 28). "Can Lucknow monuments survive quake?" *The Times of India*, Retreived August, 2016 from http://timesofindia.indiatimes.com.

Maravelaki-Kalaitzaki, P., Bakolas, A., & Moropoulou, A. (2003). "Physico-chemical study of Cretan ancient mortars." *Cement and concrete research*, 33(5), 651-661.

Maravelaki-Kalaitzaki, P. (2007). "Hydraulic lime mortars with siloxane for waterproofing historic masonry." *Cement and concrete research*, 37(2), 283-290.

McDaniel, C. C., and Archer, G. C. (2010). "Full-scale, Real-time Building Dynamics Laboratory." *9th US National and 10th Canadian Conference on Earthquake Engineering.*

Moropoulou, A., Cakmak, A. S., Biscontin, G., Bakolas, A., & Zendri, E. (2002). "Advanced Byzantine cement based composites resisting earthquake stresses: the crushed brick/lime mortars of Justinian's Hagia Sophia." *Construction and Building Materials*, 16(8), 543-552.

Moropoulou, A., Bakolas, A., and Anagnostopoulou, S. (2005). "Composite materials in ancient structures." *Cement and Concrete Composites*, 27(2), 295-300.

Masonry Standards Joint Committee (MSJC). (2002). *Building Code Requirements for Masonry Structures.* ACI 530-02/ASCE 5-02/TMS 402-02, The Masonry Institute, Boulder, American Concrete Institute, ASCE, Farmington Hills, MI, Reston, VA.

Niedbal, N. (1984). "Analytical determination of real normal modes from measured complex responses." *Proceedings of the 25th Structures, Structural Dynamics and Materials Conference*, Palm Springs, CA, 292-295.

Padhaye, M. G., Vinayaka, M. R., and Hasabnis, S. V. (1964). "Design of lime-surkhi mortar mixes for masonry." *Symposium on pozzolons – Their survey manufacture and utilization*, MERI, Nashik.

Parloo, E. (2003). "Application of frequency-domain system identification techniques in the field of operational modal analysis." *Doctoral Thesis*, Vrije Universiteit Brussel, Belgium.

Pastor, M., Binda, M., and Harčarik, T. (2012). "Modal assurance criterion." *Procedia Engineering*, 48, 543-548.

Peña, F., Lourenço, P. B., Mendes, N., and Oliveira, D. V. (2010). "Numerical models for the seismic assessment of an old masonry tower." *Engineering Structures*, 32(5), 1466-1478.

Peña, F., and Manzano, J. (2015). "Dynamical characterization of typical Mexican colonial churches." *Seismic Assessment, Behavior and Retrofit of Heritage Buildings and Monuments* 297-319, Springer.

Psycharis, I. N., Pantazopoulou, S. J., and Papadrakakis, M. (2015). *Seismic Assessment, Behavior and Retrofit of Heritage Buildings and Monuments*, Vol. 37, Springer, Berlin, Germany.

Rai, D. C., and Dhanapal, S. (2013). "Bricks and mortars in Lucknow monuments of c. 17-18 century." *Current Science*, 104(2), 238-244.

Rai, D. C., and Dhanapal, S. (2015a). "Mineralogical and Mechanical Properties of Masonry and Mortars of the Lucknow Monuments Circa the 18th Century." *International Journal of Architectural Heritage*, 9(3), 300-309.

Rai, D. C., Raj, S. B., and Sagar, S. L. (2015b). "Performance of residential buildings during the M 7.8 Gorkha (Nepal) earthquake of 25 April 2015." *Current Science*, 109(11), 2126-2135.

Rai, D. C., Singhal, V., Mondal, G., Parool, N., Pradhan, T., and Mitra, K. (2012). "The M 6.9 Sikkim (India--Nepal Border) earthquake of 18 September." *Current Science*, 102(10), 1437.

Ramos, L. F., Marques, L., Lourenço, P. B., De Roeck, G., Campos-Costa, A., and Roque, J. (2010). "Monitoring historical masonry structures with operational modal analysis: two case studies." *Mechanical Systems and Signal Processing*, 24(5), 1291-1305.

Rendon, A. R. (2011). "Determination of The Modal Parameters of A Five Story Reinforced Concrete Structure Using Ultra-Low Level Excitation And Computational Analysis." *Masters' Thesis,* Dept. of Architecture and Environmental Design, California Polytechnic State University, San Luis Obispo, California.

Rilem, T. C. (1994). *LUM B6 Diagonal tensile strength tests of small wall specimens*. RILEM Recommendations for the testing and use of constructions materials, 488-489.

Rivera, D., Meli, R, Sánchez, R., and Orozco, B. (2008). "Evaluation of the measured seismic response of the Mexico City Cathedral." *Earthquake Engineering & Structural Dynamics*, 37(10), 1249-1268.

Roca, P., González, J., Oñate, E., and Lourenço, P. (1998). "Experimental and numerical issues in the modelling of the mechanical behaviour of masonry." *Structural Analysis of Historical Constructions II.* CIMNE, Barcelona.

Stefanidou, M., Pachta, V., Konopissi, S., Karkadelidou, F., & Papayianni, I. (2014). "Analysis and characterization of hydraulic mortars from ancient cisterns and baths in Greece." *Materials and Structures*, 47(4), 571-580.

Sharda, S. (2012, November 27). "Rumi Darwaza: Monumental epitaph awaits bearers of History." *The Times of India*, Retreived August, 2016 from http://timesofindia.indiatimes.com.

Simulia. (2011). *ABAQUS Analysis User's Manual, Version 6.13-3.* Dassault Systemes, Providence, RI, USA.

Singhal, V. (2014). "Effect of toothing and openings on bi-directional seismic behaviour of confined masonry walls." *Doctoral Thesis*, Dept. of Civil Engineering, Indian Institute of Technology Kanpur, Kanpur, India.

Taliercio, A., and Binda, L. (2007). "The Basilica of San Vitale in Ravenna: Investigation on the current structural faults and their mid-term evolution." *Journal of Cultural Heritage*, 8(2), 99-118.

Teutonico, J. M., McCaig, I., Burns, C., and Ashurst, J. (1993). "The Smeaton project: factors affecting the properties of lime-based mortars." *APT bulletin*, 25(3/4), 32-49.

UNESCO. (2001). "UNESCO mission to Gujarat, India, for the conservation of earthquake-damaged cultural properties.", Retreived August, 2016 from http://conservationtech.com.

Vacher, P., Jacquier, B., and Bucharles, A. (2010). "Extensions of the MAC criterion to complex modes." *Proceedings of ISMA International Conference on Noise and Vibration Engineering,* Leuven, Belgium.

Verhosek, J. T. (2006). "Characterization and Assessment of Argamasa Applied as a Water-Resistant Masonry Surface Finish on the Dome of the Capilla de Nuestra Señora del Rosario Iglesia San José , San Juan, Puerto Rico." *Master's Thesis,* The School of Design, University of Pennsylvania, Philadelphia, Pennsylvania.

Vintzileou, E., and Miltiadou-Fezans, A. (2008). "Mechanical properties of three-leaf stone masonry grouted with ternary or hydraulic lime-based grouts." *Engineering Structures*, 30(8), 2265-2276.

Welch, P. D. (1967). "The use of fast Fourier transform for the estimation of power spectra: A method based on time averaging over short, modified periodograms." *IEEE Transactions on audio and electroacoustics*, 15(2), 70-73.

APPENDIX A

FREQUENCY DOMAIN DECOMPOSITION ALGORITHM – MATLAB IMPLEMENTATION

The following MATLAB code was used for estimating the modal parameters for dynamic characterization of the monument structure. The code is an implementation of Frequency Domain Decomposition (FDD) Algorithm.

```
% Initialization
close all
clear
clc
% ------------------------------------------------------

file=['**.lvm'];
[t,velA,velB,velC,velD,acc_sh]=textread(strcat(file,'.lvm'),'%f
%f %f %f %f %f','headerlines',23);

Ts=t(2,1)-t(1,1);
Fs = 1/Ts;
fnyq = Fs/2;
fcutin=0.3;
fcutoff=15;
window_length=8192*16;
overlap_length=window_length*(1/2);
f_points=window_length;

b = fir1(8192,[fcutin/fnyq fcutoff/fnyq],'bandpass');
velA=filtfilt(b,1,velA);
velB=filtfilt(b,1,velB);
velC=filtfilt(b,1,velC);
velD=filtfilt(b,1,velD);
response = [velA,velB,velC,velD];

fig=1;


% ------------------------------------------------------%
Compute Power Spectral as per Welch's Modified Periodogram
Method
% PSD function computes the cross power spectral density matrix
% Uses Hanning window for preventing spectral leakage

for j=1:size(response,2)
```

```
[PSD(:,j),W]=pwelch(response(:,j),hanning(window_length),overlap
_length,f_points,Fs);
end

figure(fig)
title('Power Spectral Density')
plot(W,PSD)
hold on
xlabel('Frequency (Hz)')
ylabel('PSD (m/s)^2/Hz')
grid on
xlim([2 3.5])
legend('Vel A', 'Vel B','Vel C','Vel D')
fig=fig+1;

% ---------------------------------------------------------%
Compute Power Spectral Density (PSD) matrix.
% CPSD function computes the cross power spectral density matrix

for I=1:size(response,2)
    for J=1:size(response,2)

[CPSD(I,J,:),F(I,J,:)]=cpsd(response(:,I),response(:,J),hanning(
window_length),overlap_length,f_points,Fs);
    end
end
Frequencies(:,1)=F(1,1,:);

figure(fig)
title('Cross Power Spectral Density')
data1 = abs(CPSD(3,1,:)); % CPSD between Vel C and Vel A
data1 = data1(:);
data2 = abs(CPSD(3,2,:)); % CPSD between Vel C and Vel B
data2 = data2(:);
data3 = abs(CPSD(4,1,:)); % CPSD between Vel D and Vel A
data3 = data3(:);
data4 = abs(CPSD(4,2,:)); % CPSD between Vel D and Vel B
data4 = data4(:);
plot(W,data1)
hold on
plot(W,data2)
plot(W,data3)
plot(W,data4)
xlabel('Frequency (Hz)')
ylabel('CPSD (m/s)^2/Hz')
grid on
xlim([2 3.5])
legend('Vel C with Vel A','Vel C with Vel B','Vel D with Vel
A','Vel D with Vel B')
fig = fig +1;
```

```
phase_angle_1 = abs(angle(CPSD(3,1,:)))/pi; % Phase angle
between Vel C and Vel A normalized by pi
phase_angle_1 = phase_angle_1(:);
phase_angle_2 = abs(angle(CPSD(3,2,:)))/pi; % Phase angle
between Vel C and Vel B normalized by pi
phase_angle_2 = phase_angle_2(:);
phase_angle_3 = abs(angle(CPSD(4,1,:)))/pi; % Phase angle
between Vel D and Vel A normalized by pi
phase_angle_3 = phase_angle_3(:);
phase_angle_4 = abs(angle(CPSD(4,2,:)))/pi; % Phase angle
between Vel D and Vel B normalized by pi
phase_angle_4 = phase_angle_4(:);

figure(fig)
title('Cross Spectral Phase Angle ')
subplot(2,2,1)
plot(Frequencies,phase_angle_1)
subplot(2,2,2)
plot(Frequencies,phase_angle_2)
subplot(2,2,3)
plot(Frequencies,phase_angle_3)
subplot(2,2,4)
plot(Frequencies,phase_angle_4)
xlabel('Frequency (Hz)')
ylabel('Phase Difference (x \pi radians)')
grid on
xlim([2 3.5])
ylim([0 1])
legend('Vel C with Vel A','Vel C with Vel B')
fig = fig +1;


% % ------------------------------------------------------% %
Modal Analysis
% % Compute SVD of PSD Matrix at each frequency
for I=1:size(CPSD,3)
    [u(:,:,i) , s(:,:,i) , v(:,:,i)] = svd(CPSD(:,:,i));
    s1(i) = s(1,1,i); % First eigen values
    modeshape(:,i)=u(:,1,i); % Mode shape
end

% % Plot first singular values of the PSD matrix
figure(fig)
plot(Frequencies,s1)
xlim([2 3.5])
xlabel('Frequency (Hz)')
ylabel('1^s^t Singular values of the PSD matrix ')
grid on
```

```
% % ------------------------------------------------------% %
Mode shape calculation
% % ------------------------------------------------
Fp=[];% Frequencies corresponding to peak
NumPeaks=1;
k=0;
[~,P1]=min(abs(Frequencies-2.1));
[~,P2]=min(abs(Frequencies-2.6));
[~,B]=max(s1(P1:P2));
Max=B+P1-1; % Index of natural frequency

Fp(end+1,:)=[Max,Frequencies(Max)];
% % Identified modal frequency
Frq=Fp(:,2);

% % % Compute mode shape for selected peak
[U, ~, ~] = svd(CPSD(:,:,Fp(1)));
mode_shape = U(:,1);

% % ------------------------------------------------------% %
Results
display('Natural Frequency:')
disp(Frq)
% Print Mode shapes
display('Mode Shape')
disp(mode_shape)



% ------------------------------------------------------%
Logarithmic Decreement Method
% ------------------------------------------------------
modematch = zeros(length(Frequencies),size(Fp,1));
MAC_acceptance = 0.9;

for k = Fp(1):length(Frequencies)
    A = (norm(u(:,1,k).'*conj(mode_shape)))^2;
    B =
(u(:,1,k).'*conj(u(:,1,k)))*(mode_shape.'*conj(mode_shape));
    MAC = A/B;
    if MAC >= MAC_acceptance
        modematch(k,1) = s(1,1,k);
    elseif MAC < MAC_acceptance;
        break
    end
end
hold on
y=get(gca,'ylim');
plot([Frequencies(k+1) Frequencies(k+1)],y,'LineStyle','-.',
'Color',[0 0 1])
```

```
for k = Fp(1)-1:-1:1;
    A = (norm(u(:,1,k).'*conj(mode_shape)))^2;
    B =
(u(:,1,k).'*conj(u(:,1,k)))*(mode_shape.'*conj(mode_shape));
    MAC = A/B;
    if MAC >= MAC_acceptance
        modematch(k,1) = s(1,1,k);
    elseif MAC < MAC_acceptance;
        break
    end
end
plot([Frequencies(k-1) Frequencies(k-1)],y,'LineStyle','-.',
'Color',[0 0 1])
fig = fig +1;


% Inverse Fast Fourier Transform
% -------------------------------------------------------
correlation = (ifft(modematch,'symmetric'));
corr_norm = (correlation-mean(correlation))/correlation(1);

figure(fig)
plot(t(1:2:2*5000),(corr_norm(1:5000)))
grid on
xlabel('Time (s)')
fig = fig +1;
[peak_mag , loc_peak] = findpeaks(abs(corr_norm(1:6000)));
fig = fig +1;

delta = zeros(length(peak_mag),1);
for i = 1:length(peak_mag)
    delta(i,1) = (2/i) * log(corr_norm(1,1)/abs(peak_mag(i)));
end

j= [1,16];
Y_delta = delta.*loc_peak + 2*log(abs(peak_mag));

figure(fig)
plot(loc_peak(j(1):j(2)), Y_delta(j(1):j(2)))
P1 = polyfit(loc_peak(j(1):j(2)),Y_delta(j(1):j(2)),1);
Y1 = P1(1)*loc_peak + P1(2);
damping_ratio = 1/sqrt(1+(2*pi/P1(1))^2)
```

APPENDIX B

TIME-HISTORY DATA RECORDS

Time history records and their auto spectral density plots are presented here for measurements made at fixed frequency (2.41 Hz) for Mode A for all test setups.

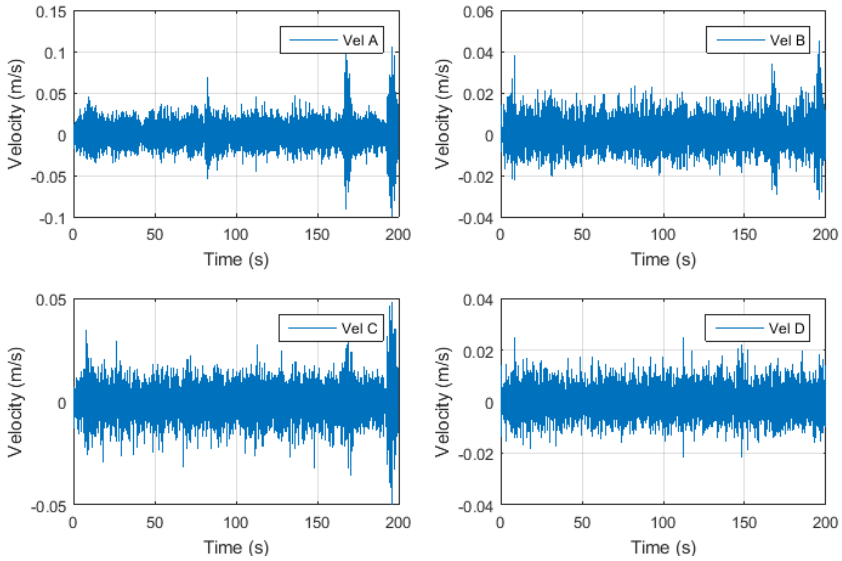

(a)

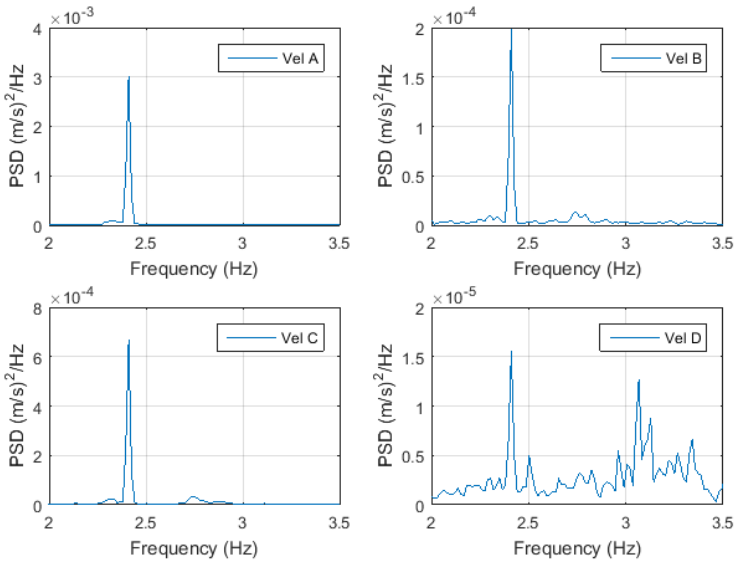

(b)

Figure B.1. Measurement record from Test setup *T1*: (a) Time-history and (b) Auto Spectral Density plots (Excitation in Y-direction)

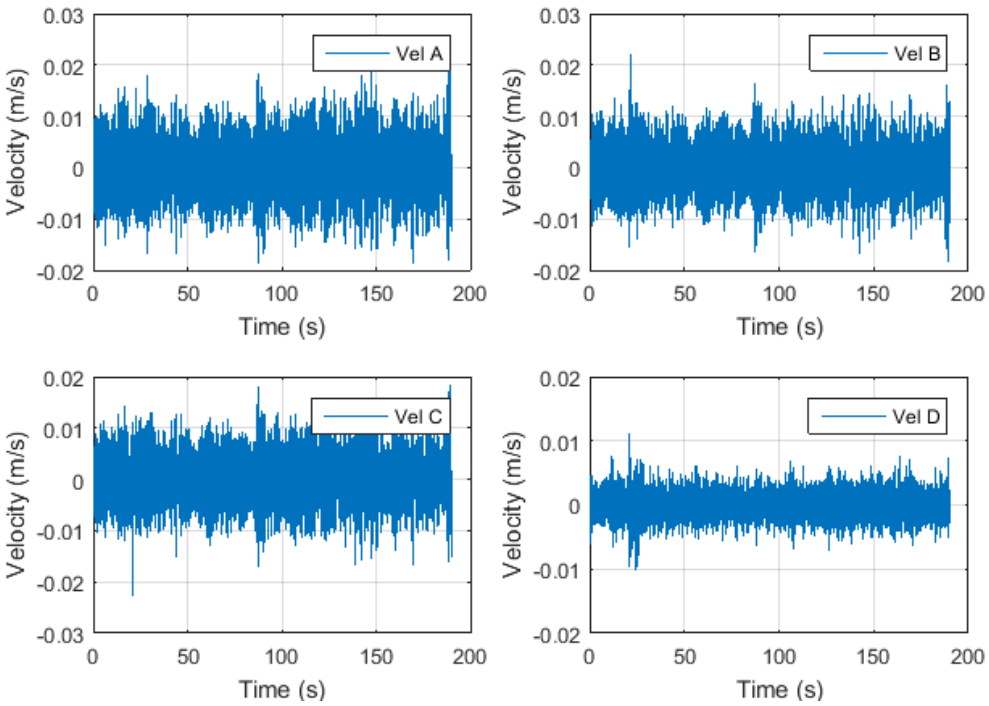

(a)

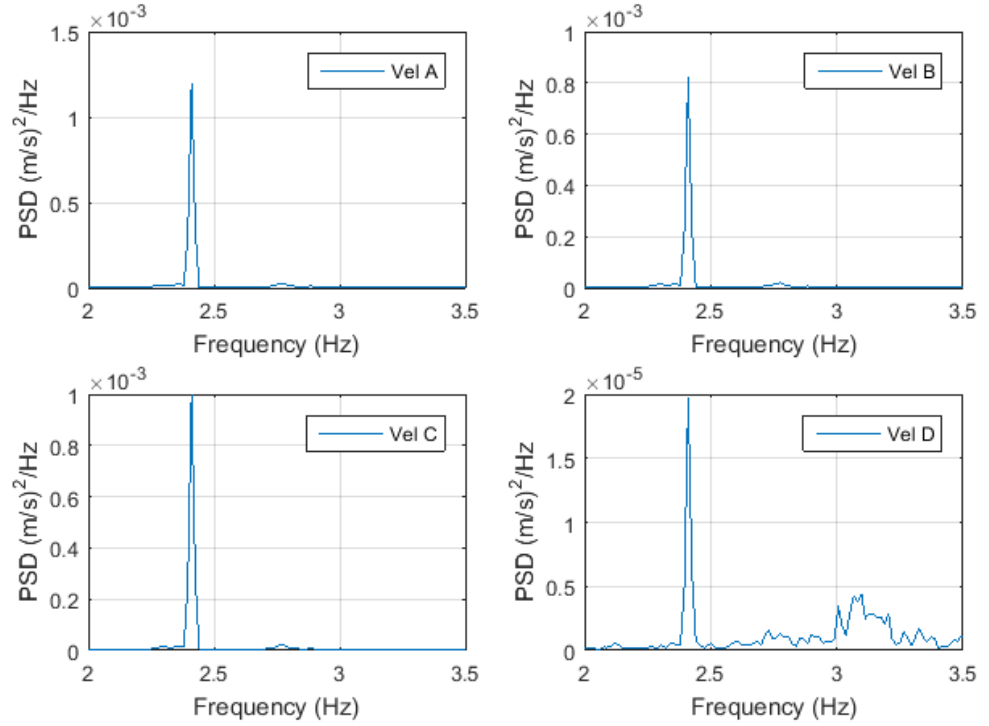

(b)

Figure 02. Measurement record from Test setup *T2*: (a) Time history and (b) Auto Spectral Density plots (Excitation in Y-direction)

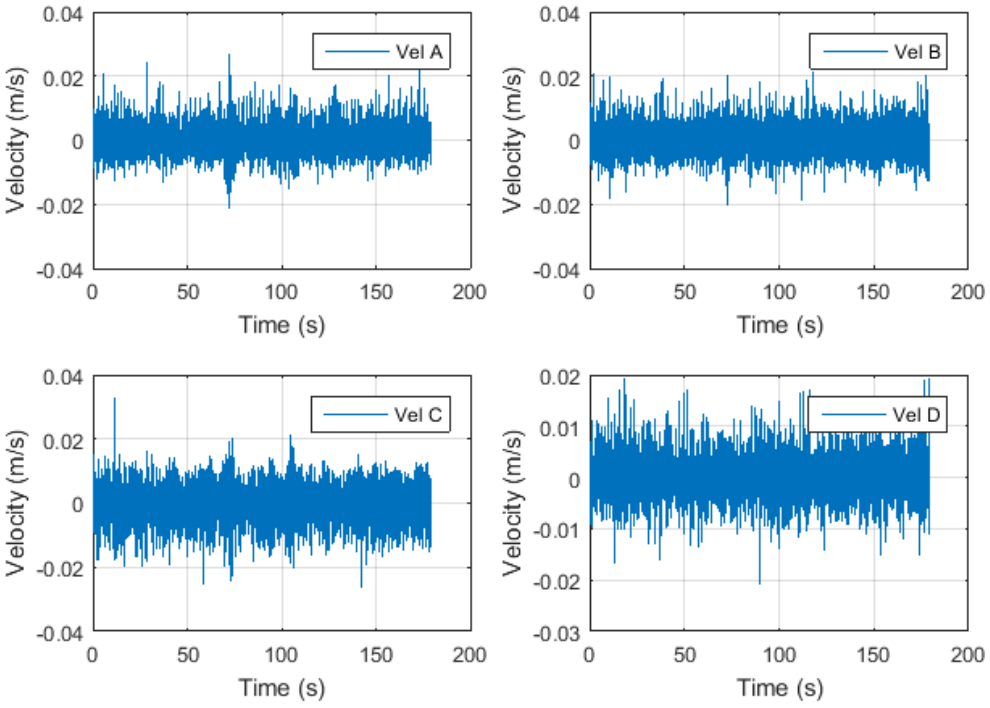

(a)

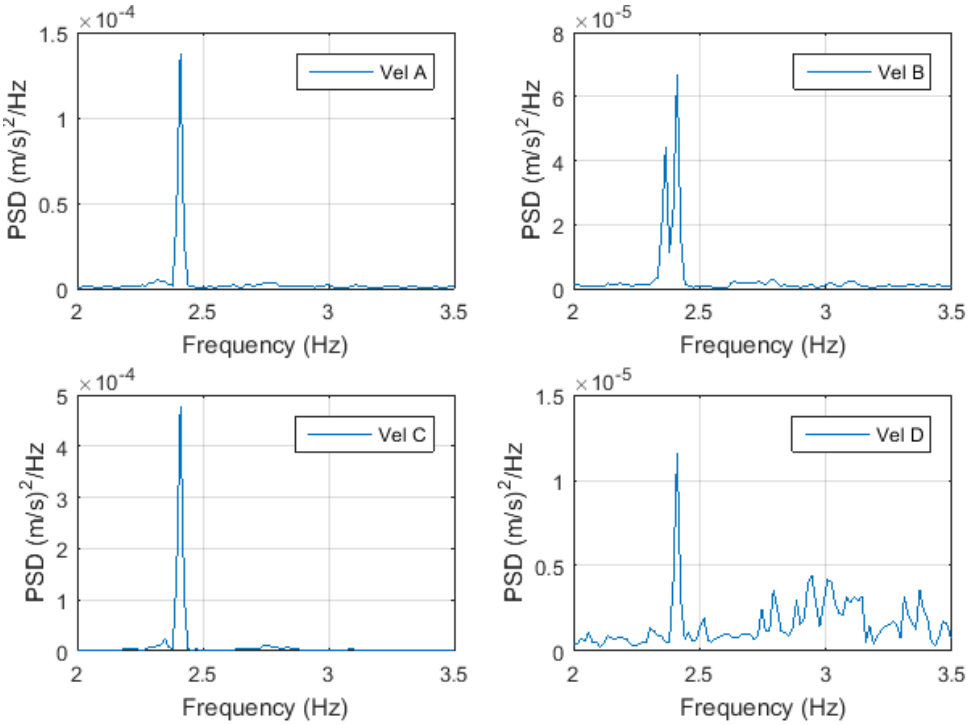

(b)

Figure 03. Measurement record from Test setup *T3*: (a) Time history and (b) Auto Spectral Density plots (Excitation in Y-direction)

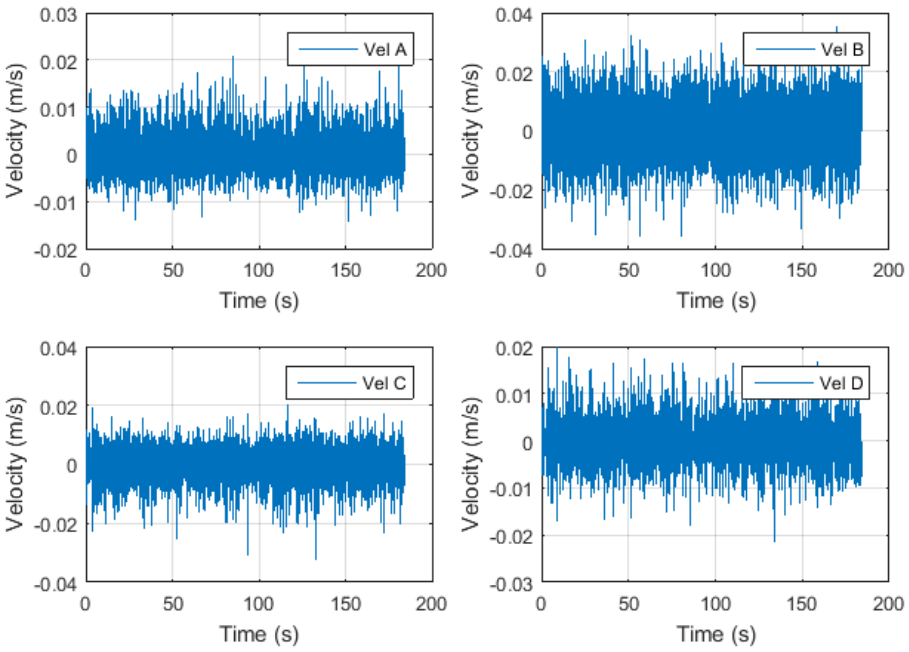

(a)

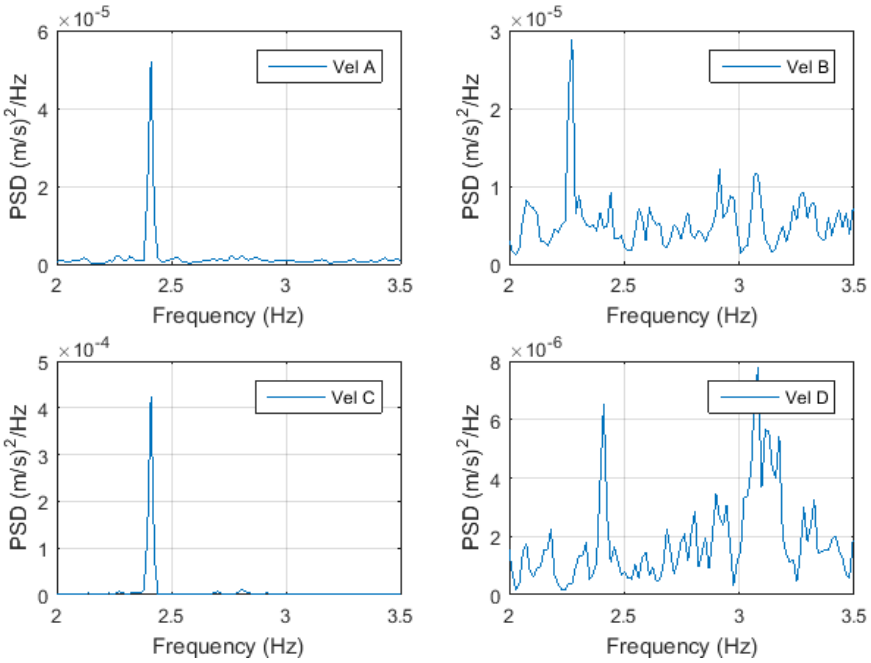

(b)

Figure 04. Measurement record from Test setup *T4*: (a) Time history and (b) Auto Spectral Density plots (Excitation in Y-direction)

It can be observed from Figure B.4 that the measurements made by Velocity meter B were not correct as the peak is not at 2.41 Hz. As a result, the modal coordinate at this DOF could not be estimated (Table 3.3).